

070
Yan
Ind
M.S.
1988

Indo-Australia plate motion determined f
AC .H3 no.Y88 15526



Yan, Chun-Yeung
SOEST Library

DEC 06 1988

INDO-AUSTRALIA PLATE MOTION DETERMINED FROM
AUSTRALIA AND TASMAN SEA HOTSPOT TRAILS

RETURN TO
HAWAII INSTITUTE OF GEOPHYSICS
LIBRARY ROOM

A THESIS SUBMITTED TO THE GRADUATE DIVISION OF THE
UNIVERSITY OF HAWAII IN PARTIAL FULFILLMENT
OF THE REQUIREMENTS FOR THE DEGREE OF

MASTER OF SCIENCE

IN GEOLOGY AND GEOPHYSICS

DECEMBER 1988

By

Chun-Yeung Yan

Thesis Committee:

Loren W. Kroenke, Chairman

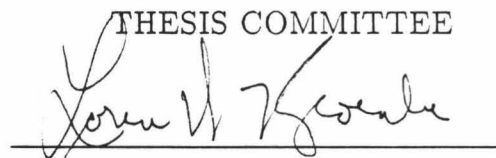
Eduard Berg

Frederick K. Duennebier

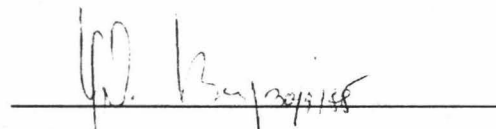
David Epp

We certify that we have read this thesis and that in our opinion it is satisfactory in scope and quality as a thesis for the degree of Master of Science in Geology and Geophysics.

THESIS COMMITTEE



Chairman







ACKNOWLEDGEMENTS

I thank Rick Hagen for proofreading the early versions of this paper and Dr. P. Coleman for providing helpful editorial comments. Their efforts to "transform" this work into proper English enabled me to express my thoughts more clearly. I am indebted to Dr. Eduard Berg for providing the BASIC computer program used to determine the poles of rotation. I am grateful to Mr. Brooks Bays for drafting assistance. Finally, I thank my fellow graduate students, Rick Hagen, Glenn Brown, and Phil Jarvis, who provided much needed support during the course of this study. This study was supported in part by a contract from the Agency for International Development.

ABSTRACT

A model of Indo-Australia Plate motion relative to hotspot trails on the eastern margin of the plate has been derived. Five poles and corresponding angles of rotation are used to describe the Indo-Australia Plate motion relative to the hotspots responsible for the Lord Howe Seamounts and Tasmantid Guyots in the Tasman Sea and Cenozoic volcanic centers in eastern Australia for the past 55 Ma. Changes in plate motion are identified at 12, 16, 28 and 43 Ma. A chain of geoid anomalies identified from the SEASAT gravity map is proposed as part of a hotspot trail active from 55 to 43 Ma. The fixed hotspot hypothesis is supported by the systematic and parallel alignment patterns of the Lord Howe Seamounts and Tasmantid Guyots with respect to parallels about the pole of rotation for these two hotspot trails for the past 28 Ma. The beginning of these hotspot trails is probably related to the end of spreading in the d'Entrecasteaux, Coral Sea, and Tasman basins. Good agreement is obtained between the Indo-Australian apparent polar wander path predicted from the model and the apparent polar wander paths obtained from other geophysical methods.

TABLE OF CONTENTS

| | |
|--|-----|
| ACKNOWLEDGEMENTS | iii |
| ABSTRACT | iv |
| LIST OF TABLES | vi |
| LIST OF ILLUSTRATIONS | vii |
| I. INTRODUCTION | 1 |
| II. BACKGROUND INVESTIGATIONS | 9 |
| III. METHODS | 19 |
| IV. RESULTS | 22 |
| V. DISCUSSION | 62 |
| VI. SUMMARY AND CONCLUSIONS | 65 |
| Appendix A: Methods for Determining Poles of Rotation | 67 |
| Appendix B1: Iteration Method for Determining Poles of Rotation | 69 |
| Appendix B2: List of Computer Program for Determining Poles of Rotation (Grid Search Method) | 74 |
| Appendix C: Contour Maps of Sigma Values | 76 |
| Appendix D: Plots of Angular Distance vs. Age | 89 |
| References | 96 |

LIST OF TABLES

| Table | | Page |
|-------|--|------|
| 1 | Determined rotation vectors | 25 |
| 2 | Predicted hotspot source locations | 26 |
| 3 | Predicted ages for the Tasman Sea seamounts | 27 |
| 4 | A comparison of predicted ages with radiometric ages | 51 |
| 5 | Poles of opening for the Southeast Indian Ridge | 58 |

LIST OF ILLUSTRATIONS

| Figure | | Page |
|--------|--|------|
| 1 | Regional map of the eastern part of the Indo-Australia Plate | 5 |
| 2 | Location of volcanic centers and seamounts on the eastern half of Indo-Australia Plate | 7 |
| 3 | Relationship between the ages and azimuth of eastern Australian volcanic centers | 12 |
| 4 | The locations and ages of the southeastern Australian basaltic lava fields | 15 |
| 5 | A straight line approximation of the Indo-Australia Plate motion . | 17 |
| 6 | Locations of poles of rotation | 24 |
| 7 | Hotspot traces generated by summation of the preferred vectors of rotation | 30 |
| 8 | Oblique Mercator grids for 12-0 Ma | 33 |
| 9 | Oblique Mercator grids for 16-12 Ma and 28-16 Ma | 35 |
| 10 | Oblique Mercator grids for 28-0 Ma | 39 |
| 11 | A plot of seamount distribution vs. angular distance from hotspot sources | 41 |
| 12 | Oblique Mercator grids for 43-28 Ma and 55-43 Ma | 43 |
| 13 | Oblique Mercator grids for 55-43 Ma without the inclusion of geoid anomalies | 46 |
| 14 | Oblique Mercator grids for 55-43 Ma with the inclusion of geoid anomalies | 48 |
| 15 | A comparison of predicted ages with radiometric ages | 54 |
| 16 | A comparison of Indo-Australian APW paths | 57 |
| 17 | Predicted Antarctic APW paths | 60 |
| 18 | Contour map of σ values for the 12- 0 Ma time span | 78 |
| 19 | Contour map of σ values for the 16-12 Ma time span | 80 |
| 20 | Contour map of σ values for the 28-16 Ma time span | 82 |
| 21 | Contour map of σ values for the 43-28 Ma time span | 84 |

| | | |
|----|--|----|
| 22 | Contour map of σ values for the 55-43 Ma time span | 86 |
| 23 | Contour map of σ values for the 28- 0 Ma time span | 88 |
| 24 | A plot of angular distance vs. radiometric age for the 43-28 Ma time span | 91 |
| 25 | A plot of angular distance vs. radiometric age for the 55-43 Ma time span (without the inclusion of geoid anomalies) | 93 |
| 26 | A plot of angular distance vs. radiometric age for the 55-43 Ma time span (with the inclusion of geoid anomalies) | 95 |

I. INTRODUCTION

The definition of a convenient frame of reference to which all plate motion can be referred is a major goal of global tectonic analysis, and greatly simplifies reconstruction of paleogeography. Although there have been numerous studies utilizing various types of frames of reference such as one continent or another (Briden et al., 1981; Smith, 1982; Whitman et al., 1983; Lawver et al., 1985; Owen, 1984; Barron, 1987), stationary geomagnetic poles (Jurdy and Van der Voo, 1974), and/or hotspots (Morgan [1981, 1983]; Duncan [1981]; Schult and Gordon, [1984]), the existence of a fixed frame of reference with respect to the mantle has not been demonstrated conclusively.

Since Wilson (1963, 1965) first postulated that volcanic chains and linear aseismic ridges are surface expressions of differential motion between the upper and central parts of mantle convection cells, and Morgan (1971, 1972a,b) first suggested that volcanic chains and linear aseismic ridges are formed by the motion of plates over fixed mantle hotspots "which are manifestations of convection in the lower mantle", there have been many studies that have questioned whether hotspots are fixed relative to each other. On the one hand, Molnar and Atwater (1973) estimated relative motions of 8-20 mm/yr between hotspots in the Atlantic and Indian oceans from plate reconstructions at anomalies 6 and 13; Burke et al. (1973) concluded from plate reconstruction in the Atlantic Ocean, that an average relative motion of 20 mm/yr has occurred between the Central and South Atlantic hotspots since the mid-Cretaceous; and Molnar and Francheteau (1975) estimated a relative motion of 10-20 mm/yr between major hotspots in the Atlantic and Indian oceans from plate reconstructions at anomalies 13 and 24. On the other hand, Minster et al. (1974) and Minster and Jordan (1978) concluded from global instantaneous plate motion models that there has been no relative motion between hotspots for the past 5-10 Ma; Morgan (1981, 1983) and Duncan (1981, 1984) concluded, albeit somewhat subjectively from the visual fitting of Atlantic hotspots, that hotspots were reasonably fixed relative to each other ($< 5\text{mm/yr}$), and thus could form a convenient reference frame.

In a recent paper, based on their combined global plate reconstructions, Molnar and Stock (1987) determined that average velocities of 10 to 20 mm/yr occurred be-

tween major hotspots in the Atlantic, Indian and Pacific oceans during the past 65 to 50 Ma, and conclude that hotspots do not define a fixed reference frame. The plate motions with respect to Atlantic hotspots used by Molnar and Stock (1987), however, were determined earlier and somewhat subjectively by Morgan (1981, 1983) and Duncan (1981). Although Molnar and Stock took into account some of the uncertainties in plate reconstruction, they used only two poles of rotation for the entire length of the Hawaiian (43-0 Ma) and Emperor (60-43 Ma) chains to describe the plate motion over the Hawaiian hotspot and they also did not consider possible plate boundaries between East and West Antarctica, both of which are questionable assumptions. In contrast, Lonsdale (1988) concludes that there has been little relative motion between the Hawaiian and Louisville hotspots for the past 70 Ma. He also shows that two poles of rotation are required in order to satisfactorily describe the geometry of Hawaiian and Louisville chains for the past 43 Ma. In summary, whether hotspots are fixed or stationary would appear to remain debatable. But if hotspots are truly fixed with respect to one another, then they could provide an ideal reference frame for mapping plate motions and reconstructing paleogeography.

Most of the observed hotspot trails, e.g. the Hawaiian-Emperor chain in the Pacific and the New England Seamounts in the northern Central Atlantic, are composed of isolated or short chains of seamounts which, at best, are partial records of plate motion. A primary requirement for defining a hotspot frame of reference is a set of fairly continuous trails of hotspot volcanism that reveal subtle changes in both rate and direction of plate motions. Furthermore, more than one hotspot trail of the same age span on the same plate, such as the Tasmanid Guyots and Lord Howe Seamounts described in this study, would help significantly to constrain the poles and angles of rotation (Harrison, 1972). Moreover, if a set of self-consistent poles and angles of rotation (i.e. vectors of rotation) that closely agrees with those hotspot trails can be determined, it would imply negligible relative motion between the hotspots. In contrast, if a set of self-consistent poles and angles of rotation that closely agrees with those hotspot trails can not be determined, it would imply relative motion between the hotspots. In this paper, hotspots are assumed to be fixed with respect to each other and thus, unless otherwise specified, it should be assumed that motions discussed in

the following sections are relative to the hotspot frame of reference. One of the results of this study will be the conclusion that the assumption is valid, i.e. the hotspots in the Tasman Sea exhibit no observable relative motion and thus are fixed with respect to each other.

The Lord Howe Seamounts, Tasmantid Guyots, and the eastern Australian volcanic centers (Fig. 1,2) collectively provide a very detailed record of Indo-Australia Plate motion relative to the hotspot frame of reference. In particular, because there are more than twenty volcanic centers along the eastern margin of Australia with reliable radiometric ages, the eastern Australian volcanic centers provide a good constraint on the timing of changes in rotation vector of the Indo-Australia Plate motion. Although Pilger (1982) dismissed the idea that hotspots are the sources for these multiple lines of volcanic centers, attributing their formation instead to the migration of intraplate extensional stress, recent studies of the geochemistry and alignment of Cenozoic volcanic activity along the eastern margin of the Indo-Australia Plate (Wellman and McDougall, 1974; Sutherland, 1981, 1983, 1985; Wellman, 1983; Kroenke, 1986; McDonough et al., 1985; Ewart, 1987; Duncan and McDougall, in press), indicate that these volcanic centers are almost certainly of hotspot origin.

The inferred source locations for three of the hotspot trails; the Lord Howe Seamounts, the Tasmantid Guyots, and one of the eastern Australian trails are located within an area covering less than 10° latitude by 15° longitude. The lateral separation between the proposed Tasmantid and Lord Howe hotspots is about 400 km (4° in angular distance). If a maximum of 20 mm/yr of relative motion occurred between these hotspots during the past 50 Ma (as proposed for the major hotspots studied by Molnar and Stock [1987]) then up to 1000 km of relative motion would have taken place between the Lord Howe and Tasmantid hotspot sources. In contrast, if a minimum of 2 mm/yr of relative motion occurred during the past 50 Ma (which is less than the 3 mm/yr relative motion proposed by Morgan [1983] for some of the Atlantic hotspots), then as much as 100 km of relative motion still would have taken place. In both examples, the amount of relative motion would be significant when compared with the distance between the Lord Howe and Tasmantid hotspot sources.

In this paper, a model is developed for Indo-Australia Plate motion using these

Figure 1 The eastern part of the Indo-Australia Plate and its surroundings showing the location of major physiographic and tectonic elements (simplified from Falconer and Tharp, 1983 and Monahan et al., 1984).

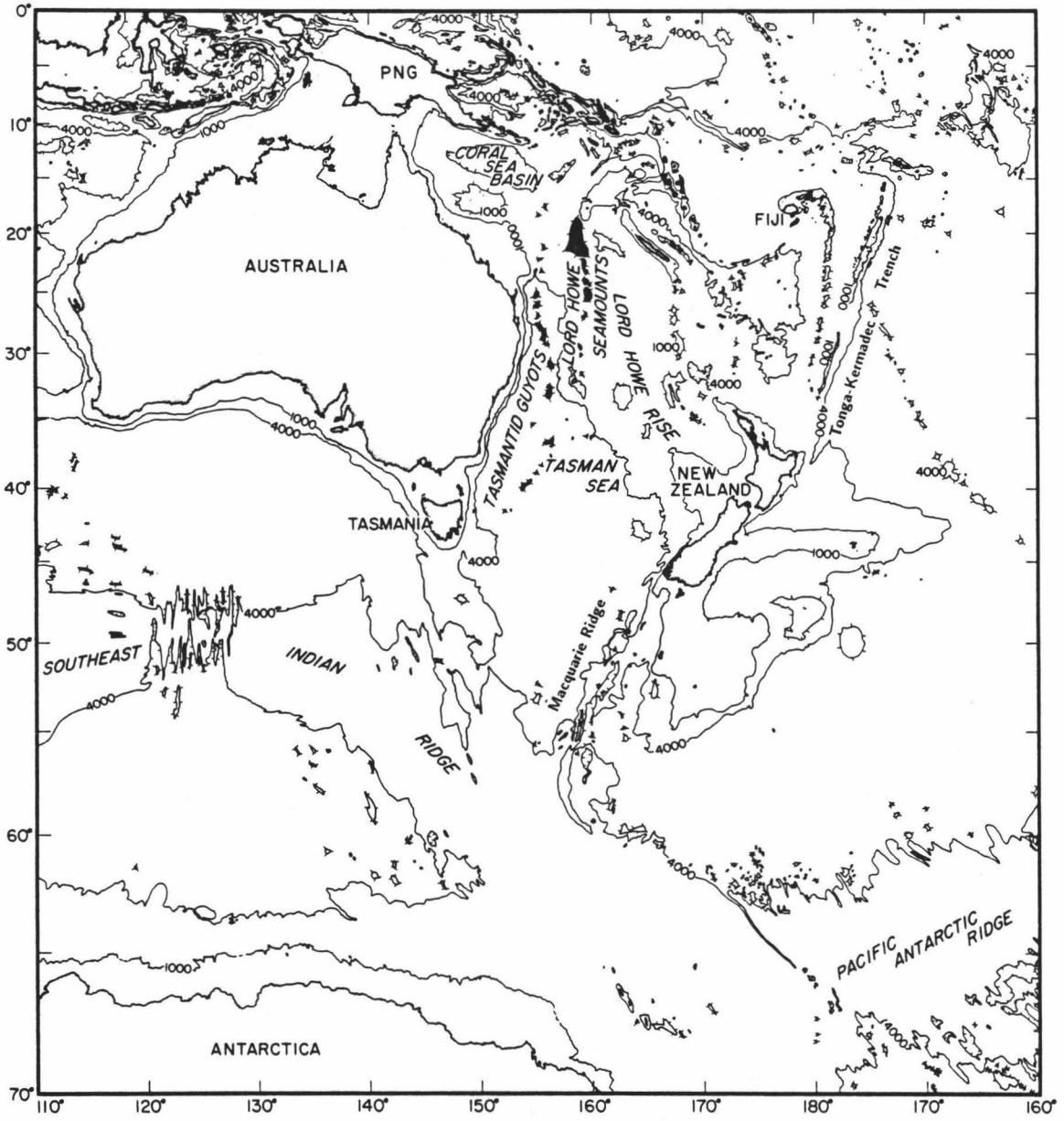
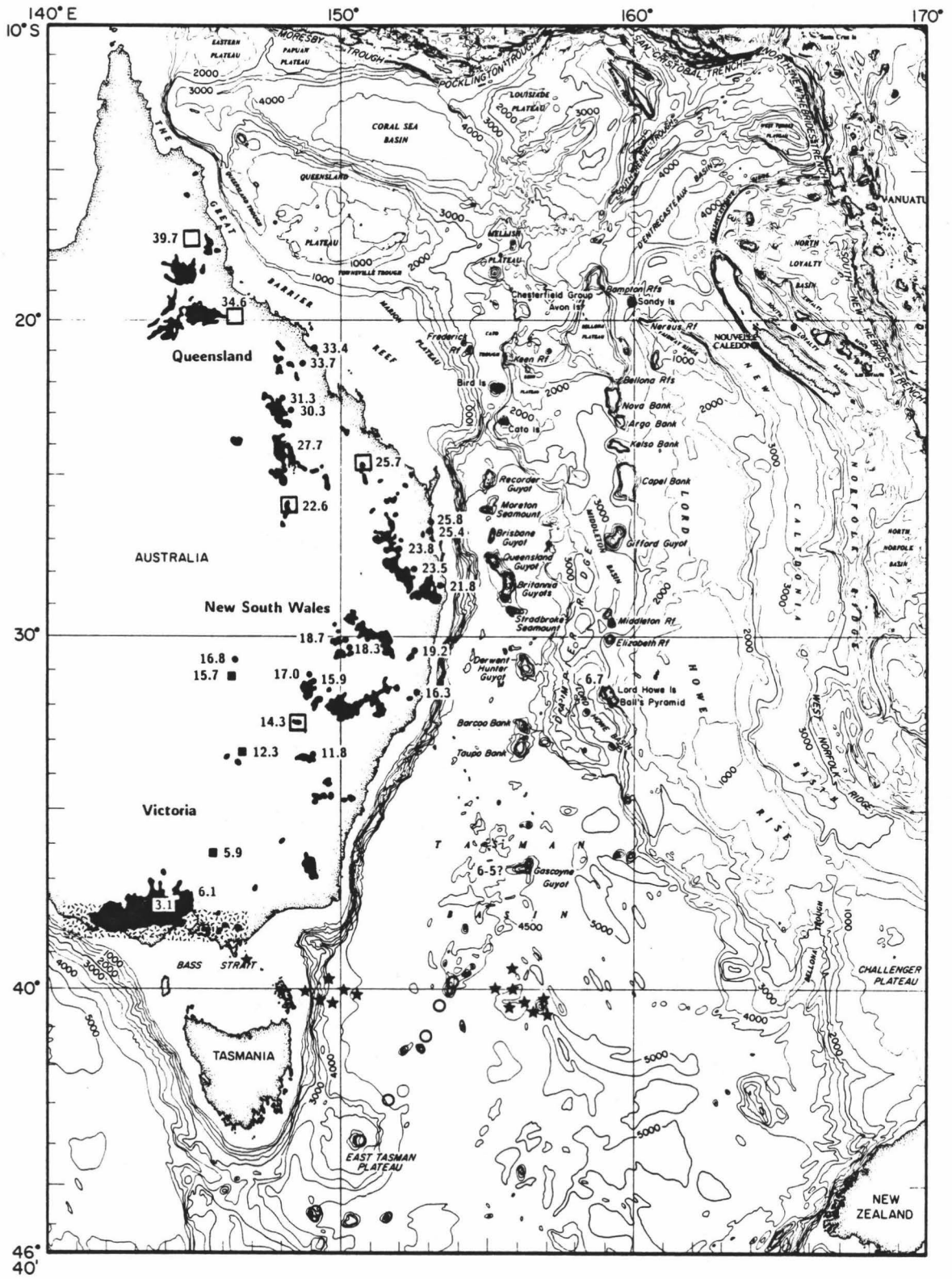


Figure 2 Location of volcanic centers and seamounts on the eastern half of the Indo-Australia Plate. The dark areas mark major centers of Cenozoic volcanism (Stephenson et al., 1980). Solid circles mark central volcanoes, solid squares mark high potassium provinces, open squares mark basaltic lava fields (see Figure 4 for the southeastern Australian basaltic lava fields), and open circles mark locations of geoid anomalies interpreted to be caused by buried seamounts. Radiometric ages for volcanic centers and seamounts are from Wellman and McDougall (1974), Wellman (1983), Sutherland (1983, 1985), and McDougall et al. (1981). The Otway electrical conductivity anomaly is shown by the dashed pattern (Lilley, 1975, 1976) and stars mark earthquake epicenters.



hotspot trails. Plate motions are described in terms of poles of rotation and rates of rotation (i.e. rotation vectors). The term trail is used herein for the actual surface manifestation of a hotspot, i.e. a chain of seamounts or volcanic centers, whereas the term trace is used for the locus of modelled past locations of the hotspot magmatic source relative to the overlying plate as determined by the respective vectors of rotation. The hotspot trails reveal a zigzag pattern of northward motion for the Indo-Australia Plate during the past 55 Ma. The Australian apparent polar wander (APW) path derived from the vectors of rotation, as will be shown later, compares favorably with the APW paths determined from other geophysical data.

II. BACKGROUND INVESTIGATIONS

Hess and Maxwell (1949) first suggested that the two, roughly north-south aligned, linear chains of seamounts located within the Tasman Sea off eastern Australia, the Lord Howe Seamounts along the western margin of the Lord Howe Rise and the Tasmantid Guyots in the middle of the Tasman Basin (Fig. 2), define fault or shear zones. Vogt and Connoly (1971) later suggested a possible hotspot origin for these two sub-parallel groups of seamount chains. The Lord Howe Seamounts can be traced northward along longitude $159^{\circ}E$ from $35^{\circ}S$ to $22^{\circ}S$ where they merge with the Bellona Plateau. In similar fashion, the Tasmantid Guyots can be traced northward along longitude $156^{\circ}E$ from $41^{\circ}S$ to $25^{\circ}S$ where they become less evident near the southern part of the Marion Plateau. The few islands and reefs in the vicinity of the eastern side of the Marion Plateau do not form an obvious alignment and their origin is less certain. Alkaline olivine basalts were collected from both of these seamount chains (Standard, 1961; Slater and Goodwin, 1973). Green et al. (1987) note that the chemistry and petrology of rocks from these seamounts match closely with those from the main cone-building stage of the Hawaiian Volcanoes along the Hawaiian-Emperor hotspot trail.

Samples and age data from both seamount chains are sparse. Lord Howe Island, an eroded tholeiitic shield volcano, near the southern end of the Lord Howe Seamounts (Fig. 2) has been dated radiometrically with a range from 6.9 to 6.4 Ma (McDougall et al., 1981). Gascoyne Seamount of the Tasmantid Guyots (Fig. 2) has a questionable date of 5.5 Ma (Sutherland, 1983). Although the present location of the hotspot source for the Lord Howe Seamounts is not well defined, a heat flow anomaly (up to 2.4 HFU [Grim, P.J., 1969; Watanabe et al., 1977]) was measured between Lord Howe Island and the location of the hotspot source postulated in this study. The present location of the hotspot source for the Tasmantid Guyots is believed to be marked by a cluster of seismicity centered at $41^{\circ}S$, $156^{\circ}E$ (Denham, 1985) near a seamount at the southern end of the chain (Fig. 2).

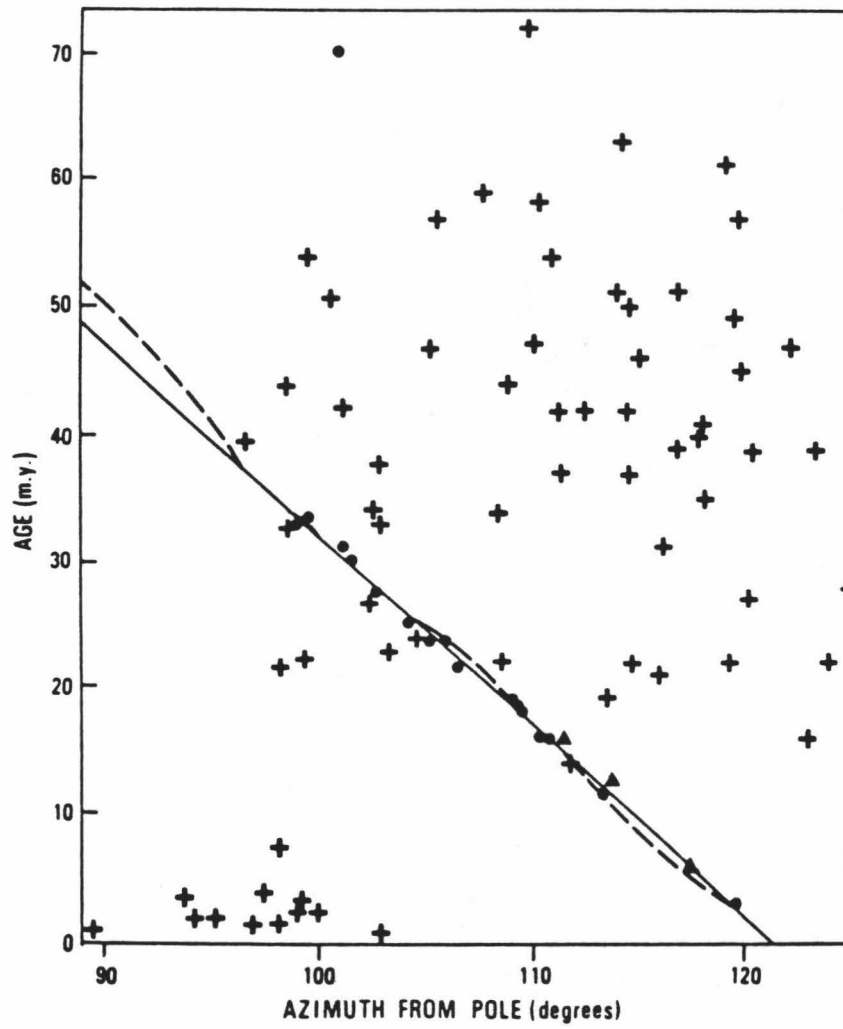
Wellman and McDougall (1974) and Wellman (1983) have summarized the radiometric age data for fifty igneous provinces along the eastern margin of Australia

(Fig. 2). From the age distribution pattern and rock types, they concluded that the central volcanoes and felsic magma of the volcanic provinces were formed by motion of the plate relative to several mantle sources. At the younger end, in the Victoria area (Fig. 2), there has been recent volcanic activity near Mount Gambier ($37.8^{\circ}S$, $140.8^{\circ}E$) about 4200 years ago (Sheard, 1978; Blackburn et al., 1982), near Mount Schank ($37.9^{\circ}S$, $140.7^{\circ}E$) about 4930 years ago (Smith and Prescott, 1987), near Tower Hill ($38.3^{\circ}S$, $142.3^{\circ}E$) about 4315 years ago (Gill, 1964), and a recent presumed underwater eruption in the Bass Strait ($38.3^{\circ}S$, $141.3^{\circ}E$) (Sprigg, 1959). The area is reported to be currently seismically active (Fig. 2) by Denham et al. (1981), and anomalous high electrical conductivity also has been reported in the Otway area (Fig. 2) by Lilley (1975, 1976), which may indicate the proximity of a heat source. In fact, Sass and Lachenbruch's (1979) study of the thermal regime of Australia indicates anomalously high heat flow in the Bass Strait area, that cannot be accounted for by crustal radioactivity. Because of the existence of thick crust (40 km, Cleary, 1973) and thick lithosphere (150-200 km, Muirhead et al., 1977), Sass and Lachenbruch concluded that intrusions into the upper crust are the sources of the thermal anomaly.

Vogt and Conolly (1971) approximated Indo-Australia Plate motions by using a single pole of rotation. From studies of African hotspots, Morgan (1981) and Duncan (1981) inferred Australia Plate motions, based on a plate circuit method (i.e. by vector addition [Le Pichon et al., 1973] and the chain rule procedure [Morgan, 1981]), that roughly agrees with the general N-S trending Australian hotspot trails. In his later paper, Morgan (1983) relied only on Atlantic hotspots to determine plate motions, citing difficulty with hotspots on other plates, in particular Indian Ocean hotspots, in constraining his model. Thus the early studies must now be viewed only as a first approximation to the motion of the Indo-Australia Plate relative to the hotspot frame of reference.

Using the results of Duncan (1981), Wellman (1983) derived a mean pole of rotation at $26.5^{\circ}N$, $33.0^{\circ}E$ for the Indo-Australia Plate motion for the past 33 Ma. Using this pole of rotation, he showed an almost linear correlation (Fig. 3) between the ages of the central volcanoes and high potassium lava fields of the eastern Australian

Figure 3 Relationship between the ages and azimuths of the eastern Australian volcanic provinces relative to the hotspot frame of reference. The azimuth is defined as “the angle subtended at the pole of rotation between the great circle through the north geographic pole and the great circle through the province” (Wellman, 1983). Crosses mark basaltic lava fields, dots show central volcanoes, and the triangles represent high potassium lava fields. The solid line is the empirical linear rotation model of Wellman (1983), and the dashed line is the rotation model of Duncan (1981). Note the good fit of the central volcanoes and the high potassium provinces as opposed to the poor fit of the basaltic lava fields whose eruptive centers are not well defined.



volcanic provinces (which he concluded were the only evidence of hotspot volcanism) and changes in azimuth of the provinces from the mean pole of rotation.

Sutherland (1981) proposed seven hotspot trails to account for the formation of all the volcanic provinces in eastern Australia and extended the age of the possible hotspot related volcanic provinces beyond 33 Ma to 55-53 Ma. Based on studies of the basaltic lava fields in southeastern Australia (Fig. 4), he included a major change in plate motion at about 29 Ma to account for the apparent difference in trend of the basaltic lava fields from the NS trending volcanic centers. Thus, the volcanic provinces can be separated into two groups by age. One group including the volcanic activity occurring from 33-0 Ma (Fig. 2) is distributed down the entire length of eastern Australia (Wellman and McDougall, 1974; Wellman, 1983), and an earlier phase of basaltic lava activity occurring from 55-30 Ma (Fig. 4), is restricted, for the most part, to southeastern Australia (Sutherland, 1981). Using two straight line fits to the volcanic centers and basaltic lava fields with a bend at 29 Ma Sutherland (1981) extrapolated the hotspot trails to the Coral Sea-Louisiade spreading system and the New Guinea collision zone, correlating them with the initiation of spreading in the Coral Sea Basin.

From the apparent congruency of the small-circle segments comprising the Lord Howe Seamounts, the Tasmantid Guyots, and Australia volcanic centers (Fig. 5), Kroenke (1986) recognized the presence of at least four hotspot trails, three of which appearing to have originated near the center of the Coral Sea Basin, the fourth appearing to have originated within the d'Entrecasteaux Basin. He also proposed that four major changes in Indo-Australia Plate motion occurred during the past 38 Ma, i.e. at 11, 16, 25 and 38 Ma. The alignment of the trails on the older side of the 38 Ma bend however was based on the presence of only a few isolated atolls and reefs and thus was subject to question. With the inclusion of the southeastern Australian basaltic lava fields shown in Figure 4, the direction of Indo-Australia Plate motion before 38 Ma can be more precisely determined and the duration of the plate motion can be extended back to 55 Ma (Sutherland, 1981) with confidence. This configuration provides the starting point for the derivation of the Indo-Australia Plate motions in this study, relative to the hotspot frame of reference, as presented below. The two

Figure 4 The locations and radiometric ages of the southeastern Australian basaltic lava fields (Sutherland, 1981). The volcanic provinces are (from north to south): Ipswich (Ip); Walcha (Wa); Barrington (Br); Airley (Ai); Mittagong(Mg); Abercrombie (Ab); Nerriga (Nr); Mittagong (Mg); Moruya(Mo); Monaro (Mn); Gelantipy (Ge); Bogong (Bo); Howitt (Hw); Toombullup (Tm); Neerim(Nm); Flinders (Fl). The open circles are geoid anomalies in the southwestern Tasman Sea (Haxby, 1987). The Ipswich and Barrington trails proposed by Sutherland (1981) are shown as solid and dashed lines respectively.

140°E

150°

150°48'

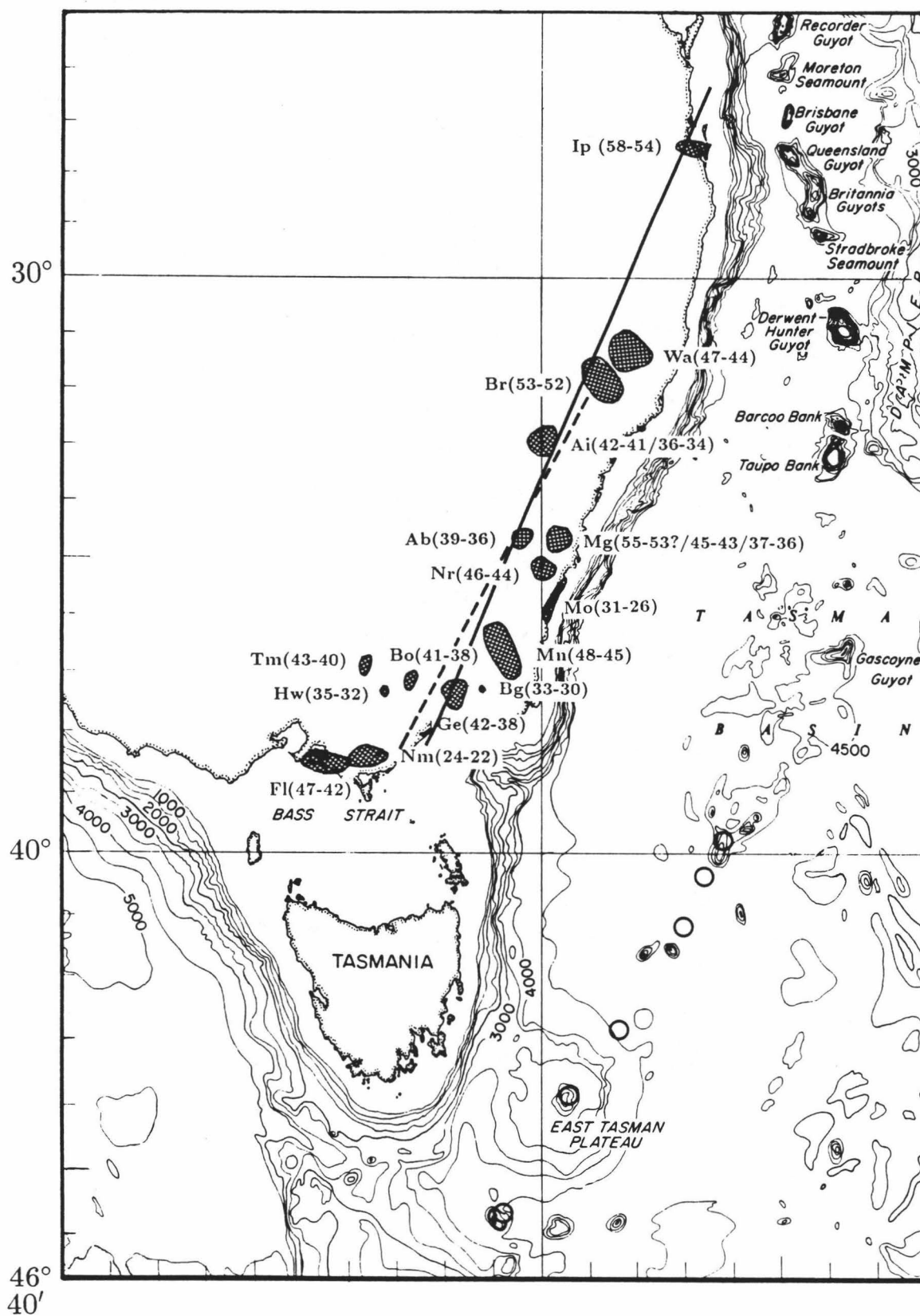
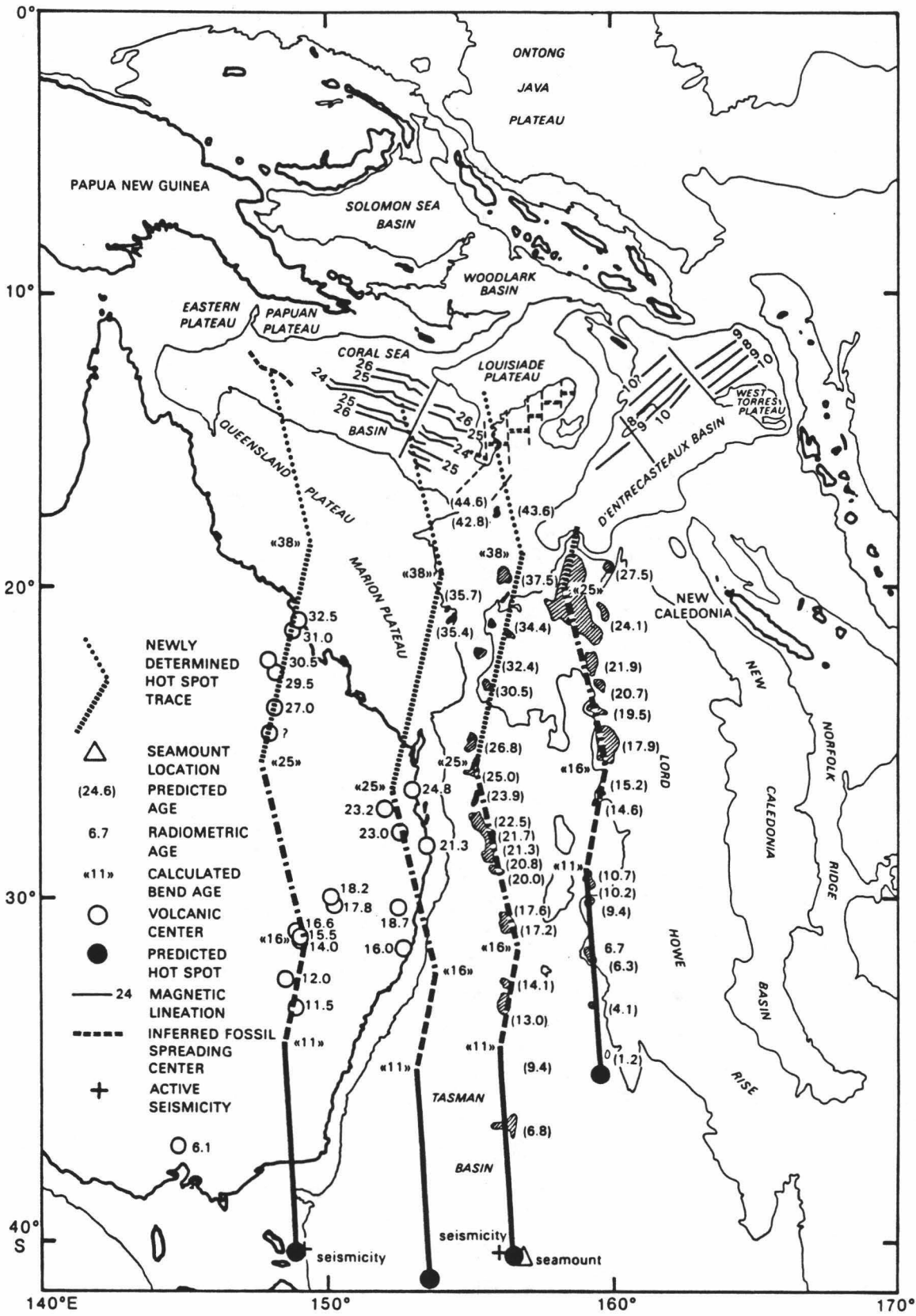


Figure 5 Straight line approximations of Indo-Australia Plate motion and times of changes in plate motion relative to eastern Australia and Tasman Sea hotspots (From Kroenke, 1986).



trails comprising the Lord Howe Seamounts and Tasmanid Guyots coupled with a single trail of volcanic centers near $148^{\circ}E$ on the eastern margin of Australia are used to obtain four poles of rotation from 43 Ma to the present. Likewise, three trails, the Ipswich and Barrington trails and the Tasman Sea geoid anomaly chain, were used to determine the pole of rotation from 55 to 43 Ma.

III. METHODS

Assuming that hotspots are fixed with respect to each other, the motion of a rigid plate on a sphere over a hotspot source during an interval of time can be defined by three parameters, the two coordinates of the pole of rotation and the angle of rotation. The pole of rotation is the geographic location on the surface of the earth, given in latitude and longitude, of the rotation vector describing the transfer of a plate from one position to another (Harrison, 1972; Klitgord and Schouten, 1986). The angle of rotation is the amount of angular motion about the pole of rotation within a certain time interval which is defined as positive in a counterclockwise sense looking down the axis of rotation i.e. using the right-handed system. The rate of angular rotation, assuming a uniform rate within that particular time interval, is given in units of degrees/Ma. Other terms that may need to be defined in order to avoid confusion are: a virtual geomagnetic pole (VGP), which is a single spot measurement of the geomagnetic field (McElhinny, 1979); the paleomagnetic pole, which refers to an average virtual geomagnetic pole; and the apparent polar wander (APW) path for a particular plate, which is defined as a time sequence of paleomagnetic poles, each of which represents the location of the geomagnetic (and presumably geographic) pole as seen by an observer on the plate at the time of formation of the rocks used to find the pole (Cox and Hart, 1986).

The goal of this study is to identify the smallest possible number of poles of rotation and their associated angles of rotation that best describe the location of seamounts in the Tasman Sea and the volcanic centers in eastern Australia. Segments of different hotspot trails, formed on the same plate by a number of hotspots during the same span of time (i.e. about the same pole of rotation), should sweep out series of congruent small-circle arcs or parallels. The angle of rotation for a time span can be estimated by fitting an oblique Mercator grid (Wong et al., 1975) about the pole of rotation on a standard Mercator projection map (Epp, 1978). Radiometric dates from the seamounts and volcanic centers can provide the data necessary to calculate the rate of plate motion between bends. The time of a change in poles of rotation (i.e. a bend time) can be determined from the interpolated ages at the intersection

of the two sets of parallels that provide the "best" visual fit to the seamounts and volcanic centers about their respective poles of rotation.

Poles of rotation were determined by minimizing values of $\sum_{j=1}^M \sum_{i=1}^{N_j} (\beta_{ij} - \bar{\beta}_j)^2$ (Harrison, 1972; Lawver and Dick, 1983; Epp, 1984; Appendices A,B). Where β_{ij} are angular distances from an assumed pole of rotation to points on parallel j , $\bar{\beta}_j$ is the average angular distance to trail j , M is the total number of hotspot trails and N_j is the total number of points, i.e. volcanic centers, along trail j . Poles of rotation were simultaneously calculated for each of the sets of trail segments representing each of the five previously discussed time spans. A trail segment comprises all the seamounts or volcanic centers formed along that trail during a particular time span. For each of the sets of trail segments, an oblique Mercator grid was generated about the calculated pole of rotation and was compared with the location of the appropriate seamounts and volcanic centers for that time span. The locations of the seamounts used in determining the poles of rotation were taken from the bathymetric charts of Kroenke et al. (1983) and Monahan et al. (1984). The center of the summit area of each seamount or guyot was used as an indication of the location of the volcanic center, i.e. the past location of the hotspot. If the edifice was sufficiently elongated to suggest the coalescence of volcanoes and had a definite trend, more than one point on the edifice was used to calculate the pole of rotation. The locations and radiometric ages of volcanic centers (Fig. 2) were taken from Wellman and McDougall (1974), McDougall et al. (1981), Wellman (1983), and Sutherland (1981, 1983, 1985).

In practice, geographic coordinates of the seamounts and volcanic centers were entered in computer programs (Appendix B) that determined the standard deviation σ , in angular distance of the data set from an assumed or estimated pole of rotation. An educated guess at the coordinates of the initial pole of rotation, such as the approximate coordinates of the point of convergence of the normals to the subparallel arcs of the seamount chains, often significantly reduced the amount of required calculations. The pole associated with the minimum σ value for the whole data set was defined as the "best" pole. The value of σ was the sole criterion used to measure how well the pole of rotation fitted the data set. The parallel that equaled the average angular distance from the best pole for the trail segment was defined as the "best" parallel

for that trail segment. Because a linear time-space correlation was found in early studies, i.e. a constant rate of rotation was present from 43 to 0 Ma, (Wellman and McDougall [1974]; Sutherland [1981, 1983]; Wellman [1983]; Duncan and McDougall [in press]), the best poles of rotation for the 12-0 Ma and 28-16 Ma time spans were not used in this study. Instead, poles of rotation were chosen within the 1.05σ limit for each of these time spans that maintained a constant rate of rotation for the past 43 Ma. The 1.05σ limit was chosen because an increase in standard deviation of 5% was considered to be significant in this study.

The time of a change in poles of rotation (i.e. a bend time) was determined from the interpolated ages at the intersection of the two sets of parallels that provide the "best" visual fit to the seamounts and volcanic centers about their respective poles of rotation. The intersections of the two sets of parallels, about their respective poles of rotation, were chosen in such a way that an equal amount of angle of rotation or congruency was maintained for all trails segments representing the same span of time. If poles of rotation that maintained both the visual fit and an equal amount of angle of rotation for each of the coeval trail segments could not be found, an adjacent parallel was chosen which maintained an equal amount of angle of rotation for all coeval trail segments. In doing so, the same geometry was maintained for all trails.

IV. RESULTS

Changes in the poles of rotation of the Indo-Australia Plate, and thus bends in the plate trajectory, were determined at 12, 16, and 28 Ma (Fig. 6) as previously discussed. The occurrence of a 43 Ma bend is inferred from the difference in location of the poles of rotation for the 43-28 Ma and 55-43 Ma trail segments (Fig. 6). The exact time and location of this bend are not certain, because of sparse data for both the older part of the 43-28 Ma time span and the younger part of the 55-43 Ma time span. There is, however, a clear indication of a change in Pacific Plate motion at 43 Ma as indicated by the Hawaiian-Emperor bend (Clague and Dalrymple, 1987) and therefore, in this study, a corresponding change in Australia Plate motion was assumed to have taken place at 43 Ma. The location of the bend was estimated by extrapolating the location of the 43 Ma position from the 28 Ma bend based on the rotation rate for that time span. The preferred set of calculated poles, angles, and rates of Indo-Australia Plate motions determined in this study are listed in Table 1 and the locations are shown in Figure 6. The hypothetical hotspot locations are listed in Table 2. Predicted ages for the seamounts based on this model are listed in Table 3. Rotation vectors determined in this study for the 12-0 Ma, 16-12 Ma, 28-16 Ma and 43-28 Ma time spans give rotation rates very close to a constant $0.7^\circ/\text{Ma}$, for the Indo-Australia Plate during the entire 43 Ma to present time span. Likewise, the rotation vector for the 55-43 Ma time span gives a rate that is also very close to $0.7^\circ/\text{Ma}$.

The hypothetical traces, constructed from the vector sums of the rotation vectors given in Table 1, fall within the charted width of most of the seamounts studied (Fig. 7). The volcanic centers located on eastern Australian continental crust, however, are not in as close agreement. Deep crustal structure, in particular deep normal faulting (including listric faulting) along the Australian rifted margin (Falvey and Mutter, 1981), may have deflected magma rising from the deep mantle sources. Or, more simply perhaps, the actual extent of volcanism may not be known due to: erosion, sediment cover, or incomplete mapping of the area. A model of a hotspot source with considerable lateral extent, i.e. a hotline model (Bonatti et al., 1977; Wellman, 1983;

Figure 6 Locations of poles of rotation for the Indo-Australia Plate from 55 Ma to the present determined from hotspot trails in the Tasman Sea and eastern Australia. Solid circles are poles of rotation at the minimum standard deviation (σ) in angular distance. Triangles mark poles of rotation that maintain a constant rate of rotation. Arrows indicate the preferred poles of rotation. Ellipses indicate the 1.05 times minimum σ values. The solid square is the pole of rotation for 55-43 Ma time span determined without the inclusion of the chain of geoid anomalies in southwestern Tasman Sea. The open square is the Indo-Australian pole relative to hotspots determined from the present day plate motion model of Minster and Jordan (1978), which is close to the pole for the 12-0 Ma time span determined in this study. Dots show the locations of hotspot traces along eastern Australia and within the Tasman Sea.

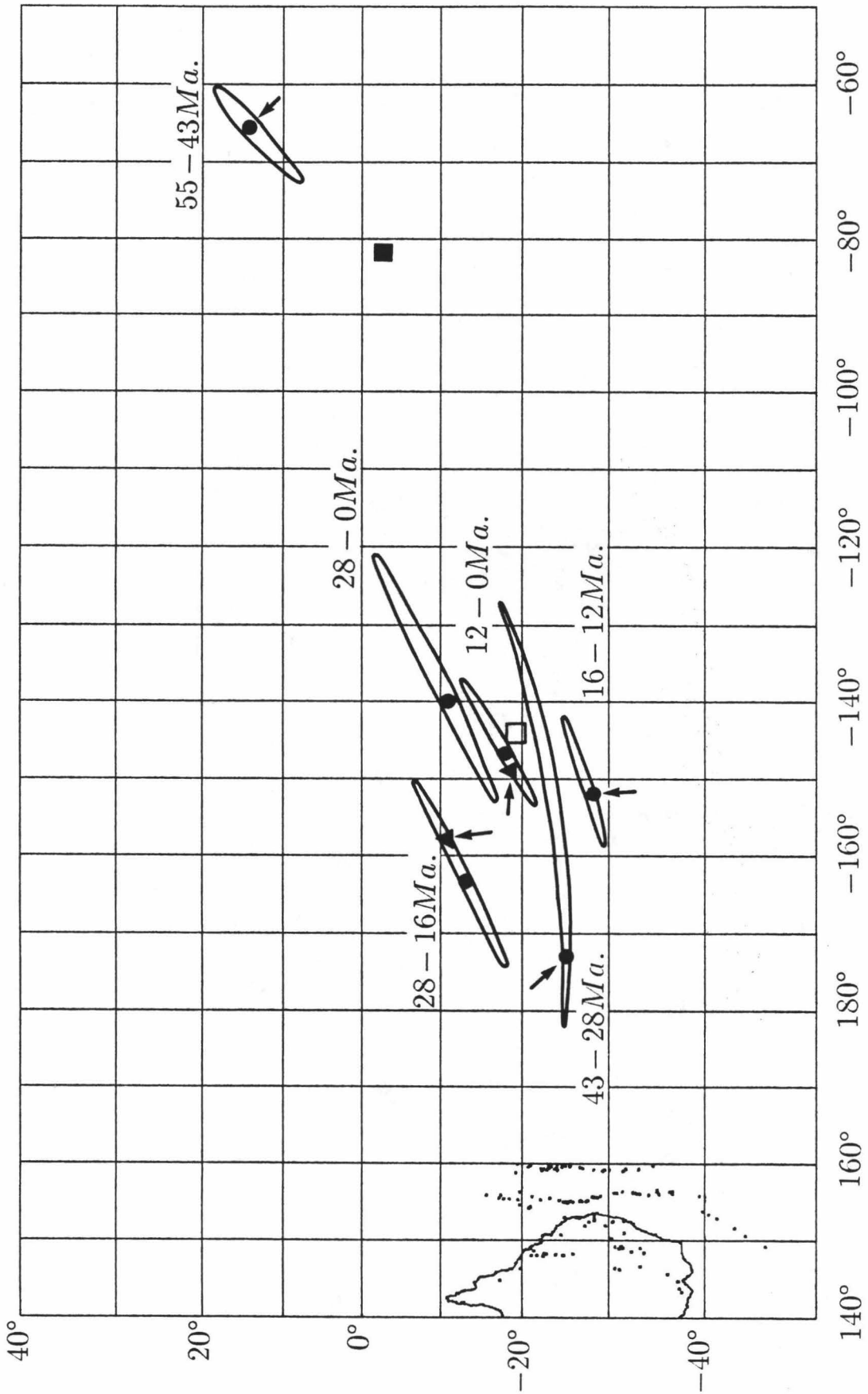


Table 1

Rotation vectors determined for the Indo-Australia Plate from hotspot trails in the Tasman Sea and eastern Australia.

a. Preferred Indo-Australian rotation vectors for the five time spans from 55 Ma to the present.

| Age | Pole of rotation | | Angle* | Rate** | Sigma Min. |
|-----------|---------------------|---------|--------|--------|------------|
| Ma | Lat. | Long. | (°) | °/Ma | (°) |
| 11.8- 0.0 | 18.8°S | 148.3°W | 8.6 | 0.7(3) | 0.109 |
| 16.4-11.8 | 28.2°S | 152.0°W | 3.4 | 0.7(4) | 0.055 |
| 27.7-16.4 | 10.8°S | 157.8°W | 8.4 | 0.7(4) | 0.103 |
| 43.0-27.7 | 25.2°S | 173.2°W | 10.7 | 0.7(0) | 0.131 |
| 55.0-43.0 | 14.4°N | 65.8°W | 8.0 | 0.6(7) | 0.211 |

b. Single Indo-Australian rotation vector determined for the past 28 Ma.

| Age | Pole of rotation | | Angle* | Rate** | Sigma Min. |
|-----------|---------------------|---------|--------|--------|------------|
| Ma | Lat. | Long. | (°) | °/Ma | (°) |
| 28.0- 0.0 | 10.4°S | 139.8°W | 15.7 | 0.5(6) | 0.350 |

* The angles of rotation for the 43.0-27.7 and 55.0-43.0 Ma time spans were calculated by multiplying the determined rates of rotation (Appendix D) by their respective time spans.

** The rates for the 11.8-0, 16.4-11.8, 27.7-16.4 and 28.0-0.0 Ma time spans were calculated by dividing the angles of rotation by their respective time spans.

Table 2

Locations of predicted hotspot sources in the Tasman Sea and eastern Australia.

| | Lat.(°S) | Long.(°E) |
|---------------------|----------|-----------|
| Lord Howe Seamounts | 34.69 | 159.48 |
| Tasmantid Guyots | 40.51 | 156.71 |
| 148°E Trail | 40.58 | 148.41 |
| 153°E Trail | 41.03 | 153.31 |
| 145°E Trail | 41.18 | 145.30 |
| 143°E Trail | 39.65 | 143.20 |
| Ipswich Trail | 52.78 | 158.80 |
| Barrington Trail | 56.86 | 159.42 |
| Geoid Chain | 63.25 | 169.55 |

Table 3
 Predicted ages for Tasman Sea seamounts and geoid anomaly chain.

a. Predicted ages and angular distances measured from the predicted hotspot source for Lord Howe Seamounts based on preferred vectors of rotation.

| | | Lat. | Long. | Predicted Ages (Ma)* | | Angular Dist.* |
|---|--------------------|-------|--------|----------------------|-----------|----------------|
| | | °S | °E | Center | Range | (°) |
| + | N. Bellona Plateau | 19.46 | 158.81 | 30.2 | — | 22.1 |
| + | | 19.88 | 158.75 | 29.1 | — | 21.4 |
| + | | 20.30 | 158.62 | 28.0 | — | 20.6 |
| + | Nova Bank | 22.55 | 159.27 | 23.3 | 23.9-22.3 | 17.1 |
| + | Argo Bank | 23.30 | 159.51 | 21.7 | 22.1-21.2 | 15.9 |
| + | Kelso Bank | 24.10 | 159.46 | 20.2 | 20.7-19.8 | 14.8 |
| + | Capel Bank | 25.10 | 159.75 | 18.1 | 19.0-16.7 | 13.3 |
| + | Gifford Guyot | 26.75 | 159.58 | 14.8 | 15.1-14.5 | 10.8 |
| + | Unnamed Seamount | 27.05 | 159.39 | 14.2 | 14.5-13.7 | 10.4 |
| + | Unnamed Seamount | 29.33 | 159.05 | 9.8 | 10.1- 9.5 | 7.1 |
| + | Middleton Reef | 29.58 | 159.21 | 9.4 | 9.6- 9.1 | 6.8 |
| + | Elizabeth Reef | 30.05 | 159.15 | 8.5 | 8.7- 8.1 | 6.2 |
| + | Lord Howe Island | 31.62 | 159.13 | 5.6 | 5.9- 5.4 | 4.1 |
| + | Ball's Pyramid | 31.85 | 159.26 | 5.2 | 5.4- 4.9 | 3.8 |
| | Flinders Seamount | 34.75 | 159.75 | 0.1 | 0.3- 0.0 | 0.0 |

b. Predicted ages and angular distances measured from the predicted hotspot sources for Tasmantid Guyots based on preferred vectors of rotation.

| | | Lat. | Long. | Predicted Ages (Ma)* | | Angular Dist.* |
|---|----------------------|-------|--------|----------------------|-----------|----------------|
| | | °S | °E | Center | Range | (°) |
| | Mellish Reef | 17.45 | 155.86 | 50.4 | 50.6-50.0 | 32.8 |
| | Unnamed Seamount | 18.44 | 155.27 | 47.9 | 48.4-47.5 | 31.3 |
| | Unnamed Seamount | 19.70 | 156.29 | 43.2 | — | 29.4 |
| + | Kenn Reef | 21.30 | 155.73 | 40.5 | 41.0-39.7 | 26.9 |
| + | Bird Island | 22.24 | 155.30 | 37.4 | 38.0-37.0 | 25.3 |
| + | Cato Island | 23.32 | 155.54 | 34.3 | 35.0-34.3 | 23.7 |
| + | Recorder Guyot | 25.10 | 155.02 | 28.8 | 29.7-27.7 | 20.9 |
| + | Mareton Seamount | 26.02 | 155.03 | 26.6 | 27.0-26.2 | 19.6 |
| + | Brisbane Guyot | 26.80 | 155.15 | 25.2 | 25.4-25.1 | 18.5 |
| + | | 27.02 | 155.10 | 24.8 | 25.1-24.6 | 18.2 |
| + | Queensland Guyot | 27.54 | 155.09 | 23.8 | 24.0-23.6 | 17.5 |
| + | | 27.70 | 155.20 | 23.5 | 23.6-23.2 | 17.3 |
| + | Britania Guyots | 28.11 | 155.67 | 22.6 | 23.0-22.8 | 16.6 |
| + | | 28.34 | 155.65 | 22.2 | 22.8-21.9 | 16.3 |
| + | | 28.73 | 155.56 | 21.6 | 21.9-21.1 | 15.9 |
| + | Stradbroke Seamount | 29.13 | 155.80 | 20.8 | 20.9-20.4 | 15.3 |
| + | Derwent-Hunter Guyot | 30.62 | 156.16 | 18.1 | 18.2-17.5 | 13.3 |
| + | | 30.86 | 156.23 | 17.4 | 17.5-16.8 | 12.7 |
| + | Barcoo Bank | 32.60 | 156.25 | 14.2 | 14.5-13.8 | 10.4 |
| + | Taupo Bank | 32.96 | 156.17 | 13.5 | 13.6-13.3 | 9.9 |
| + | | 33.22 | 156.12 | 12.9 | 13.3-12.3 | 9.4 |
| + | Unnamed Seamount | 35.45 | 156.41 | 9.3 | 9.3- 8.8 | 6.8 |
| + | Gascoyne Guyot | 36.70 | 156.31 | 6.7 | 7.2- 6.2 | 4.9 |
| + | Unnamed Seamount | 40.42 | 156.75 | 0.3 | 0.4- 0.0 | 0.2 |

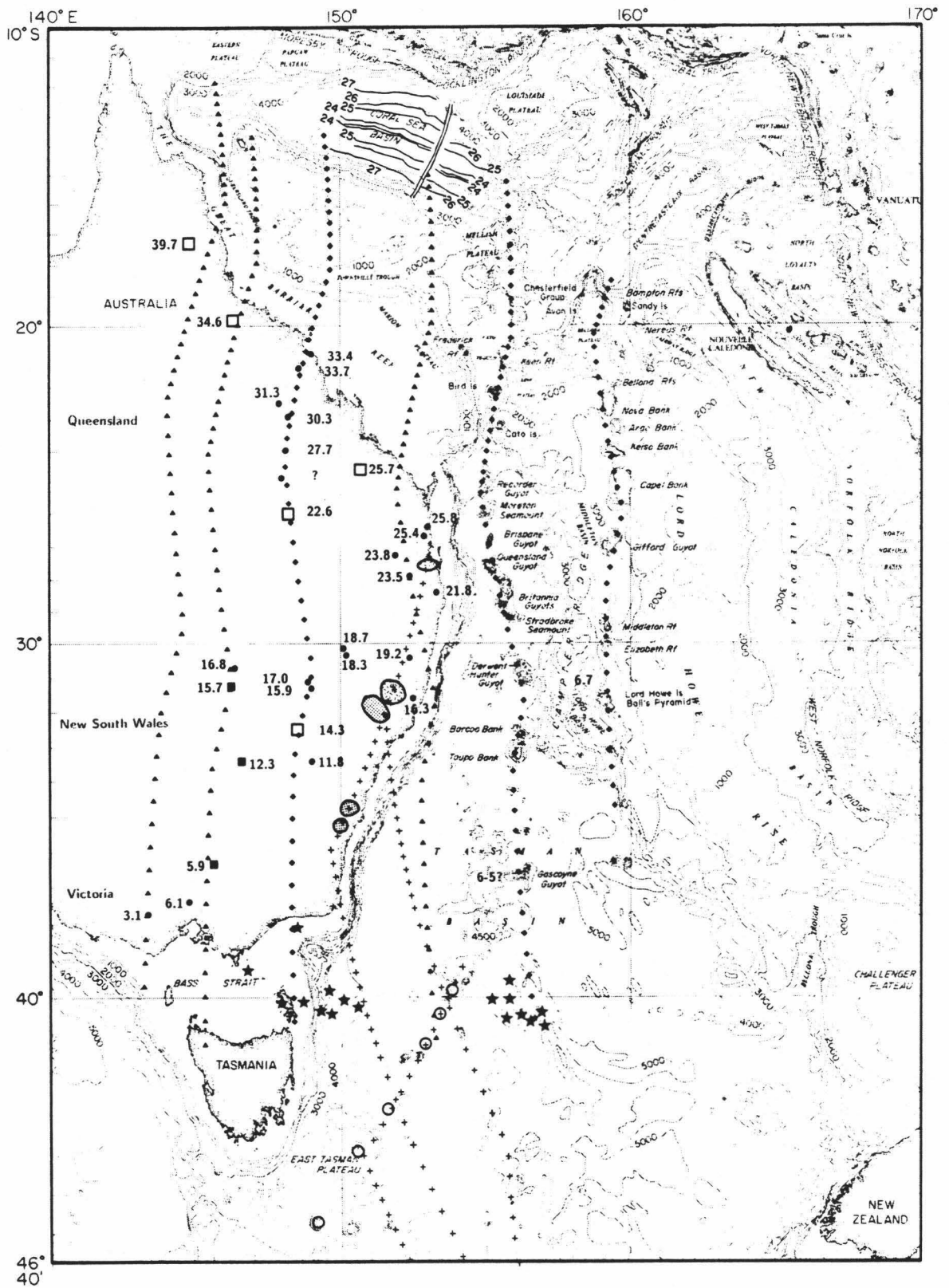
c. Predicted ages and angular distances measured from the predicted hotspot sources for the Geoid Anomaly chain based on preferred vectors of rotation.

| | Lat. °S | Long. °E | Predicted Ages (Ma)* Center | Angular Dist.* (°) |
|---|------------|-------------|--------------------------------|-----------------------|
| + | 39.77 | 153.83 | 53.3 | 37.9 |
| + | 40.39 | 153.38 | 51.7 | 36.9 |
| + | 41.17 | 152.89 | 49.7 | 35.5 |
| + | 42.84 | 151.59 | 45.0 | 32.4 |
| + | 43.85 | 150.57 | 42.6 | 30.8 |
| + | 45.63 | 149.18 | ? | — |

* Predicted age (Ma) and angular distance (°) are determined by projecting the locations of seamounts, volcanic centers and geoid anomalies along meridians onto the best parallels about the poles of rotation determined in this study. The age of the center of the seamount, cluster of volcanic centers, or geoid anomaly is given first, followed by the range in age over the length of the edifice, cluster of volcanic centers, or anomaly.

+ Volcanic features that were included as part of the input data used to determine the poles of absolute motion presented in Table 1.

Figure 7 Hotspot traces generated by summation of the preferred vectors of rotation for the past 55 Ma. Solid circles mark central volcanoes, solid squares mark high potassium provinces, open squares mark basaltic lava fields, and open circles mark locations of geoid anomalies interpreted to be caused by buried seamounts. The Ipswich Trail (coarsely dashed areas) and the Barrington Trail (finely dotted areas) are basaltic lava fields from Sutherland (1981). Diamonds and crosses mark locations of traces determined from the model. The diamonds show the locations of the traces for the Lord Howe Seamounts, Tasmantid Guyots, and the eastern Australian volcanic centers. The crosses mark the locations of the traces for the southeastern Australian basaltic lava fields (solid irregular areas) and the geoid anomaly chain (open circles) in the southwestern Tasman Sea. Triangles indicate the predicted traces for volcanic centers not used in constraining the model. The spacing between symbols for the reconstructed traces represents 1 Ma interval.



Sutherland, 1985), could be another possible explanation.

The 12-0 Ma time span is mostly constrained by the Lord Howe Seamounts (Fig. 8) comprising a total of six seamounts and islands. In contrast, the Tasmantid Guyots contain only three seamounts in this time span, the southernmost one being associated with seismicity and, although their positions agree well with the inferred hotspot trace for that time span, their relatively small number and uneven distribution precludes the detection of any change in plate motion within that time span. Likewise, three volcanic centers of possible hotspot origin (Figs. 2,7) are present in eastern Australia during this period (Wellman, 1983). These three volcanic centers do not exhibit any obvious alignment or age progression pattern, however, and thus do not appear to be associated with a single trail. In northern Queensland, the late Cenozoic basaltic lava fields also do not indicate any apparent age progression pattern (Stephenson et al., 1980). One of the volcanic centers associated with the obvious eastern Australian trail, the 11.8 Ma center, appears to be located close to a bend, i.e. where a predicted parallel congruent to the 12-0 Ma seamount trace intersects the parallel which best fits the volcanic centers to the north for the 16-12 Ma time span. This volcanic center thus provides the age control for the 12 Ma bend.

The 16-12 Ma trail segments are represented by the alignment of Gifford Guyot and an adjacent unnamed seamount in the Lord Howe Seamounts, and Barcoo and Taupo banks in the Tasmantid Guyots (Fig. 9). These edifices show a distinct subparallel SSE alignment that is different from seamounts to the north and south in both chains. The time and location of the 16 Ma bend are interpolated between the 28 Ma and 12 Ma bends by assuming constant rate of rotation from 28 to 12 Ma.

The 28-16 Ma trail segments are well constrained by four seamounts in the Lord Howe Seamounts and five seamounts in the Tasmantid Guyots (Fig. 9), that are evenly distributed over most of the length of each trail segment. In addition, the elongate shapes of Capel and Nova banks in the Lord Howe Seamounts and Derwent-Hunter Guyot in the Tasmantid Guyots also appear to be good indicators of the probable trend of plate motion during this time span. The Argo-Kelso banks in the Lord Howe Seamounts and the Queensland, Britannia, and Stradbroke guyots in the Tasmantid Guyots which were formed during the middle of this time span (about 22

Figure 8 Sections of oblique Mercator grids about the pole at $18.8^{\circ}S$, $148.3^{\circ}W$ (12-0 Ma) were superimposed on seamounts and volcanic centers within the 12-0 Ma time span. Grid spacing is 0.4° parallel by 1.0° meridian. The solid circles are central volcanoes, the solid squares are high potassium provinces, the open square is a basaltic lava field, the open circles are geoid anomalies, and the stars are earthquake epicenters.

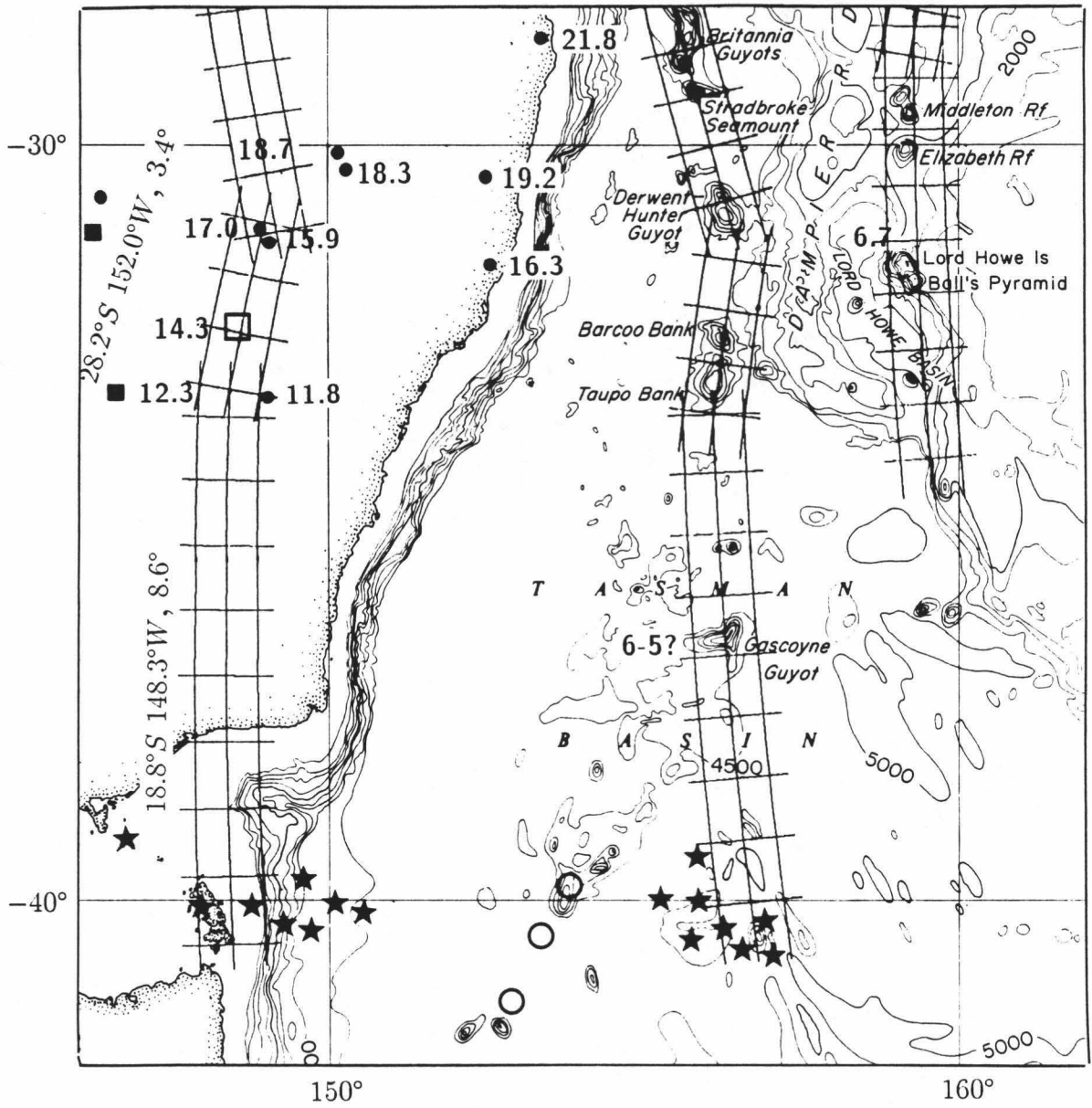
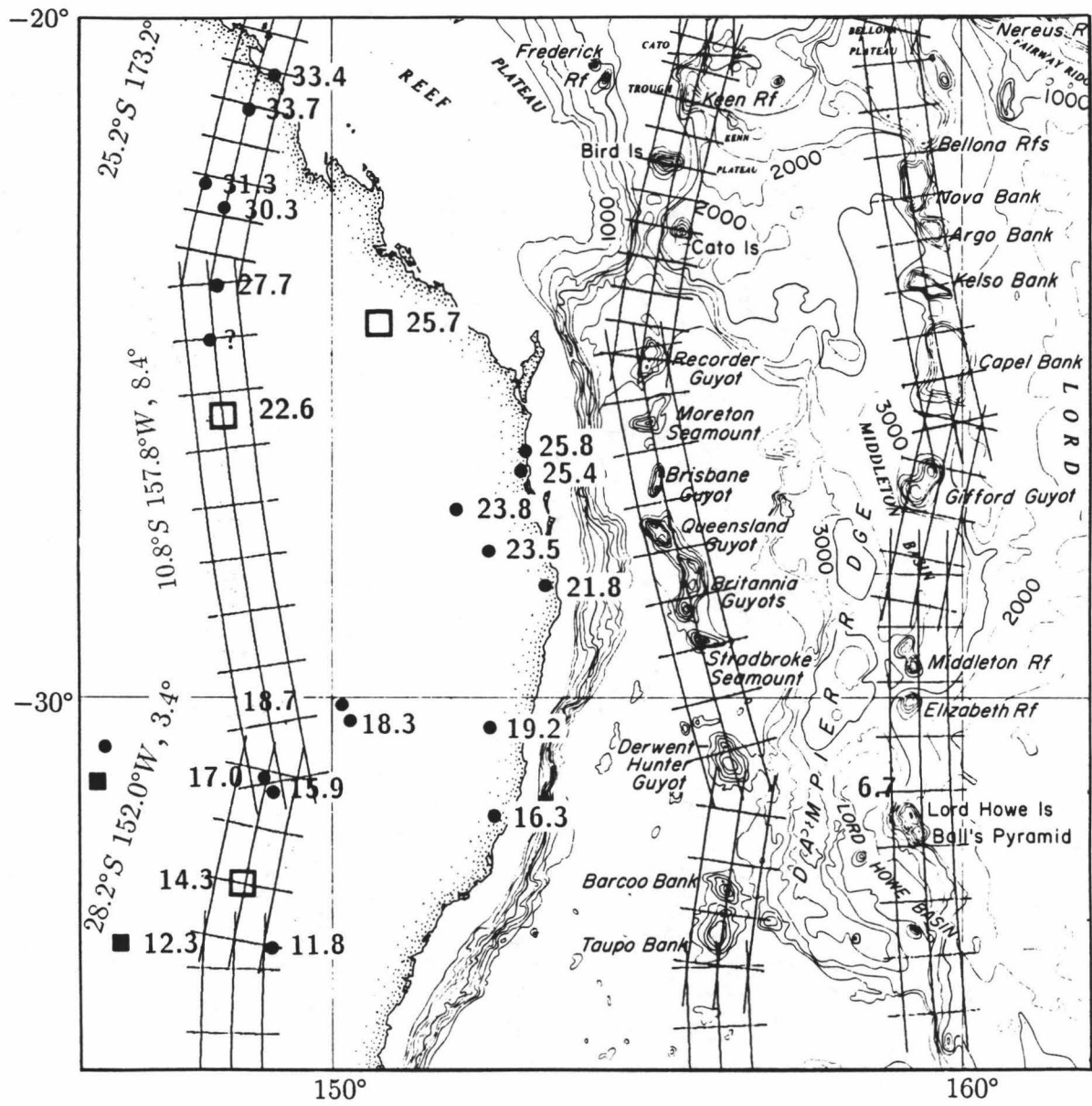


Figure 9 Sections of oblique Mercator grids about the poles at $28.2^{\circ}S$, $152.0^{\circ}W$ (16-12 Ma) and $10.8^{\circ}S$, $157.8^{\circ}W$ (28-16 Ma) are superimposed on seamounts and volcanic centers within the 16-12 Ma and 28-16 Ma time spans. Grid spacing is 0.4° parallel by 1.0° meridian. The solid circles are central volcanoes, the solid squares are high potassium provinces, and the open squares are basaltic lava fields.



Ma), have trends suggesting some perturbation in the plate motion. Nevertheless, a reasonable pole of rotation can be obtained that allows the best parallel of the preferred pole of rotation to pass through most of the shallowest points of the seamounts of both chains (Fig. 9).

In contrast to the Lord Howe Seamounts and Tasmantid Guyots, there are fewer continental hotspot-related volcanic centers for the 28-16 Ma time span along the single eastern Australian trail used to control this study (Fig. 9). One of the eastern Australian volcanic centers, the 27.7 Ma center, appears to be located close to a bend where the predicted parallel for the 28-16 Ma volcanic centers intersects the parallel which best fits the volcanic centers to the north for the 43-28 Ma time span. This volcanic center thus provides the age control for the 28 Ma bend. Most of the other eastern Australian volcanic centers within the 28-16 Ma time span appear to form a diffuse pattern along the coast and, for reason given earlier, were not used in determining the pole of rotation for this time span.

Although the rotation vectors determined for the three time spans between 28 Ma and the present satisfactorily account for the alignment of the Tasman Sea seamounts and most of the eastern Australian volcanic centers (within 0.4° of the hypothetical trace), there is still a possibility that a single rotation vector would be sufficient to describe the plate motion for the entire time period, with any variation in alignment being due to a small relative motion between hotspots. The relatively large number of Lord Howe Seamounts and Tasmantid Guyots and the close proximity of these two chains provide a unique opportunity to test whether these hotspots are indeed fixed. This fixity hypothesis can be verified by calculating a single pole of rotation based on the entire 28-0 Ma data set and by comparing departures in seamount locations from the best parallel about that pole as is discussed below.

The lack of a well defined symmetrical distribution pattern of these seamounts with respect to the best parallels would imply varying relative motion between the two hotspots. A systematic, non-parallel departure of seamount locations might imply a constant relative motion between these two hotspot sources. A systematic, parallel departure of seamount locations would imply changes in plate motion without relative hotspot motion and would require more than one pole of rotation to satisfactorily

describe the actual Indo-Australia Plate motion.

In Figure 10, parallels about the single best pole of rotation for the past 28 Ma are compared with the location of Tasman Sea seamount trails. Although most of the Lord Howe Seamounts and Tasmantid Guyots fall within one and a half degree swath of the two best fitting parallels about the pole of rotation, a small but systematic, parallel departure of the seamount locations with respect to the best small circles about the pole of rotation can be observed. This systematic, parallel departure supports a model of multiple, simple changes in plate motion and also supports the original assumption that these hotspots are fixed with respect to each other. In Figure 11, differences of seamount locations (distribution), in angular distance, from the best parallels about the best pole of rotation for the past 28 Ma are plotted against the angular distance of the seamounts from the hotspot sources. The systematic, roughly parallel distribution pattern also suggests that a series of simple changes in plate motion has occurred during the past 28 Ma with no significant relative motion between these hotspots.

The 43-28 Ma trail segments appear to be best represented by the Tasmantid Guyots (Fig. 12). Few edifices are recognizable, however, in the older part of this trail segment, and thus control for determining the pole of rotation for this time span depends heavily on guyots in the young part of this segment. The youngest part of the trail segments (34-28 Ma) are equally well represented by the alignment of the northern portion of the Bellona Plateau in the Lord Howe Seamounts and the alignment of Recorder Guyot in the Tasmantid Guyots (Fig. 12). The Bellona Plateau, located to the north of Nova Bank in the Lord Howe Seamounts, may mark the northern terminus of the Lord Howe Seamounts. A total of three points are chosen along the middle portion of the northern half of the Bellona Plateau, on the assumption that they may represent the average location of the hotspot trail.

Indeed, the alignment of the northern half of the Bellona Plateau sub-parallel the alignment of Recorder Guyot, Cato and Bird islands and Kenn Reef in the Tasmantid Guyots. The southern half of Bellona Plateau is too broad to indicate the location of any change in plate motion. The Bellona Reefs, the Avon Islands, the Chesterfield Group and the Bampton Reefs on the Bellona Plateau may simply indicate reef

Figure 10 Sections of oblique Mercator grids about the pole at $10.4^{\circ}S$, $139.8^{\circ}W$ (28-0 Ma) are superimposed on the Tasmantid Guyots and Lord Howe Seamounts. The dotted patterns indicate elements of symmetry. Grids spacing is 0.4° parallel by 1.0° meridian. The solid circles are central volcanoes, the open square is a basaltic lava field. Note the close correspondence in amount and direction of offset between the two seamount trails.

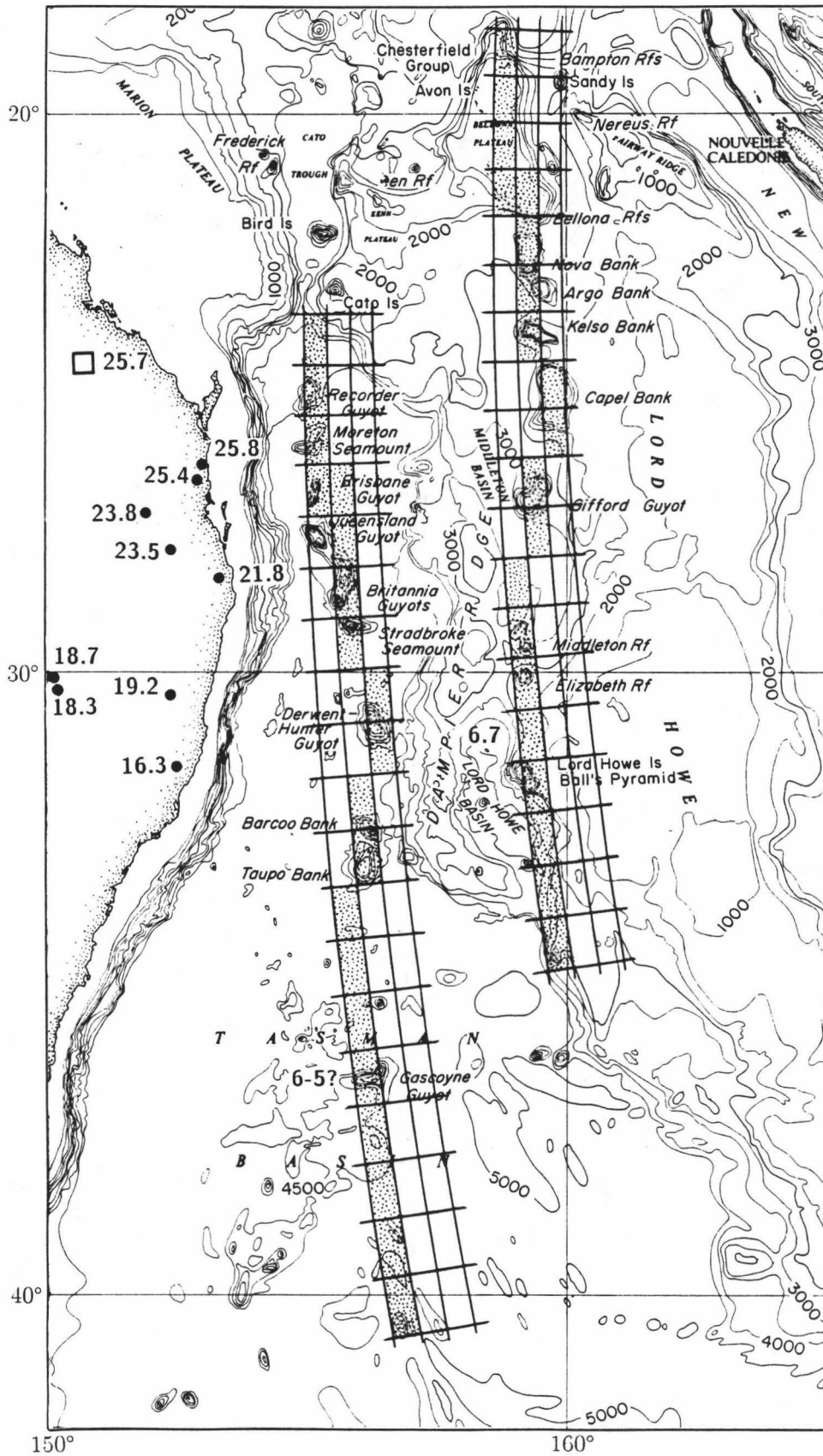


Figure 11 Seamount distribution plotted in terms of the seamount location from the best parallel versus the angular distance along the hotspot trail measured from the predicted hotspot source about a pole of rotation at $10.4^{\circ}S$, $139.8^{\circ}W$ for the past 28 Ma. The zero abscissa represents the best parallel about the 28-0 Ma pole of rotation. Open squares are the Lord Howe Seamounts, and solid squares are the Tasmanid Guyots, arrows show the approximate locations of bends (Ma) along the trails.

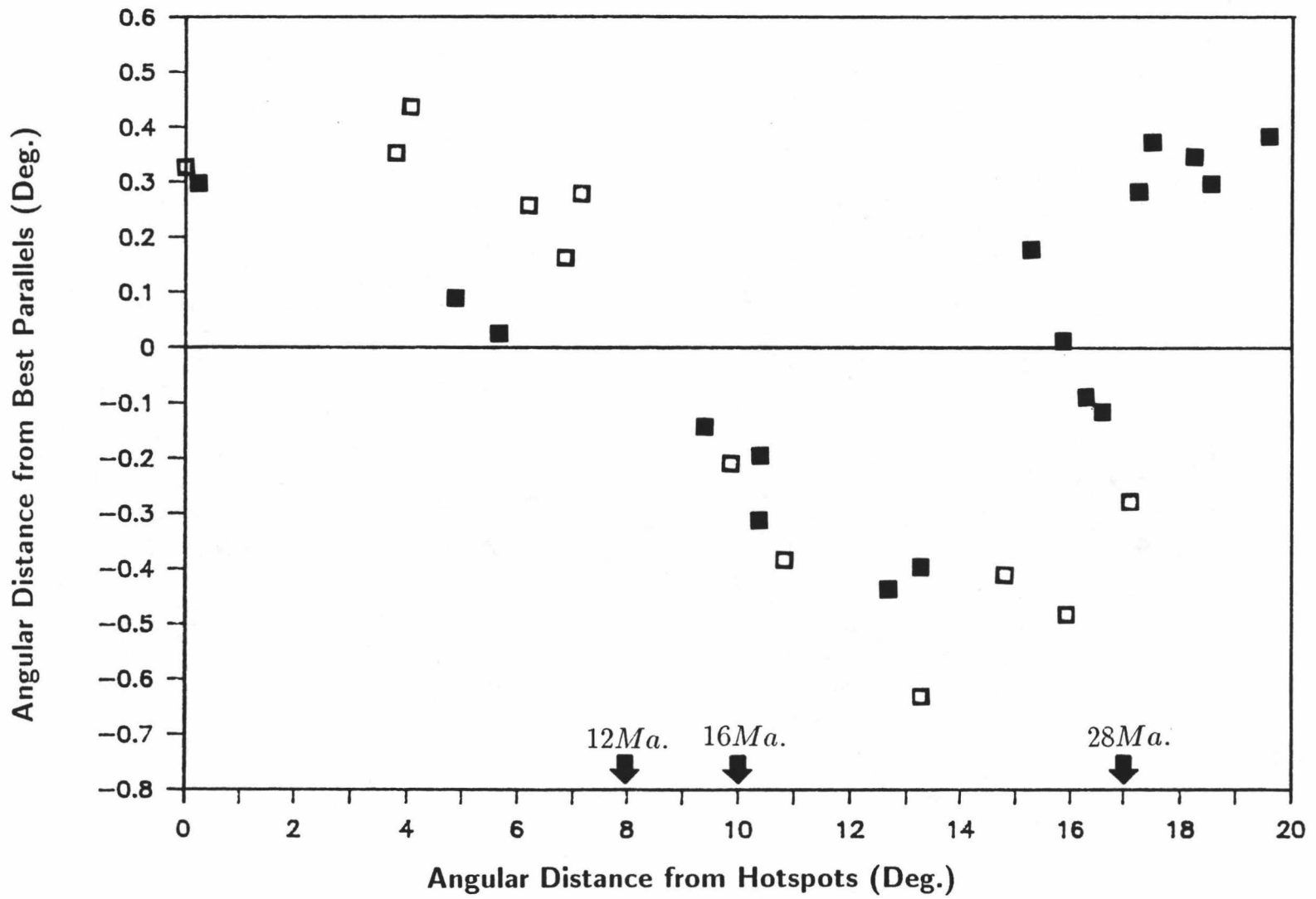
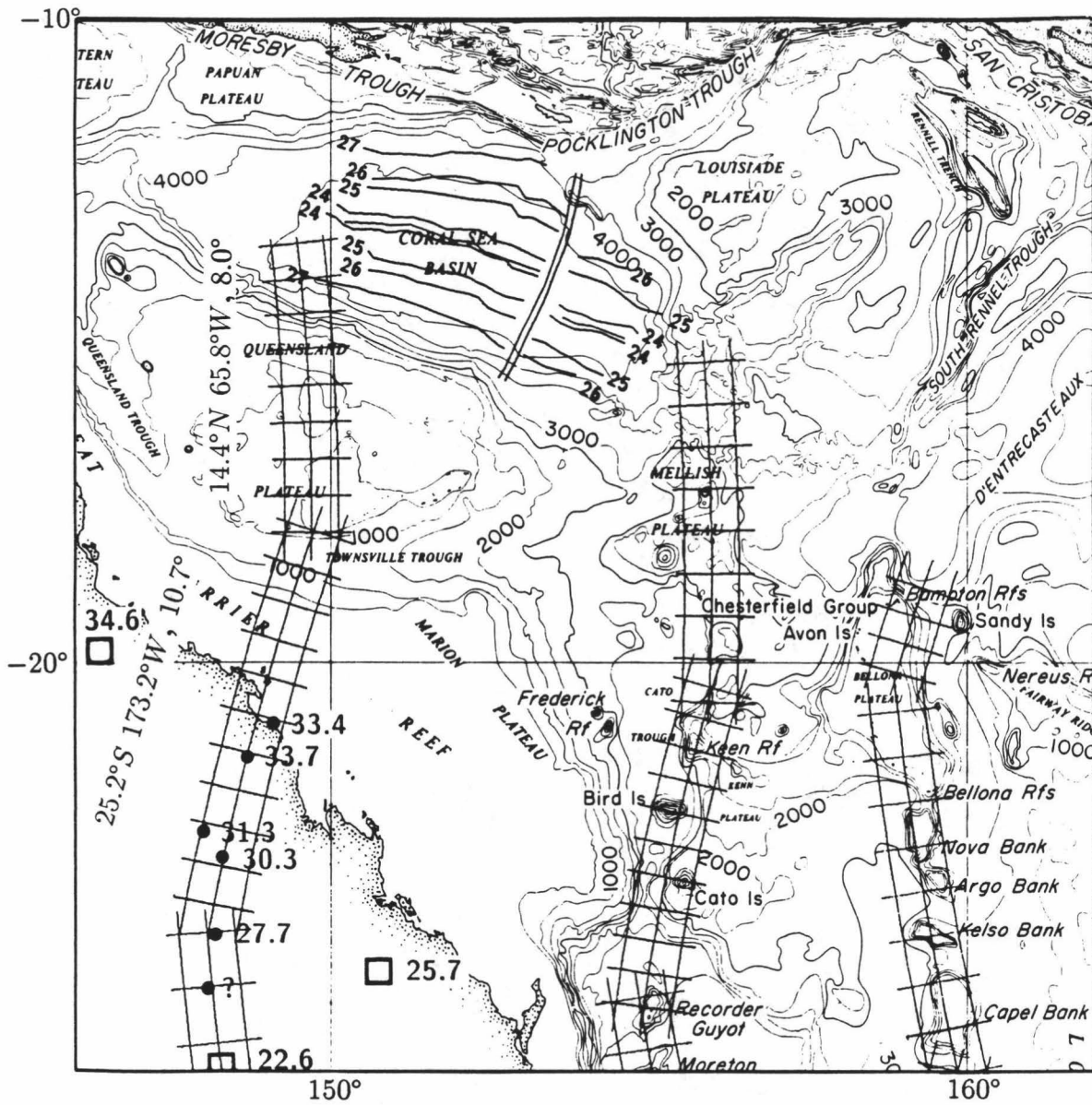


Figure 12 Sections of oblique Mercator grids about the poles at $25.2^{\circ} S, 173.2^{\circ} W$ (43-28 Ma) and $14.4^{\circ} N, 65.8^{\circ} W$ (55-43 Ma) are superimposed on seamounts and volcanic centers within the 43-28 Ma and 55-43 Ma time span. Grid spacing is 0.4° parallel by 1.0° meridian. The solid circles are central volcanoes and the open squares are basaltic lava fields.



buildup on the perimeter of the plateau and not the locus of the possible hotspot trail. Thus it is the change in alignment at the Recorder Guyot (Fig. 12) that appears to provide an indication of a change in plate motion and a suggestion of the trend of the new trajectory. The rate of rotation for the 43-28 Ma time span is based on the ages of four volcanic centers along longitude 148° near the northeastern coast of Australia (Fig. 12).

The pole of rotation for the 55-43 Ma time span, by necessity, must be based on the age groupings of the basaltic lava provinces in southeastern Australia as proposed by Sutherland (1981). However, neither the exact locations of the volcanic centers nor the age progression pattern for the 55-29 Ma time span (Figs. 4,13) are well defined. Moreover, because long durations of volcanism (up to 50 Ma) have been reported in some of these basaltic lava fields, only those within the time span of 55-29 Ma were included in the groupings (Sutherland, personal communication, 1987). Although a general SSW age progression (from older to younger) is indicated by the distribution pattern of basaltic lava fields, the exact locations of the eruptive centers are not known and thus the calculated rotation vector for this time span is not well constrained. Circular approximation, therefore, was used by Sutherland (1981) to outline the provinces and approximate the locations of the volcanic centers along the Barrington (55 to 40 Ma) and the Ipswich (58 to 30 Ma) trails (Fig. 4).

A better indication of the direction of plate motion during the 55-43 Ma time span may be obtained from the alignment of a chain of five small geoid anomalies (open circles in Figs. 13,14) in the southwestern Tasman Basin off the southeastern margin of Australia. Positions for the geoid anomalies were obtained from the SEASAT gravity map of Haxby (1987). The lack of correlation between the geoid anomalies and bathymetry (Fig. 14) is believed by the writer to result from inundation by sediment derived from the Australian continent. Thus, the geoid anomalies are interpreted herein to represent a partially buried linear chain of seamounts, similar to those believed to represent undetected seamounts elsewhere in the South Pacific area (Sandwell, 1984; Baudry et al., 1987). Furthermore, the 55-43 Ma pole of rotation, calculated from the southeastern Australian basaltic lava fields provides the only small circle arc segment that roughly parallels the alignment of the Tasman Sea

Figure 13 Sections of oblique Mercator grids about the pole at $2.85^{\circ}N$, $81.75^{\circ}W$ (the 55-43 Ma pole is determined without the inclusion of the chain of geoid anomalies in the southwestern Tasman Sea) are superimposed on the Ipswich Trail (coarsely dashed areas) and the Barrington Trail (finely dotted areas) basaltic lava fields (Sutherland, 1981). Grids spacing is 0.4° parallel by 1.0° meridian. The open circles are geoid anomalies (Haxby, 1987). Volcanic provinces are: Barrington (Br); Ipswich (Ip); Mittagong (Mg); Nerriga (Nr); Walcha (Wa).

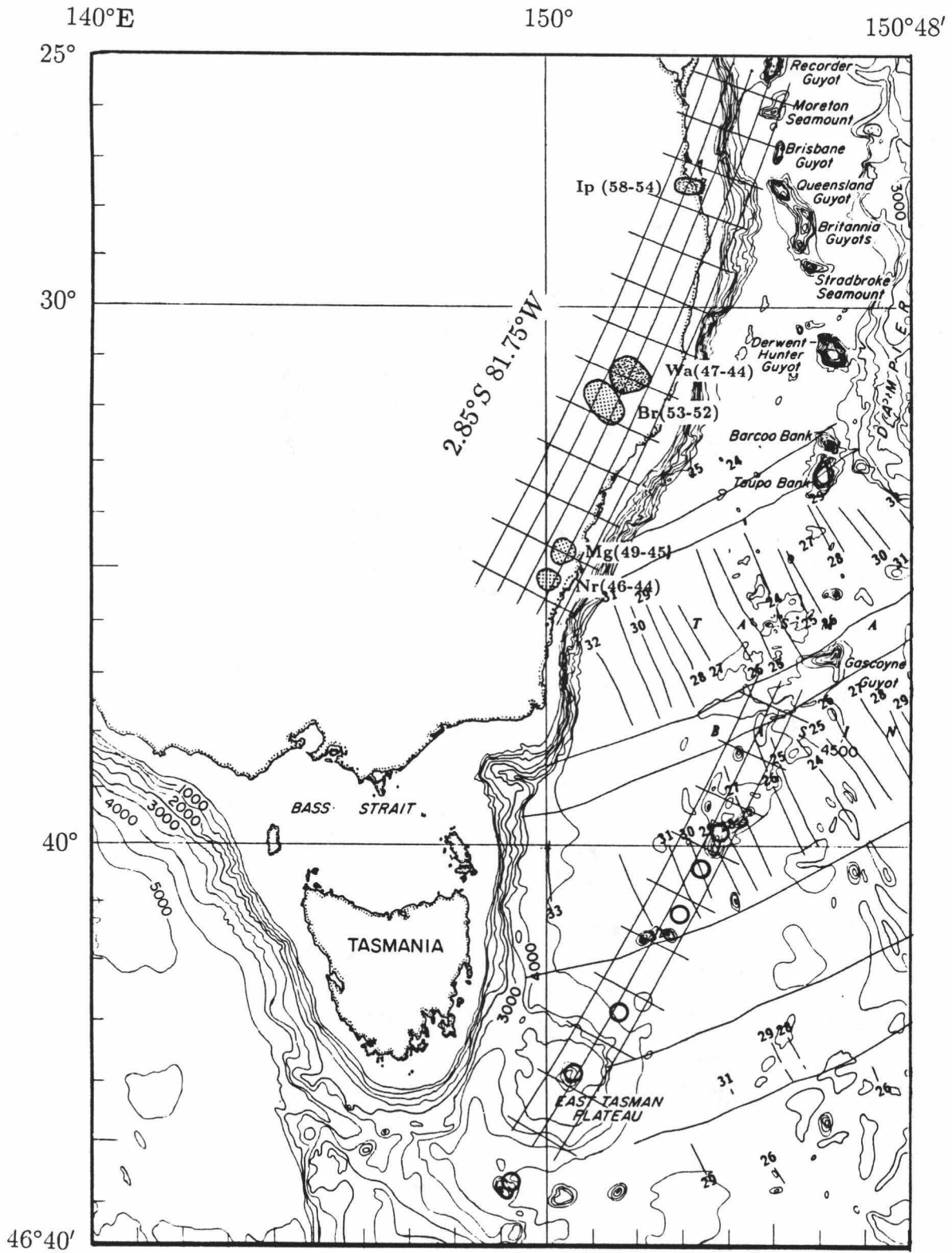


Figure 14 Sections of oblique Mercator grids at $14.4^{\circ}N$, $65.8^{\circ}W$ (the 55-43 Ma pole of rotation determined with the inclusion of the chain of geoid anomalies in the southwestern Tasman Sea) are superimposed on the Ipswich Trail (coarsely dashed areas) and the Barrington Trail (finely dotted areas) basaltic lava fields (Sutherland, 1981). Grids spacing is 0.4° parallel by 1.0° meridian. The open circles are geoid anomalies (Haxby, 1987). The volcanic provinces are: Barrington (Br); Ipswich (Ip); Mittagong (Mg); Nerriga (Nr); Walcha (Wa).

geoid anomaly chain.

Because of this singular agreement between the trail of geoid anomalies and the parallels about the 55-43 Ma pole (Fig. 13), and in view of the age of Tasman Basin seafloor (Hayes and Ringis, 1973; Weissel and Hayes, 1977; Shaw, 1979) where the youngest magnetic anomaly which has been identified is 24 (55 Ma, Kent and Gradstein, 1986), the linear chain of geoid anomaly is interpreted to be caused by a chain of seamounts formed at a hotspot on the Indo-Australia Plate during the 55-43 Ma time span. Thus, a total of three hotspot trails are recognized as forming during the 55-43 Ma time span: the Ipswich and Barrington trails starting at about $27^{\circ}S$ and $32^{\circ}S$ and the chain of geoid anomaly starting at about $40^{\circ}S$. A new pole of rotation, therefore, has been determined from the alignment of both the geoid anomaly chain and the two trails of southeastern Australian basaltic lava fields (Fig. 14). The rate of Indo-Australia Plate rotation for this time span (about $0.7^{\circ}/Ma$, Table 1), calculated from the five southeastern Australian basaltic lava fields is close to the calculated rates of rotation for the other time spans. The large difference in locations between the poles of rotation for the 55-43 Ma time span and those for the four time spans from 43-0 Ma (Fig. 6) also supports the assumption that a major change in Indo-Australia Plate motion occurred about 43 Ma.

Although some uncertainty in the determination of the new pole of rotation remains, the new pole, based on both the trails of basaltic lava fields and the chain of geoid anomalies (Fig. 14), provides as good a fit to the trends and age progression patterns of the basaltic lava fields as that based solely on the basaltic lava fields (Fig. 13). Moreover, using the new pole of rotation, the projected Tasmantid Guyot and the eastern Australian volcanic center traces begin north of the southern boundary of the Coral Sea Basin (Fig. 7) at about 55 Ma, the approximate age for cessation of spreading in the basin between anomalies 23 and 24 (Weissel and Watts, 1979).

There are some isolated dated volcanic centers that might be part of other hotspot trails (indicated in Figs. 2,7) but which were not used in determining the rotation vectors. The possible hotspot origin of these volcanic centers was tested by aligning the younger end of a predicted trace of appropriate age on each of the isolated volcanic centers and checking the agreement with the ages of the volcanic centers

intersected at the older end of the trace. Close agreement between predicted and observed radiometric ages of the volcanic centers at the far ends of these traces would indicate that these volcanic centers were of hotspot origin and would also test the validity of the model.

In all, there are twenty-three volcanic centers scattered along eastern Australia that were not used in determining Indo-Australian rotation rates (Fig. 7). Ten of these are located along the eastern margin of the Australian continent, seven east of $151^{\circ}E$ and three between $150^{\circ}E$ and $151^{\circ}E$. The seven volcanic centers east of $151^{\circ}E$ appear to have been formed along a separate hotspot trace. The hotspot which formed this trace, if still active, would be located today at $41.0^{\circ}E, 153.3^{\circ}E$. Five volcanic centers located along longitude $148^{\circ}E$ appear to belong to the $148^{\circ}E$ trail. The three centers between $150^{\circ}E$ and $151^{\circ}E$ have ages that fall within the 28-16 Ma time span of that trace and thus may be part of the same trace. Of the eight remaining volcanic centers, located west of $148^{\circ}E$, five may form a trace along $145^{\circ}E$ and three may form another trace along $143^{\circ}E$. The predicted age of the basaltic lava field at about $20^{\circ}S$, obtained by assigning it to the $143^{\circ}E$ trace, is in good agreement with the radiometric age for that field and is thus treated as part of that trace. It is noteworthy that the predicted ages of all of these volcanic centers differ at most by 2.4 Ma from their radiometric ages (Table 4). The remarkably good agreement between all of the predicted and radiometric ages along the newly identified traces further attests to the validity of the model.

Linear regression was performed between the predicted ages and the radiometric ages for the twenty-eight dated Australian volcanic centers (Table 4) and the two dated Tasman Sea seamounts in order to test the Indo-Australia Plate motion model for the last 43 Ma. Six out of the thirty volcanic centers and seamounts were used to constrain the rotation rate of the model, i.e. the predicted ages for the volcanic centers were controlled by the ages of the two volcanic centers near the 28 and 12 Ma bends and the four volcanic centers along $148^{\circ}E$ older than 28 Ma. Linear regression between the predicted ages and the radiometric ages (Table 4) for the 30 volcanic centers and seamounts yields the following relationship:

Table 4

A comparison of predicted ages with radiometric ages for dated seamounts in the Tasman Sea and volcanic centers in eastern Australia.

a. Summary of locations and ages of volcanic centers that were used as age control in this study.

| | Volcanic Province | Lat. | Long. | Radiometric Age | | Predicted | Residual | Rock Type* | Ref.** |
|---|-------------------|------|-------|-----------------|-------------|-----------|-----------|------------|--------|
| | | °S | °E | Ave. Ma | Range Ma | Age Ma | Age Ma | | |
| + | Hillsborough | 20.9 | 149.0 | 33.4 | 34.1-31.3 | 35.8 | -2.4 | a | 3 |
| + | Nebo | 21.4 | 148.6 | 33.7 | 35.1-28.4 | 34.4 | -0.7 | a | 3 |
| + | Clermont N | 22.5 | 147.9 | 31.3 | | 31.4 | -0.1 | a | 3 |
| + | Clermont S | 22.9 | 148.2 | 30.3 | 35.2-27.4 | 30.6 | -0.3 | a | 3 |
| + | Springsure | 24.0 | 148.1 | 27.7 | 33.6-23.9 | 27.7 | | a | 3 |
| | Orange | 33.4 | 149.0 | 11.8 | 13.0-11.2 | 11.8 | | a | 3 |

b. Summary of locations and ages of volcanic centers and seamounts that were not used as age control in this study.

| | Volcanic Province | Lat. | Long. | Radiometric Age | | Predicted | Residual | Rock Type* | Ref.** |
|---|-------------------|-------|--------|-----------------|-------------|-----------|-----------|------------|--------|
| | | °S | °E | Ave. Ma | Range Ma | Age Ma | Age Ma | | |
| | Lord Howe I. | 31.5 | 159.0 | 6.9 | | 5.7 | 1.2 | d | 2 |
| | Gascoygne | 36.6 | 156.3 | 6-5? | | 6.7 | -1.2 | d | 4 |
| | Unnamed | 17.3 | 144.8 | 39.7 | | 38.9 | 0.8 | c | 3 |
| | Unnamed | 19.8 | 146.3 | 34.6 | | 34.6 | 0.0 | c | 3 |
| | Unnamed | 24.6 | 150.7 | 25.7 | | 26.4 | -0.7 | c | 3 |
| + | Blackland | 24.85 | 148.0 | ? | | 26.4 | | a | 1 |
| + | Unnamed | 26.0 | 148.2 | 22.6 | | 24.5 | -1.9 | c | 3 |
| | Mt. Cooroy | 26.4 | 153.0 | 25.8 | | 25.7 | 0.1 | a | 4 |
| + | Glass House | 26.7 | 152.9 | 25.4 | 27.3-25.2 | 25.2 | 0.2 | a | 3 |
| | Toowoomba | 27.3 | 151.9 | 23.8 | | 24.4 | -0.6 | a | 3 |
| | Main Range | 27.9 | 152.4 | 23.5 | 27.2-22.6 | 23.2 | 0.3 | a | 3 |
| + | Tweed | 28.4 | 153.3 | 21.8 | | 22.3 | -0.5 | a | 3 |
| | Nandewar N | 30.1 | 150.1 | 18.7 | 21.0-17.4 | 17.2 | 1.5 | a | 3 |
| | Nandewar S | 30.3 | 150.2 | 18.3 | | 16.8 | 1.5 | a | 3 |
| | Ebor | 30.4 | 152.4 | 19.2 | | 18.9 | 0.3 | a | 3 |
| | Unnamed | 30.68 | 146.35 | 16.8 | | 16.9 | -0.1 | b | 5 |
| + | Warrumbungle N | 31.1 | 148.9 | 17.0 | | 15.7 | 1.3 | a | 3 |
| + | Warrumbungle C | 31.3 | 149.0 | 15.9 | 17.1-13.6 | 15.4 | 0.5 | a | 3 |
| | Unnamed | 31.2 | 146.2 | 15.7 | 12.2/15.7 | 16.7 | -1.0 | b | 3,5 |
| | Comboyne | 31.6 | 152.5 | 16.3 | 16.4-16.1 | 16.3 | 0.0 | a | 3 |
| + | Unnamed | 32.5 | 148.5 | 14.3 | | 13.2 | 1.1 | a,c | 3 |
| | Unnamed | 33.4 | 146.6 | 12.3 | 10.4-14.8 | 12.7 | -0.4 | b | 3 |
| | Unnamed | 36.3 | 145.6 | 5.9 | | 7.8 | -1.9 | b | 3,4 |
| | Macedon | 37.35 | 144.7 | 6.1 | | 6.1 | 0.0 | a | 1,4 |
| | Unnamed | 37.7 | 143.3 | 3.1 | 0.6-7.0 | 3.1 | 0.0 | a | 3 |

* Volcanic features that were cited in the above references: a. central volcano provinces; b. high potassium provinces; c. basaltic lava fields; d. oceanic islands or seamounts.

** Age data are compiled from the literatures cited in the following references: 1. Wellman and McDougall, 1974; 2. McDougall et al., 1981, 3. Wellman, 1983, 4. Sutherland, 1983, 5. Sutherland, 1985.

+ Volcanic features that were included as part of the input data used to determine the poles of absolute motion presented in Table 1.

$$\text{Age (Ma)} = -0.050 + 1.0075 (\pm 0.019)(x \text{ Ma})$$

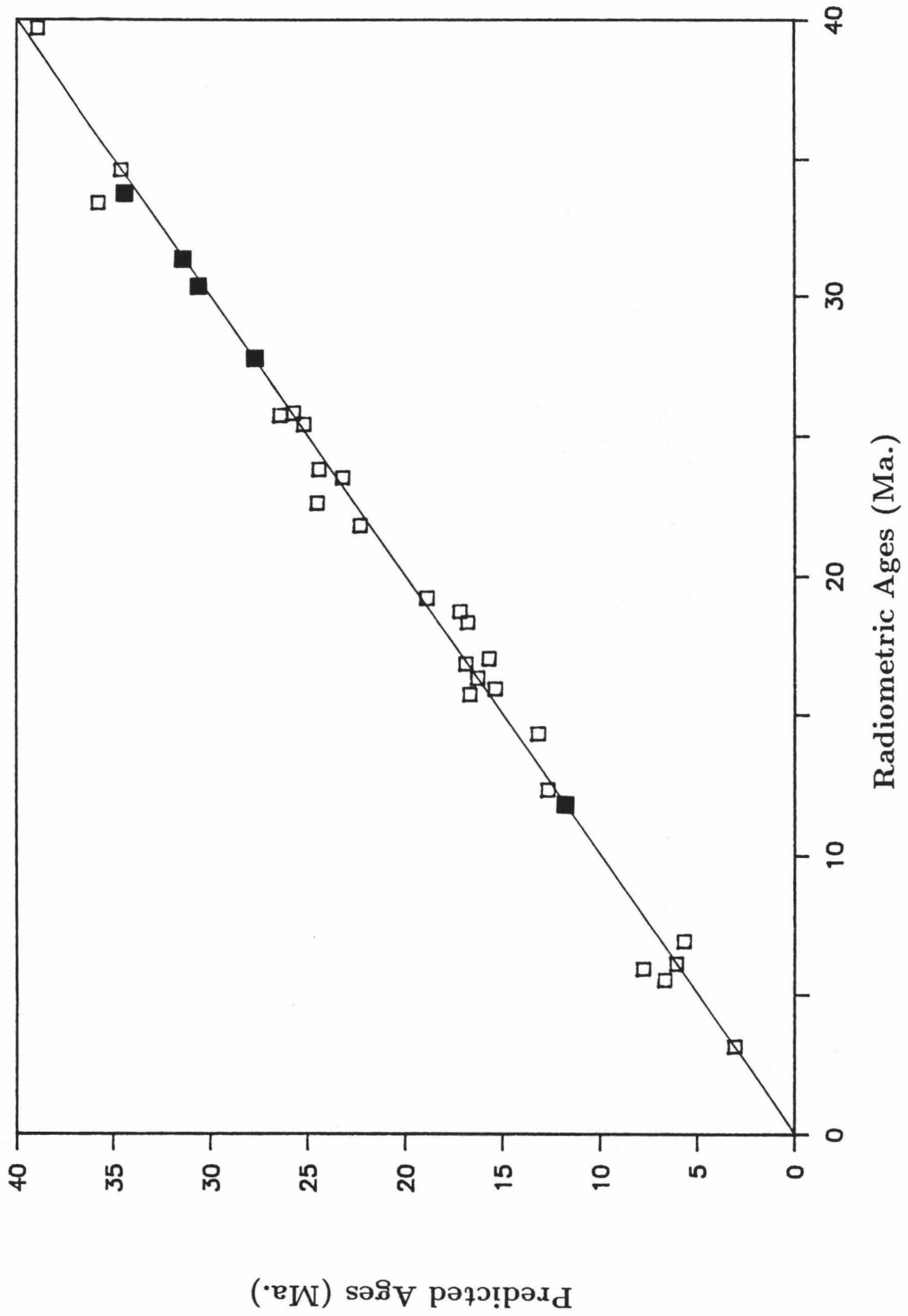
where x is the radiometric determined age.

The standard error of the predicted ages is 0.978 Ma which is within the uncertainty in the mean ages for the volcanic centers of 0.5 to 1.0 Ma (Wellman and McDougall, 1974). The correlation coefficient for the regression is 0.995. A plot of the predicted versus the radiometric ages is shown in Figure 15. The high degree of correlation between the predicted ages and the radiometric ages supports the proposed model.

An independent test of the newly determined Indo-Australia Plate motion vectors relative to the hotspot frame of reference, for the past 55 Ma, can be made by comparing the Indo-Australian APW path predicted from the hotspot model with that determined by paleomagnetic methods. The predicted path, derived by assigning an Indo-Australian hotspot source to the south pole and assuming the geomagnetic and the geographic poles were coincident through time, is shown in Figure 16 together with the APW paths obtained by the various paleomagnetic methods discussed below.

McElhinny et al. (1974) obtained a set of five paleomagnetic poles from 357 basaltic volcanic rocks with K-Ar ages from 60-0 Ma from eastern Australia. These poles trace a "distinct zigzag pattern about longitude 120° with a westerly excursion around 30 Ma and a knee around 18 Ma". Embleton and McElhinny (1982) constructed a Tertiary APW path from a filtered analysis of Australian weathered laterite profiles. The resultant virtual geomagnetic poles likewise trace a zigzag pattern close to longitude $120^\circ E$, which was also chosen as the reference meridian. The choice of $120^\circ E$ as the reference meridian, however, was not critical in determining the resultant smooth curve according to Embleton and McElhinny. In a study of the late Mesozoic and Cenozoic sedimentary sequences by Idnurm (1985), it was found that the sediment derived Australian APW path differed from the basalt-derived path of McElhinny et al. (1974) by "the absence of a large westward excursion and zigzag irregularities", "a substantially straight Cenozoic trajectory", and "a non-uniform rate". Although the data showed a more-or-less co-linear APW path along longitude $120^\circ E$ within the confidence ellipses, a zigzag pattern remains a distinct possibility

Figure 15 A comparison of the predicted versus the radiometric ages (in Ma) for eastern Australian volcanic centers. Solid squares are dated volcanic centers used to constrain the rotation rate for the model, and open squares are dated volcanic centers not used to constrain rotation rate for the model.



and, indeed, could be present based on Idnurm's actual paleomagnetic poles locations. Thus these studies all seem to indicate a more-or-less zigzag, southward APW path aligned along longitude $120^{\circ}E$ during the past 43 Ma and, based on the late Mesozoic-Cenozoic sedimentary sequences, a predominately westward path prior to 43 Ma.

The predicted APW path derived from this study (Fig. 16) also shows a slightly zigzag, southward path along longitude $120^{\circ}E$ during the past 43 Ma and a distinctly westward path from 55 to 43 Ma. The small differences between the pole positions derived from the hotspot model and those derived by Idnurm (1985) fall within the uncertainties in the paleomagnetic pole locations. Furthermore, the incorporation of non-dipole components in the Australian paleomagnetic data, which suggests a significant change in Indo-Australia Plate motion between 26 and about 60 Ma after dipole correction (Idnurm, 1986), does not seem necessary. Thus it is concluded that the Indo-Australia Plate rotation vectors determined from the hotspot model are reliable and produce an APW path comparable to those from paleomagnetic studies for the past 55 Ma. This agreement between the Australian APW paths determined from the hotspot model and the paleomagnetic studies also supports the conclusion of Livermore et al., 1984 that there has been little true polar wander during Cenozoic.

The newly determined Indo-Australian rotation vectors were also used to predict the Cenozoic Antarctic APW path by taking into account the divergent motion across the Southeast Indian Ridge (Weissel and Hayes, 1972; Weissel et al., 1977; Konig, 1987; Cande and Mutter, 1982) through the method of vector summation. Because there are two different models for the initial opening of the Southeast Indian Ridge, however, based on two different interpretations of the magnetic anomalies older than anomaly 18 (Table 5), two sets of Cenozoic APW paths have been generated (Fig. 17). The first model, proposed by Weissel and Hayes (1972) and Weissel et al. (1977) suggests a relatively rapid initial phase of opening for the Southeast Indian Ridge from anomalies 24 to 18 (55 to 43 Ma, Kent and Gradstein, 1986). In contrast, the second model proposed by Cande and Mutter (1982), suggests a relatively slow initial phase of opening for the Southeast Indian Ridge from anomaly 33 to 18 (76 to 43 Ma.) The two Antarctic APW paths, predicted by the above models, both show a very small Cenozoic Antarctica Plate motion relative to the geographic South Pole

Figure 16 A comparison of the Australian Apparent Polar Wandering (APW) path predicted by the hotspot model, with APW paths determined by other geophysical studies. The open circles trace the APW path for Australia (in 1 Ma increment) determined by summing the preferred Indo-Australian vectors of rotation (this paper). The double open circles show bend times determined in this study. The solid squares mark the APW path determined from Australian Cenozoic volcanic rocks (McElhinny, et al., 1974). The solid circles mark the filtered APW path determined from the magnetic properties of laterites and weathered profiles in Australia (Embleton and McElhinny, 1982). The stars mark the APW path determined from Australian sedimentary sequences (OP is the mean of five overprinted magnetization poles from south-eastern Australia [Schmidt and Embleton, 1981]; K1 is the Otway Group pole [Idnum, 1985]).

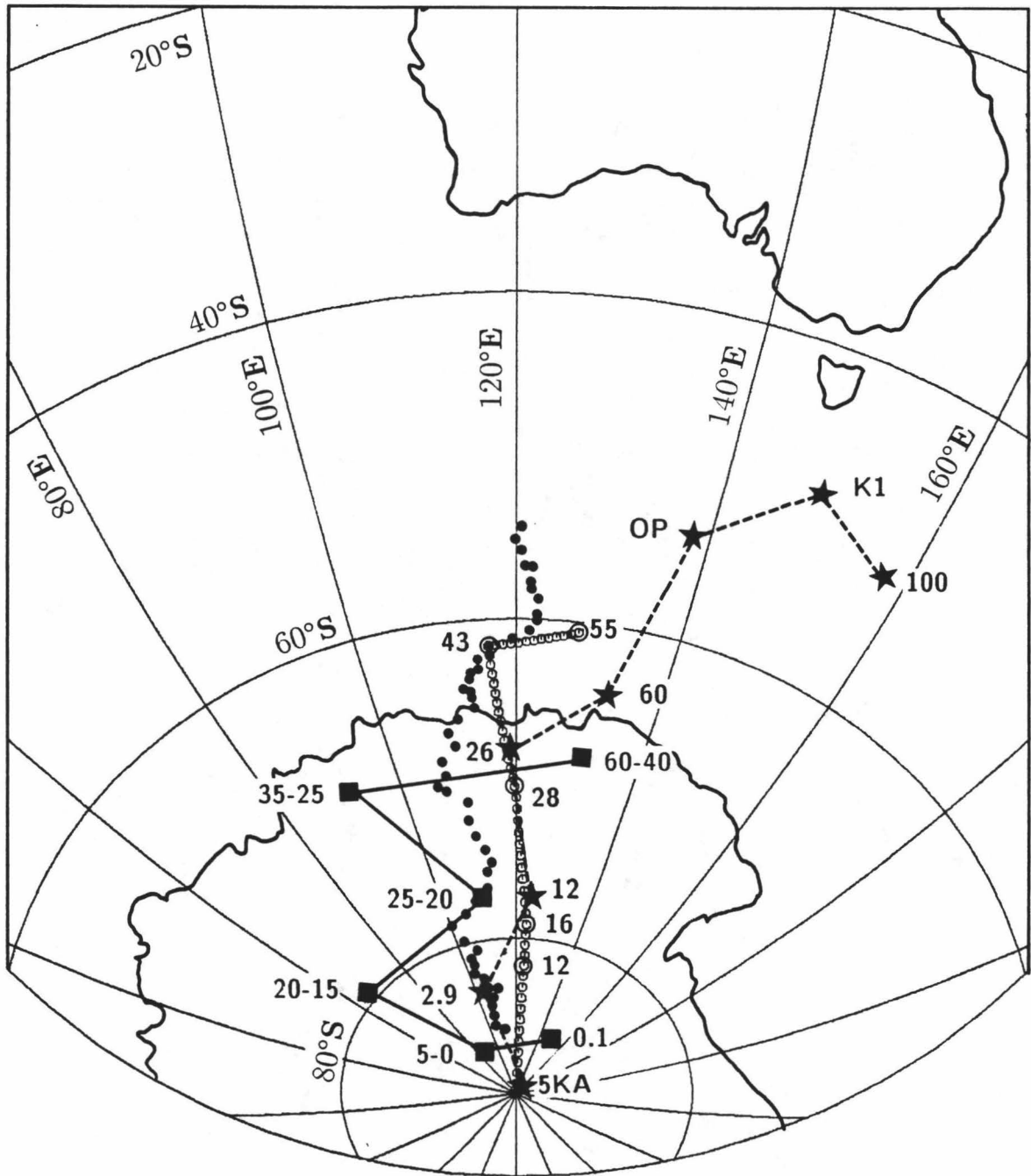


Table 5
Poles of opening for the Southeast Indian Ridge

a. Parameters for finite rotations of Australia relative to Antarctica determined by Weissel et al. (1977) based on the magnetic anomaly identification of Weissel and Hayes (1972) after anomaly 18 (43 Ma).

| Anomaly no. | Time | Pole Location | | Rotation Angle |
|-------------|------|---------------|------------|----------------|
| | Ma | Lat. (°N) | Long. (°E) | (°) |
| 5 | 9.6 | 9.7 | 36.5 | 06.75 |
| 6 | 19.9 | 13.8 | 34.6 | 12.0 |
| 8 | 27.8 | 14.25 | 33.25 | 16.0 |
| 12 | 33.8 | 12.5 | 34.4 | 18.9 |
| 13 | 37.0 | 11.9 | 34.4 | 20.5 |
| 18 | 42.3 | 10.3 | 34.75 | 23.6 |

b. Parameters for finite rotations of Australia relative to Antarctica determined by König (1987) based on the magnetic anomaly identification of Cande and Mutter (1982) and Weissel et al. (1977) prior to anomaly 18 (43 Ma).

| Anomaly No.** | | Time*** | | Pole Location | | Rotation Angle |
|----------------------|----|---------|-----------|---------------|-----------|----------------|
| | | Ma | | Lat.(°N) | Long.(°E) | (°) |
| A | B | A | B | | | |
| 20 | 19 | ~45.5 | 43.8 | 13.0 | 31.5 | 24.10 |
| 21-24 | 20 | ~52 | 45.5 | 9.0 | 32.3 | 24.68 |
| 27-31 | * | ~66 | 46.5-48.5 | 5.0 | 34.5 | 25.55 |
| 32-33 | 21 | ~76 | 49.5 | 5.0 | 34.5 | 26.37 |
| Pre-final Separation | | >80 | >50.5 | 5.0 | 34.5 | 26.6 |
| 34 | 22 | 84 | 52 | 1.5 | 37.0 | 27.58 |
| Reconstruction | | >94 | >54 | 1.5 | 37.0 | 30.05 |

** Anomaly identifications in column A after Cande and Mutter (1982). Anomaly identifications in column B after Weissel and Hayes (1972).

*** Time in column A pertains to anomaly identifications of Cande and Mutter (1982). Time in column B pertains to anomaly identifications of Weissel and Hayes (1972).

Figure 17 Predicted Antarctic APW paths from 52 Ma to the present obtained by vector summation of the Indo-Australia Plate motions determined in this study and the poles of opening for the Southeast Indian Ridge. The open circles mark the predicted Antarctic APW path based on the anomaly identifications of Weissel and Hayes (1972). The crosses mark the predicted Antarctic APW path based on the anomaly identifications of Cande and Mutter (1982) which differs from that of Weissel and Hayes (1972) only prior to 43 Ma. The poles of opening for the Southeast Indian Ridge for both paths were determined by Weissel et al. (1977) from anomaly 18 (43 Ma) to the present and Konig (1987) prior to anomaly 18 (43 Ma). Arrows point to locations of corresponding times of changes in Indo-Australia Plate motion. The spacing between symbols for the predicted traces represents 1 Ma interval.

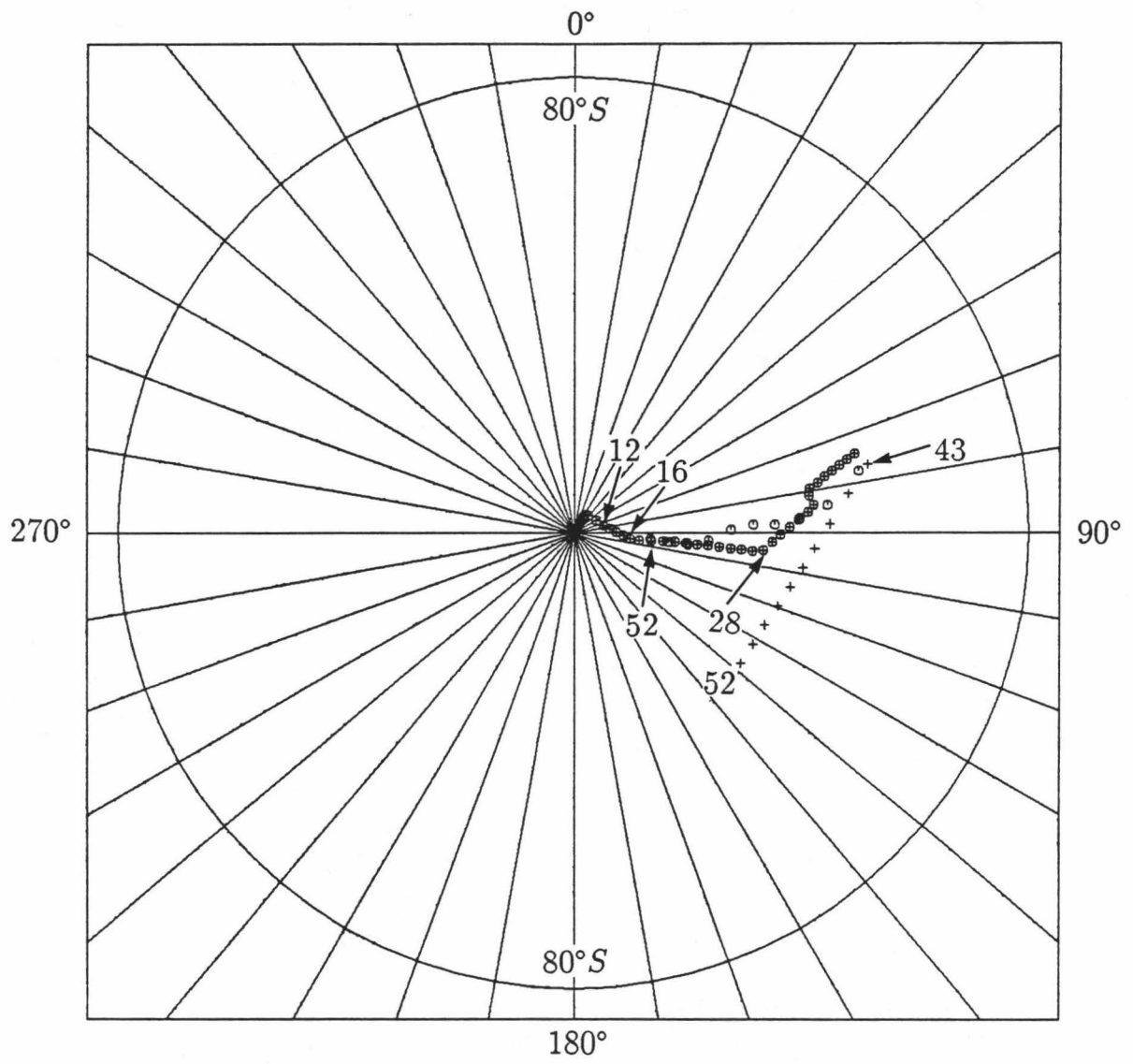


(Fig. 17). APW paths determined from Antarctic paleomagnetic data (Briden et al., 1981; Watts et al., 1984; Idnurm, 1986) also suggest a small amount of Antarctica Plate motion relative to the South Pole. Because of the APW paths from different data sets are associated with large confidence ellipses clustered around the South Pole, it is difficult to favor one model over the other.

V. DISCUSSION

Based on a study of basaltic lava fields in southeast Australia, Sutherland (1981) extended the time span of the Australian Cenozoic volcanism beyond 34 Ma. He projected hotspot trails back to the Coral Sea Basin-Louisiade Plateau (Sutherland, 1981, 1983) and the South Rennel Trough (Sutherland, 1985) spreading structures and speculated that the hotspot trails originated with the initiation of spreading along these structures. Kroenke (1986) proposed a model for the Australia Plate motion based on the alignment of seamount chains in the Tasman Sea and the eastern Australian volcanic centers. He also extrapolated the hotspot trails into the Coral Sea and d'Entrecasteaux basins and speculated that the hotspot trails originated with the cessation of spreading in these basins. Although these correlations are conjectural at best, there is some evidence based on this study, albeit tenuous, favoring correlation of the origin of these hotspot trails with the cessation of spreading in the basins.

From the more-or-less east-west lines of coeval volcanic activity, based on the ages and locations of the Tasmantid Guyots and the eastern Australian volcanic centers alone, a hotline model could be inferred in similar fashion to that proposed by Sutherland (1981, 1983). In order to align the origins of the trails along the southern edge of the Coral Sea Basin however, as proposed by Sutherland (1981, 1983) to occur at the beginning of spreading (anomaly 27, Shaw, 1979), a smaller rotation rate than that obtained herein for the 55-43 Ma time span would be required. In contrast to Sutherland's interpretation, these trails, as reconstructed in this study, appear to start at 55 Ma (anomaly 24) just south of the fossil spreading center in the Coral Sea Basin, concomitant with the cessation of spreading at anomaly 24 (Shaw, 1979; Weissel and Watts, 1979), with the start of the Tasmantid Guyot chain appearing to occur at the eastern-most extension of the fossil Coral Sea Ridge. None of these trails appear to extend across the Coral Sea Basin.

The small circle arc segments or parallels delineating the Lord Howe Seamount trace are offset to the northeast of the congruent parallels delineating the coeval volcanic edifices of the Tasmantid Guyots. Such an offset would imply a more northerly origin for the Lord Howe Seamounts than the Tasmantid Guyots, yet the Lord Howe

Seamounts can be traced no further north than the northern end of the Bellona Plateau (Fig. 2). To the north of the Bellona Plateau, the age of the central part of the d'Entrecasteaux Basin is roughly 30 Ma, i.e. about anomaly 10 (Larue et al., 1977), which is close to the age of the northernmost part of the Bellona Plateau as predicted by this study. This coincidence in ages suggests that hotspot volcanism indeed may have been initiated about the time of cessation of spreading in the d'Entrecasteaux Basin (about 30 Ma) which is in contrast to the apparent initiation of the Tasmantid hotspot volcanism at 55 Ma. The apparent differences in space and time between the initiation of the Lord Howe and Tasmantid volcanism imply that these two hotspots were formed independently, and thus should be decoupled from each other. The pattern of systematic, parallel variations in seamount locations from the pole of rotation for the past 28 Ma for these two hotspot trails also shows that a series of simple changes in plate motion has taken place and that no significant relative motion between these two hotspots has occurred.

A scenario for the origin of the Tasmantid and the eastern Australian hotspots is proposed as follows: As divergence was initiated south of the Southeast Indian Ridge at anomaly 22 or 34 (Weissel and Hayes, 1972; Weissel et al., 1977; Konig, 1987; Cande and Mutter, 1982), the entire Indo-Australia Plate began to move northward, overrunning the smaller Coral Sea spreading system, effectively inhibiting spreading. Spreading center magma sources coalesced to form point sources along the now extinct Coral Sea spreading ridge. As the Indo-Australia Plate continued to move northward, hotspot trails comprising the Tasmantid Guyots and the eastern Australian volcanic centers were left behind. Today, two east-west trending clusters of seismicity (Fig. 2,7), provide the only clue to the possible location of the relic Coral Sea spreading center.

The southeastern Australian basaltic lava fields (55 to 30 Ma) and the buried seamounts believed to be responsible for the SEASAT geoid anomalies, i.e. the geoid anomaly chain, may be related to the spreading history of the Tasman Basin. The progressive SSW decrease in ages of the southeastern basaltic lava fields (Sutherland, 1981) together with their proximity to the Tasman Sea suggest a possible landward migration of volcanism to the southwest out of the Tasman Basin. The Tasman

Basin was active from 74 to 55 Ma (anomalies 33 to 24, Weissel and Hayes, 1977; Shaw, 1979) with a slight northwestward component of Indo-Australia Plate motion. Magnetic anomalies 25 and 24 were mapped just off the southeastern coast of the Australian continent near latitude $33^{\circ}S$ (Weissel and Hayes, 1977; Shaw, 1979). The start of the Barrington Trail (Sutherland, 1981), which trends from the NNE to the SSW (oldest to youngest), is marked by the Barrington volcanic center dated at 53-52 Ma. If hotspot volcanism originated at the end of spreading along the Tasman ridge crest at anomaly 24, a NNE directed opening of the Southeast Indian Ridge at the same time would move the Australian continent back directly over the location of the Tasman Basin spreading center at anomaly 24. The pole of rotation for 55-43 Ma, calculated herein from the southeast Australian basaltic lava fields and the geoid anomaly chain, indicates just such a NNE directed plate motion. The origin of the southeastern basaltic lava fields and the geoid anomaly chain thus could be related to the end of spreading in the Tasman Basin and the onset of NNE directed spreading along the of Southeast Indian Ridge.

VI. SUMMARY AND CONCLUSIONS

A model of Indo-Australia Plate motion is proposed based on the seamount and geoid anomaly chains in the Tasman Sea, and the volcanic centers along eastern Australia. The model, which assumes the various hotspots that formed these features remained fixed relative to each other, describes Indo-Australia Plate motion from 55 Ma to the present in terms of five rotation vectors (Table 1). Three hotspot trails, the Lord Howe Seamounts, Tasmantid Guyots and one trail of eastern Australian volcanic centers, were used to determine the plate rotation vectors from 43 Ma to the present. Likewise, three trails, the Ipswich and Barrington trails and the Tasman Sea geoid anomaly chain, were used to determine the rotation vector from 55 to 43 Ma. Four changes in direction or bends in Indo-Australia Plate motion are recognized at 12, 16, 28, and 43 Ma. Corresponding systematic, parallel departures of Tasman Sea trails from the best fitting traces, determined from a single pole for the past 28 Ma, suggest that multiple, albeit simple, changes in plate motion have occurred and confirm that little or no relative motion has taken place between the Lord Howe and the Tasmantid hotspots. A major change in direction of plate motion is believed to have occurred at 43 Ma because of the large difference between the location of the 55-43 Ma pole of rotation and those of the other poles. Rotation rates of about $0.7^\circ/Ma$ were determined for each of the five time spans, from 55 Ma to the present. Ages for the Tasman Sea seamounts are predicted based on this model (Table 3). A high degree of correlation was found between predicted ages of the seamounts and volcanic centers, based on the newly determined rotation vectors and observed ages, based on radiometric dates. Three additional hotspot trails are recognized from the agreement between predicted and observed radiometric ages of other volcanic centers. An APW path determined from the hotspot model appears to be comparable to those determined by paleomagnetic methods and indicates the reliability of the model. The start of the Lord Howe trail seems to correlate with the cessation of spreading in the d'Entrecasteaux Basin at about 30 Ma and the start of the Tasmantid and the eastern Australian trails seem to correlate with the cessation of spreading in the Coral Sea Basin at 55 Ma. The start of the Ipswich and Barrington trails (in

southeastern Australia) and the geoid anomaly chain (in the Tasman Basin) likewise seem to correlate with the cessation of spreading in the Tasman Basin at 55 Ma.

Appendix A:

Methods for Determining Poles of Rotation

Two methods were used to locate the minimum σ value for the data set and the results compared. In the iteration method, the σ value is determined at an estimated pole of rotation and then the sum of error square Ψ (defined below) is minimized in a least-square sense (Appendix B1) to obtain an adjustment to the coordinates of the pole of rotation. The adjusted pole of rotation is then used as the estimated pole of rotation to determine a further adjustment, and the process is repeated until a stable σ value is reached or only very small changes in the calculated pole of rotation are noted.

The standard deviation (σ) angular distance at a assumed pole is:

$$\sigma = \sqrt{\frac{\Psi}{(\sum_{j=1}^M N_j) - (M + 2)}}$$

where

$$\Psi = \sum_{j=1}^M \sum_{i=1}^{N_j} (\beta_{ij} - \bar{\beta}_j)^2$$

β_{ij} = the angular distance between the assumed pole and any point i along trail j

$\bar{\beta}_j$ = the average angular distance between the assumed pole and all points along parallel j

M = number of trails

N_j = number of volcanic centers in trace j

Ψ = the sum of squares of the errors to each data point in angular distance from the calculated parallels.

(Harrison, 1972; Epp, 1984).

The fit for each trace segment was improved subjectively by either eliminating some of the eastern Australian volcanic centers of questionable affinity or adding points along a submarine volcanic ridge exhibiting a well defined trend that approximated the postulated direction of motion.

Although the calculated final poles of rotation as discussed above have relatively small angular distance standard deviations (σ) as compared to the dimensions of seamounts used in this study, some of the calculated σ values converge very slowly towards the minimum value. There is, therefore, a possibility that the pole of rotation thus determined is not at the actual minimum σ value for the data set and the pole determined is not the best pole.

In the second method, i.e. a grid search minimization (Lawver and Dick, 1983; Appendix B2), the σ values were calculated for poles in a defined grid pattern for the data set. No minimization of the Ψ value is needed in this method because the σ values are calculated for the whole grid at a specified interval. In practice, the σ values are first determined at a larger grid interval, and the precision of the location is improved by progressively reducing the scale of the grid. Because the standard deviation of the Ψ values is generally about 0.1° , a grid interval of 0.1° for locating the pole is chosen. Once the values are obtained for each point of the grid, they are contoured at fixed increments (0.05X in close and 1.00X further out). Different grid searches were made for each of the five time spans identified.

Note that if a pole on the 2.00X contour is used, the standard deviation of the data is twice the standard deviation of the minimum. I consider an increase in standard deviation of 5% to be significant. Thus it is reasonable to assume that the "true" pole is within the 1.05X contour. Any pole location within the 1.05 σ contour yields a standard deviation that is not significantly higher than the standard deviation obtained using the "best" pole. In general, any pole of rotation within the 1.05X contour value can be used as a pole of rotation for that time span without noticeable discrepancies between the parallels representing trace segments and the actual seamounts location. An additional constraint on the location of each trace segment along each trail for a particular time span is that the lengths of the coeval segments must subtend the same angle of rotation about the pole.

Appendix B1:

Iteration Method for Determining Poles of Rotation

A least-square method for minimization of the value $\sum_{i=1}^N (\Delta\beta_i)^2$ with respect to $\Delta\theta$ and $\Delta\xi$ for determining a pole of rotation for congruent hotspot trails is derived as follows:

Chains of seamounts formed by fixed hotspot sources on a single plate can be approximated on the earth's surface by congruent small circle arcs or parallels generated by rotating a point i about a pole of rotation p with coordinates (θ, ξ) .

The coordinates of point i are given by (θ_i, ξ_i)

where:

θ_i = the co-latitude of point i = 90.0 - latitude of point i

ξ_i = the longitude of point i of the present day geodetic system.

A constant angle β_i at the center of the earth is maintained between point (θ_i, ξ_i) and the pole of rotation (θ, ξ) .

Considering the simplest case with only one hotspot trace on a plate.

$$\begin{aligned} \cos\beta_i &= (\theta_i, \xi_i) \cdot (\theta, \xi) \\ &= (\sin\theta_i \cos\xi_i \sin\theta \cos\xi + \sin\theta_i \sin\xi_i \sin\theta \sin\xi + \cos\theta_i \cos\theta) \\ &= \sin\theta_i \sin\theta \cos(\xi - \xi_i) + \cos\theta_i \cos\theta = B_i \end{aligned} \quad (1)$$

$$\beta_i = \cos^{-1} B_i \quad (2)$$

Let β be the angle between the pole of rotation and the hotspot trail.

If $\Delta\beta_i$ is the mislocation of (θ_i, ξ_i) away from the hotspot trail, then

$$\Delta\beta_i = \beta - \beta_i \quad (3)$$

Expanding (3) at pole p using a Taylor series,

$$\Delta\beta_i = \bar{\beta} - \left(\beta_i + \frac{\partial}{\partial\theta} \beta_i \Delta\theta + \frac{\partial}{\partial\xi} \beta_i \Delta\xi \right)$$

where $\bar{\beta}$ is the average of β_i from points 1 to N on the trail.

Minimizing the square sum of error $\Delta\beta_i$, $\sum_{i=1}^N (\Delta\beta_i)^2$, by partial differentiation of the value β_i with respect to $\Delta\theta$ and $\Delta\xi$:

$$\begin{aligned} \frac{\partial}{\partial \Delta\theta} \left(\sum_{i=1}^N (\Delta\beta_i)^2 \right) &= 2 \sum_{i=1}^N \Delta\beta_i \left(\frac{\partial}{\partial \Delta\theta} \Delta\beta_i \right) \\ &= 2 \sum_{i=1}^N \Delta\beta_i K_\theta = 0 \end{aligned} \quad (4)$$

$$\begin{aligned} \frac{\partial}{\partial \Delta\xi} \left(\sum_{i=1}^N (\Delta\beta_i)^2 \right) &= 2 \sum_{i=1}^N \Delta\beta_i \left(\frac{\partial}{\partial \Delta\xi} \Delta\beta_i \right) \\ &= 2 \sum_{i=1}^N \Delta\beta_i K_\xi = 0 \end{aligned} \quad (5)$$

Determine K_θ and K_ξ about pole p for point i .

From (4)

$$\begin{aligned} K_\theta &= \left(\frac{\partial}{\partial \Delta\theta} \Delta\beta_i \right) \\ &= \frac{\partial}{\partial \Delta\theta} [\bar{\beta} - (\beta_i + \frac{\partial}{\partial \theta} \beta_i \Delta\theta + \frac{\partial}{\partial \xi} \beta_i \Delta\xi)] \\ &= -\frac{\partial}{\partial \theta} \beta_i \\ &= -\frac{\partial}{\partial \theta} \cos^{-1} B_i \\ &= -\left(\frac{-1}{\sqrt{1 - B_i^2}} \right) \frac{\partial}{\partial \theta} B_i \\ &= -\left(\frac{-1}{\sqrt{1 - B_i^2}} \right) [\cos\theta \sin\theta; \cos(\xi_i - \xi) - \sin\theta \cos\theta_i] \end{aligned}$$

From (5)

$$\begin{aligned}
K_\xi &= \left(\frac{\partial}{\partial \Delta \xi} \Delta \beta_i \right) \\
&= \frac{\partial}{\partial \Delta \xi} \left[\bar{\beta} - \left(\beta_i + \frac{\partial}{\partial \theta} \beta_i \Delta \theta + \frac{\partial}{\partial \xi} \beta_i \Delta \xi \right) \right] \\
&= -\frac{\partial}{\partial \xi} \beta_i \\
&= -\frac{\partial}{\partial \xi} \cos^{-1} B_i \\
&= -\left(\frac{-1}{\sqrt{1 - B_i^2}} \right) \frac{\partial}{\partial \xi} B_i \\
&= -\left(\frac{-1}{\sqrt{1 - B_i^2}} \right) \sin \theta \sin \theta_i \sin(\xi_i - \xi)
\end{aligned}$$

Rearranging equation (4) and (5):

From (4)

$$\begin{aligned}
2 \sum_{i=1}^N \Delta \beta_i K_\theta &= 0 \\
2 \sum_{i=1}^N \left[\left(\bar{\beta} - \left(\beta_i + \frac{\partial}{\partial \theta} \beta_i \Delta \theta + \frac{\partial}{\partial \xi} \beta_i \Delta \xi \right) \right) K_\theta \right] &= 0 \\
\sum_{i=1}^N (\bar{\beta} - \beta_i) K_\theta + K_\theta^2 \Delta \theta + K_\theta K_\xi \Delta \xi &= 0 \\
\Delta \theta \left(\sum_{i=1}^N K_\theta^2 \right) + \Delta \xi \sum_{i=1}^N K_\xi K_\theta &= \sum_{i=1}^N (\beta_i - \bar{\beta}) K_\theta \tag{6}
\end{aligned}$$

From (5)

$$\begin{aligned}
2 \sum_{i=1}^N \Delta \beta_i K_\xi &= 0 \\
2 \sum_{i=1}^N \left[\left(\bar{\beta} - \left(\beta_i + \frac{\partial}{\partial \theta} \beta_i \Delta \theta + \frac{\partial}{\partial \xi} \beta_i \Delta \xi \right) \right) K_\xi \right] &= 0 \\
\sum_{i=1}^N (\bar{\beta} - \beta_i) K_\xi + K_\theta K_\xi \Delta \theta + K_\xi^2 \Delta \xi &= 0 \\
\Delta \theta \sum_{i=1}^N K_\theta K_\xi + \Delta \xi \left(\sum_{i=1}^N K_\xi^2 \right) &= \sum_{i=1}^N (\beta_i - \bar{\beta}) K_\xi \tag{7}
\end{aligned}$$

Rearrange (6) and (7) into a matrix equation:

$$\begin{pmatrix} \sum_{i=1}^N K_{\theta}^2 & \sum_{i=1}^N K_{\xi} K_{\theta} \\ \sum_{i=1}^N K_{\theta} K_{\xi} & \sum_{i=1}^N K_{\xi}^2 \end{pmatrix} \begin{pmatrix} \Delta\theta \\ \Delta\xi \end{pmatrix} = \begin{pmatrix} \sum_{i=1}^N (\beta_i - \bar{\beta}) K_{\theta} \\ \sum_{i=1}^N (\beta_i - \bar{\beta}) K_{\xi} \end{pmatrix}$$

Solving for $\Delta\theta$ and $\Delta\xi$

$$\Delta\theta = \frac{-\sum_{i=1}^N (\beta_i - \bar{\beta}) K_{\theta} \sum_{i=1}^N K_{\xi}^2 + \sum_{i=1}^N (\beta_i - \bar{\beta}) K_{\xi} \sum_{i=1}^N K_{\theta} K_{\xi}}{\sum_{i=1}^N K_{\theta}^2 \sum_{i=1}^N K_{\xi}^2 - (\sum_{i=1}^N K_{\theta} K_{\xi})^2}$$

$$\Delta\xi = \frac{-\sum_{i=1}^N (\beta_i - \bar{\beta}) K_{\xi} \sum_{i=1}^N K_{\theta}^2 + \sum_{i=1}^N (\beta_i - \bar{\beta}) K_{\theta} \sum_{i=1}^N K_{\theta} K_{\xi}}{\sum_{i=1}^N K_{\theta}^2 \sum_{i=1}^N K_{\xi}^2 - (\sum_{i=1}^N K_{\theta} K_{\xi})^2}$$

This can be generalized for M number of hotspot trails on a plate with β_{ij} .

In practice a BASIC computer program, POLEROT (E. Berg, personal communication), is used to determine a pole of rotation by a least-squares minimization of the angular distance between data points along hotspot trails and the pole of rotation, subtended through the center of the Earth.

```

100 'Program POLEROT.BAS
110 DEFDBL A-F,L,P,S
120 DEFINT I,N,J,M
130 'An assumed initial pole of rotation for the data set
135 'LATP=18.80# : LONP=31.70#
140 ' M = number of hotspot trails in the data set
150 M=2 :DIM N(M),SB(M),EE(M) :NN=0' =# of iteration
160 N(1)=8:N(2)=5 'number of data points in trail N(1), N(2) etc.
165 N=13 'total number of data points
170 DIM LAT(M,N),LON(M,N),LA(M,N),LO(M,N),CB(M,N),B(M,N),DFIB(M,N),DDETAB(M,N),E
180 '
190 LAT(1,1)=-29.33#:LON(1,1)=159.05#
200 LAT(1,2)=-29.58#:LON(1,2)=159.21#
210 LAT(1,3)=-30.05#:LON(1,3)=159.15#
220 LAT(1,4)=-31.62#:LON(1,4)=159.13#
230 LAT(1,5)=-31.85#:LON(1,5)=159.26#
240 LAT(1,6)=-33.20#:LON(1,6)=159.25#
250 LAT(1,7)=-34.75#:LON(1,7)=159.75#
260 LAT(1,8)=-28.30#:LON(1,8)=159.22#
280 LAT(2,1)=-35.46#:LON(2,1)=156.41#
300 LAT(2,2)=-35.45#:LON(2,2)=156.18#
310 LAT(2,3)=-36.70#:LON(2,3)=156.31#
320 LAT(2,4)=-40.42#:LON(2,4)=156.75#
330 LAT(2,5)=-34.30#:LON(2,5)=155.95#
400 PI=3.141592653589793#
410 P2=PI/2#
420 LAP=LATP*P2/90#: LOP=LONP*P2/90#
430 FOR J = 1 TO M
440 FOR I = 1 TO N(J)
450 LA(J,I)=LAT(J,I)*P2/90#
460 LO(J,I)=LON(J,I)*P2/90#
470 NEXT I
480 NEXT J
490 GOSUB 1000 'GO SUBROUTINE 1
500 'Partial Derivatives
510 FOR J = 1 TO M
520 FOR I = 1 TO N(J)
530 A=-1#/SQRT(1-CB(J,I)*CB(J,I))
540 DFIB(J,I)=A*SIN(P2-LA(J,I))*SIN(P2-LAP)

```

```

550 DFIB(J,I)=DFIB(J,I)*(-COS(LO(J,I))*SIN(LOP)+SIN(LO(J,I))*COS(LOP))
560 DDETAB(J,I)=-A*COS(P2-LA(J,I))*SIN(P2-LAP)
570 DDETAB(J,I)=DDETAB(J,I)+A*SIN(P2-LA(J,I))*COS(P2-LAP)*COS(LO(J,I)-LOP)
580 NEXT I
590 NEXT J
600 D1=0:D2=0:F1=0:F2=0:DETA1=0:DETA2=0
610 FOR J = 1 TO M
620 FOR I = 1 TO N(J)
630 D1=E(J,I)*DFIB(J,I)+D1
640 D2=E(J,I)*DDETAB(J,I)+D2
650 F1=DFIB(J,I)*DFIB(J,I)+F1
660 F2=DFIB(J,I)*DDETAB(J,I)+F2 'also = deta1
670 DETA2=DDETAB(J,I)*DDETAB(J,I)+DETA2
680 NEXT
690 NEXT
700 'eq are: D1 + F1*dlop + F2*(-dlap) = 0 sign reversed ddeta=-dfi
710 ' D2 + F2*dlop + deta2*(-dlap) = 0
715 DNOM=F1*DETA2-F2*F2
720 DLAP= (D2*F1-F2*D1)/DNOM '= - deldeta
725 SIGLAP=SQR(DETA2/DNOM) :PRINT "siglap=";SIGLAP
730 'DLOP=-D1/F1+F2/F1*DLAP
735 SIGLOP=SQR(F1/DNOM) :PRINT "siglop=";SIGLOP
740 DLOP= (-D1*DETA2+D2*F2)/DNOM
750 LAP=LAP+DLAP ' new pole
760 LOP=LOP+DLOP
770 LATP=LAP*90#/P2 : DLATP=DLAP*90#/P2
780 LONP=LOP*90#/P2 : DLONP=DLOP*90#/P2
790 GOSUB 1000 'G O SUBROUTINE 1
800 PRINT" LAT sigma adjust LON sigma adjust s
810 PRINT USING "###.##### ";LATP,EEE*SIGLAP*90/P2,DLATP,LONP,EEE*SIGLOP*90/P2,
815 PRINT" ":PRINT" distance to hot spot trace with error"
820 FOR J = 1 TO M
830 PRINT USING "###.##### ";SB(J)*90/P2,EE(J)*90/P2:NEXT
835 PRINT "iteration #";NN
840 PRINT" to iterate press : cont"
845 NN=NN+1
847 PRINT"latp= :lonp= :goto 420"
850 STOP
860 GOTO 500
1000 ' SUBROUTINE I for calculating differences in angular distance
1010 FOR J = 1 TO M
1020 SB(J)=0 ' CB= cos angle pole to point, b=angle in rad
1030 FOR I = 1 TO N(J)
1040 CB(J,I)=COS(P2-LA(J,I))*COS(P2-LAP)
1050 CB(J,I)=CB(J,I)+SIN(P2-LA(J,I))*SIN(P2-LAP)*COS(LOP-LO(J,I))
1060 B(J,I)=P2-ATN(CB(J,I)/SQR(-CB(J,I)*CB(J,I)+1)) ' =arc cos cb(i)
1070 'PRINT USING "###.#### ";B(j,I)*90/P2,CB(j,I),COS(LOP-LO(j,I))
1080 SB(J)=SB(J)+B(J,I)
1090 NEXT
1100 PRINT " "
1110 SB(J)=SB(J)/N(J)
1120 NEXT J
1130 EEE=0 :MM=0
1140 FOR J = 1 TO M :EE(J)=0
1150 FOR I = 1 TO N(J)
1160 E(J,I)=B(J,I)-SB(J)
1170 PRINT USING "###.### ";B(J,I)*90/P2,E(J,I)*90/P2,(B(J,I)-E(J,I))*90/P2
1180 EE(J)=E(J,I)*E(J,I) + EE(J)
1190 NEXT I
1200 EEE = EE(J) + EEE
1210 EE(J)=SQR(EE(J)/(N(J)-2))
1220 MM = MM + N(J) 'total # of data points 'Sigma for trail j
1225 PRINT " "
1230 NEXT J
1240 EEE = SQR(EEE/(MM-2)) 'Sigma for j trails
1250 RETURN

```

Appendix B2:

List of Computer Program for Determining Poles of Rotation (Grid Search Method).

```

C      A FORTRAN computer program (written by the author) is used to
C calculate the standard deviations, in angular distances, between data
C points along hotspot trails and the assumed poles of rotation subtended
C at the center of the Earth. The poles of rotation locate at grid points
C within the defined grid limits from which the search for the minimum
C poles are made.
C
C      1. AINCR = AMOUNT OF INCREMENTS FOR GRID
C      2. WT    = VALUE OF NORMALIZED FOR CONTOURING
C
C      3. INDEX =1 NO NORMALIZATION OF DATA
C              =2 NORMALIZED ALL VALUE WITH WT      ( 1,1  GRID )
C                                                       2,2
C      4. IWRITE =1 OUTPUT VALUE AS GRID  F7.5      1,3  LIST
C              =2 OUTPUT VALUE AS GRID  F5.0      2,3
C              =3 OUTPUT VALUE AS LIST  F10.5
C              =4 LIST THE DIFFERENCE OF EACH DATA POINTS
C
C      1  1  0.1234  2  1
C      NJ, AINCR,  WT,  INDEX, IWRITE
C      NJ    = NUMBER OF TRACE,
C      AINCR = GRID DIVISION
C      WT    = VALUE OF NORMALIZATION
C      INDEX = NORMALIZATION OF DATA
C      IWRITE = OUTPUT FORMAT
C
C      EACH LINE SHOULD HAVE AT LEAST 3 DATA POINTS
C      A MAXIMUM OF 6 TRAILS
C      LATMIN, LONGMIN = MIN. LIMIT OF LAT., LONG. TO ITERATE
C      LATMAX, LONGMAX = MAX. LIMIT OF LAT., LONG. TO ITERATE
C
C      REAL LAT, LONG, PI2, PI4, LATMIN, LATMAX, LONGMIN, LONGMAX
C      DIMENSION LAT(6,50), LONG(6,50), BETA(6,50), BETAV(6), SIGMA(6),
C      +          K(6), CPOLE(51)
C      DATA RAD /.1745329E-1/
C      PI2=360.*RAD
C      PI4=PI2/4
C      CMIN = 90.
C      READ (10,*) NJ, AINCR, WT, INDEX, IWRITE
C      READ (10,*) LATMIN, LATMAX, LONGMIN, LONGMAX
C      IF (IWRITE.EQ.1) WRITE(20,100) NJ,LATMIN,LATMAX, LONGMIN, LONGMAX
100  FORMAT('NO. OF TRACE,  INPUT LAT.,LONG. LIMIT',/,
C      +          5X,I5,4F6.1)
C
C      READ IN LAT. AND LONG. OF THE DATA POINTS
C      N=0
10  IF (N.GE.NJ) GO TO 20
    IF (N.LT.NJ) N=N+1
    DO 30 I =1 ,50
20  READ(10,200) NN, LAT(N,I), LONG(N,I)
    FORMAT(I1,F6.2,1X,F7.2)
    IF(NN.EQ.9) THEN
      GO TO 40
    END IF
    LAT(N,I)=(90-LAT(N,I))*RAD
    LONG(N,I)=LONG(N,I)*RAD
    K(N)=K(N)+1
30  IF(NN.GT.0.AND.NN.LT.9) GO TO 10
20  DO 50 IJ = 1,1000
    ALONG=(LONGMIN+IJ*AINCR)
    IF (ALONG.LE.LONGMAX) THEN
      AALONG=ALONG
      ALONG=ALONG*RAD

```

```

ELSE
GO TO 999
END IF
IK=1
DO 60 J = 1,1000
IJK=J
ALAT=(LATMIN+J*AINCR)
IF (ALAT.LE.LATMAX) THEN
AALAT=ALAT
ALAT=(90-ALAT)*RAD
ELSE
GO TO 998
END IF
C RESET THE VALUES
DO 70 N=1,NJ
DO 70 I=1,K(N)
BETA(N,I)=0.
BETAV(N)=0.
70 SIGMA(N)=0.
SSIGMA=0.
JS=0
C
C CALCULATE THE ANGLE, BETA(I), BETWEEN THE POLE AND DATA POINTS
C
DO 80 N=1,NJ
DO 90 I=1,K(N)
BE=COS(LAT(N,I))*COS(ALAT)+SIN(LAT(N,I))*SIN(ALAT)*COS(ALONG-
+ LONG(N,I))
BETA(N,I)=ACOS(BE)
90 BETAV(N)=BETAV(N)+BETA(N,I)
BETAV(N) = BETAV(N)/K(N)
IF (IWRITE.EQ.4) THEN
WRITE(30,300) AALAT, AALONG, BETAV(N)/RAD, N, NJ
END IF
300 FORMAT(3F10.5,2I5,/)
C
C CALCULATE THE ERROR FOR EACH TRACE SIGMA(N)
C THE ERROR FOR ALL TRACES SSIGMA
C
DO 91 I=1,K(N)
91 SIGMA(N)=SIGMA(N)+(BETA(N,I)-BETAV(N))**2
SSIGMA=SSIGMA+SIGMA(N)
SIGMA(N)=SQRT(SIGMA(N)/(K(N)-2))
JS=JS+K(N)
80 CONTINUE
SSIGMA=SQRT(SSIGMA/(JS-NJ-2))/RAD
C CHANGE IN SCALE FOR CONTOURING
C
IF (INDEX.EQ.1) CPOLE(IK)=SSIGMA
IF (INDEX.EQ.2) CPOLE(IK)=(SSIGMA-WT)/WT*100
IF (IWRITE.EQ.3) WRITE(20,400) AALONG, AALAT, CPOLE(IK), IK
400 FORMAT(3F10.5,I5)
C
C FIND MINIMUM VALUE
IF(SSIGMA.LT.CMIN) THEN
CMIN=SSIGMA
CLAT=AALAT
CLONG=AALONG
END IF
IK=IK+1
60 CONTINUE
998 IF (IWRITE.EQ.1) WRITE(20,500) AALONG, (CPOLE(IM), IM=1, IJK)
C GRID
IF (IWRITE.EQ.2) WRITE(20,600) AALONG, (CPOLE(IM), IM=1, IJK)
50 CONTINUE
C FOR CONTOUR INPUT FILE
999 IF (IWRITE.EQ.1) WRITE(20,*) CMIN, CLAT,CLONG
500 FORMAT(' ',F5.1,1X,51(F7.5))
600 FORMAT(' ',F5.1,1X,51(F5.0))
STOP
END

```

Appendix C:
Contour Maps of Sigma Values

Contour maps of standard deviation (σ) of the poles of rotation in angular distance for the 12-0, 16-12, 28-16, 43-28, 55-43 and 28-0 Ma time spans showing the locations of the minimum σ values and preferred poles determined in this study.

Figure 18 Contour map of standard deviation (σ) of the poles of rotation in angular distance for the 12-0 Ma time span. Contour levels are chosen at either 0.05 or 1.00 increments of the minimum standard deviation of angular distance (0.109°) as indicated. The dotted pattern is the distribution of data points contoured. Solid dot marks the location of the minimum σ value. Triangle marks the location of the preferred pole. Open square marks the location of the Indo-Australian pole relative to hotspots from Minster and Jordan (1978).

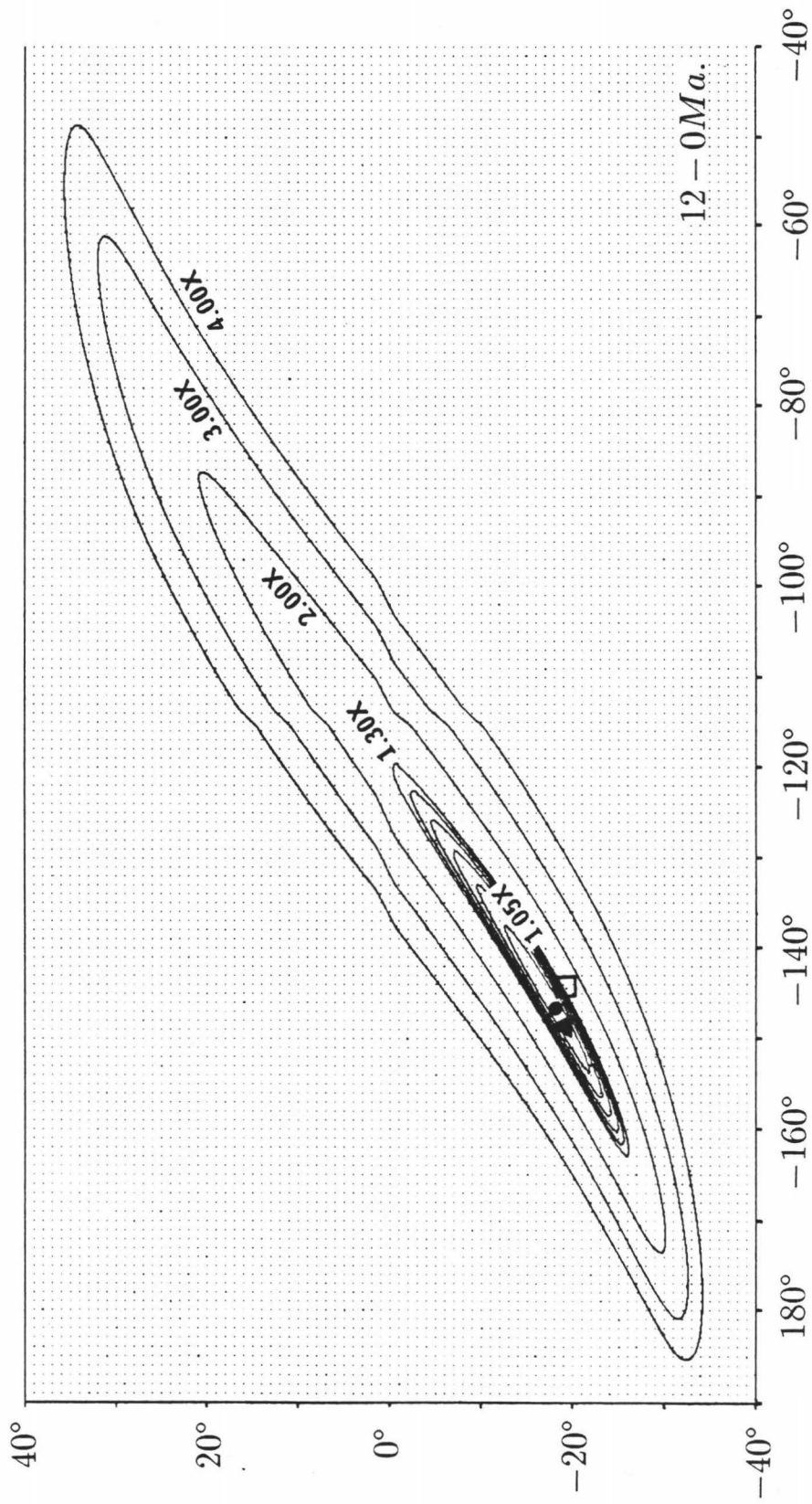


Figure 19 Contour map of standard deviation (σ) of the poles of rotation in angular distance for the 16-12 Ma time span. Contour levels are chosen at either 0.05 or 1.00 increments of the minimum standard deviation of angular distance (0.055°) as indicated. The dotted pattern is the distribution of data points contoured. Solid dot marks the location of the minimum σ value.

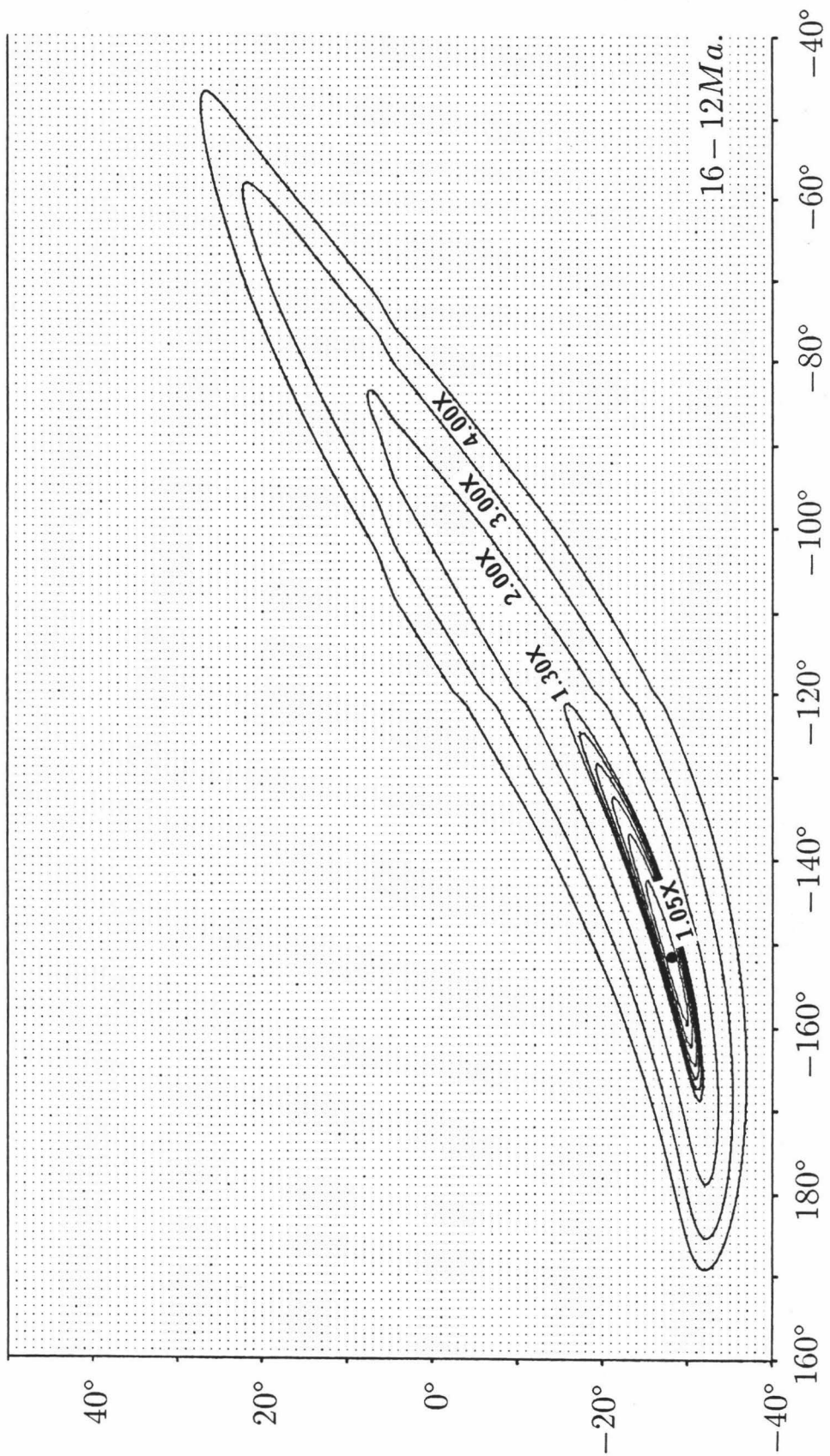


Figure 20 Contour map of standard deviation (σ) of the poles of rotation in angular distance for the 28-16 Ma time span. Contour levels are chosen at either 0.05 or 1.00 increments of the minimum standard deviation of angular distance (0.103°) as indicated. The dotted pattern is the distribution of data points contoured. Solid dot marks the location of the minimum σ value. Triangle marks the location of the preferred pole.

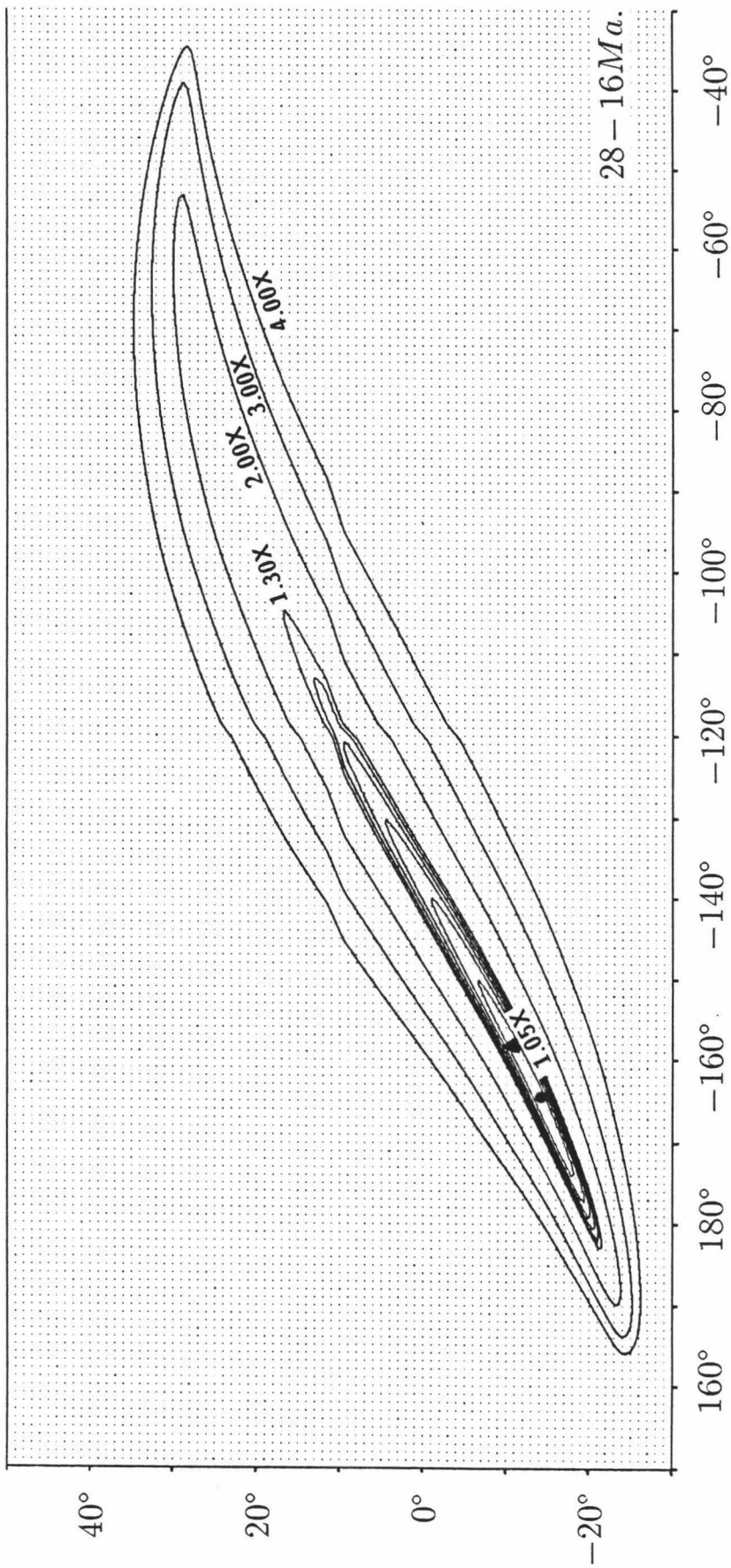


Figure 21 Contour map of standard deviation (σ) of the poles of rotation in angular distance for the 43-28 Ma time span. Contour levels are chosen at either 0.05 or 1.00 increments of the minimum standard deviation of angular distance (0.131°) as indicated. The dotted pattern is the distribution of data points contoured. Solid dot marks the location of the minimum σ value.

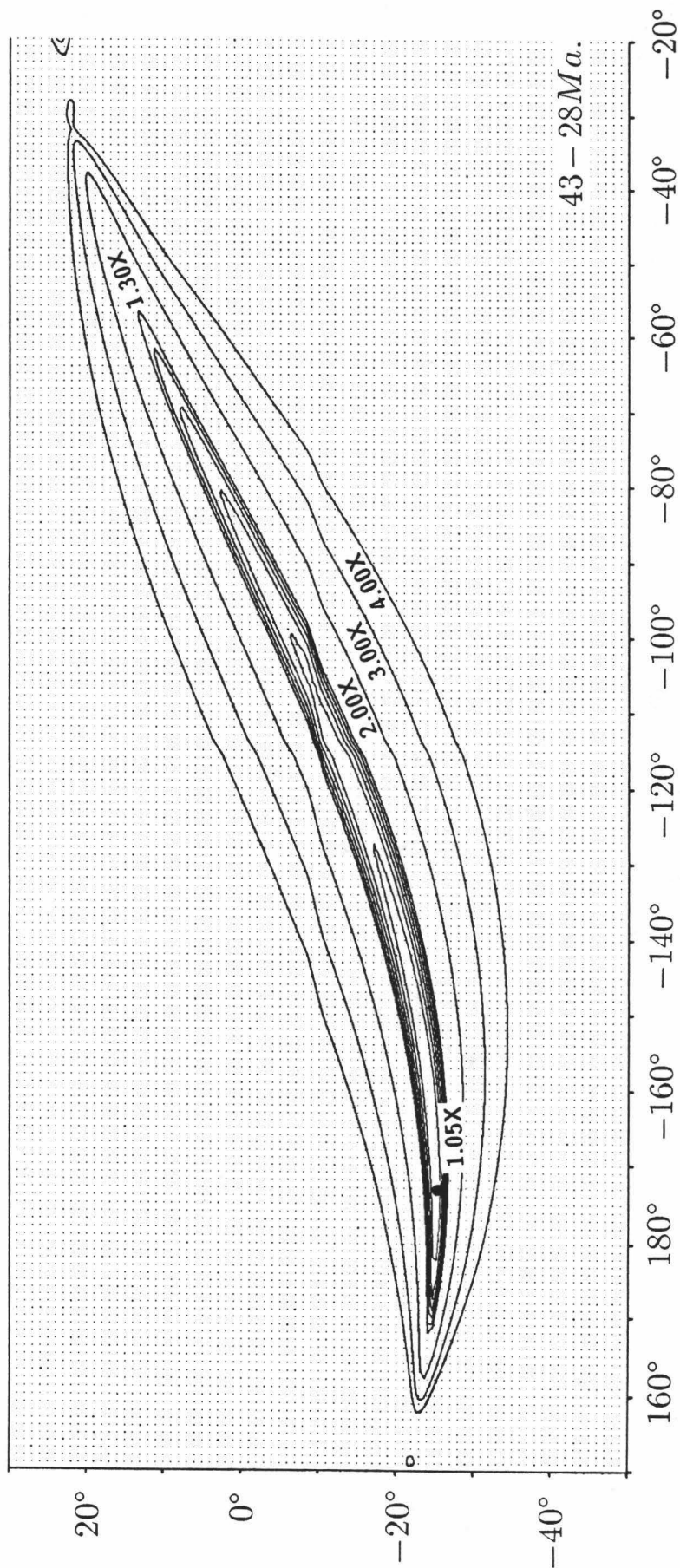


Figure 22 Contour map of standard deviation (σ) of the poles of rotation in angular distance for the 55-43 Ma time span. Contour levels are chosen at either 0.05 or 1.00 increments of the minimum standard deviation of angular distance (0.211°) as indicated. The dotted pattern is the distribution of data points contoured. Solid dot marks the location of the minimum σ value. Solid square marks the location of the calculated pole without the inclusion of the geoid anomalies.

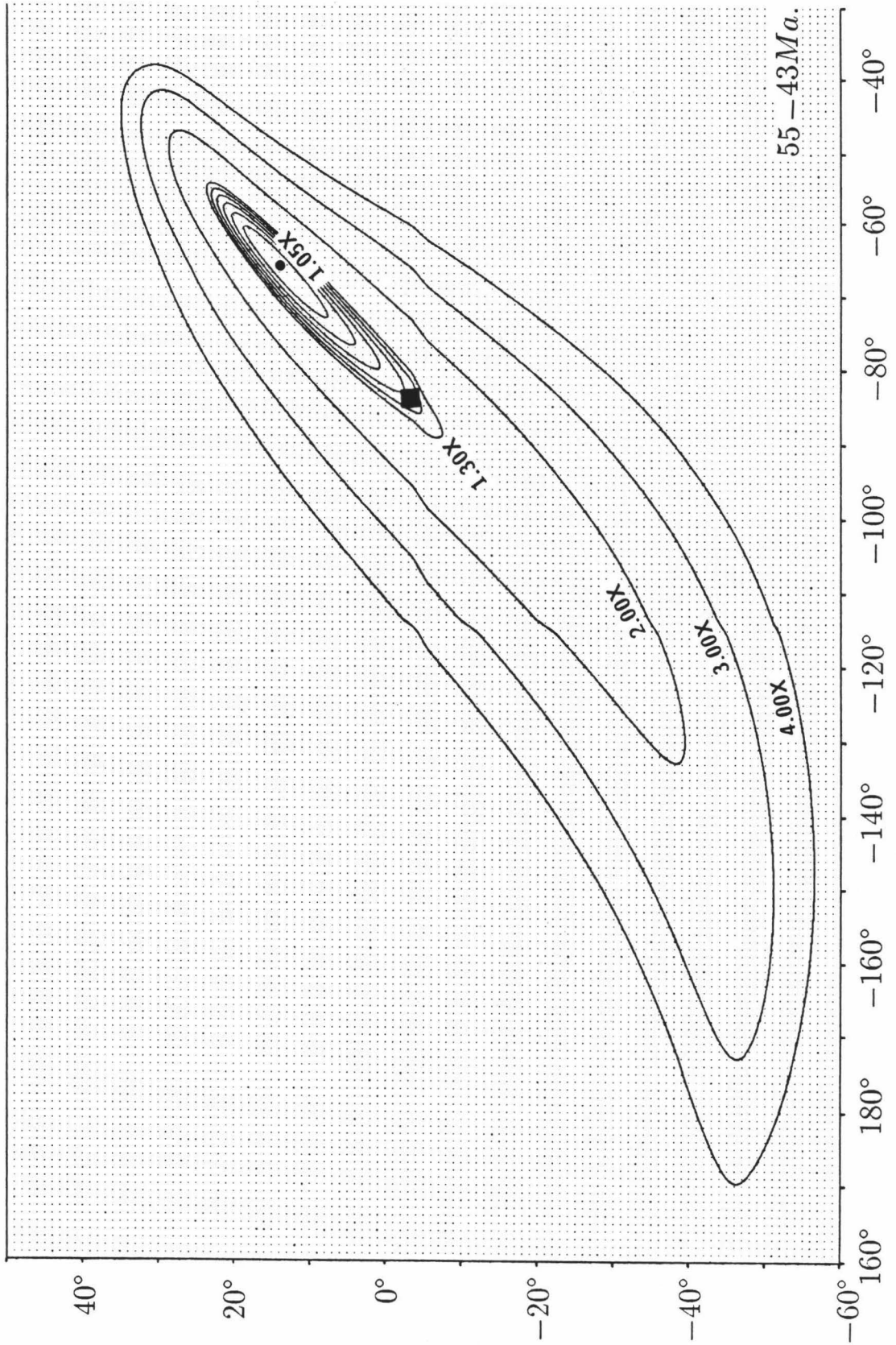
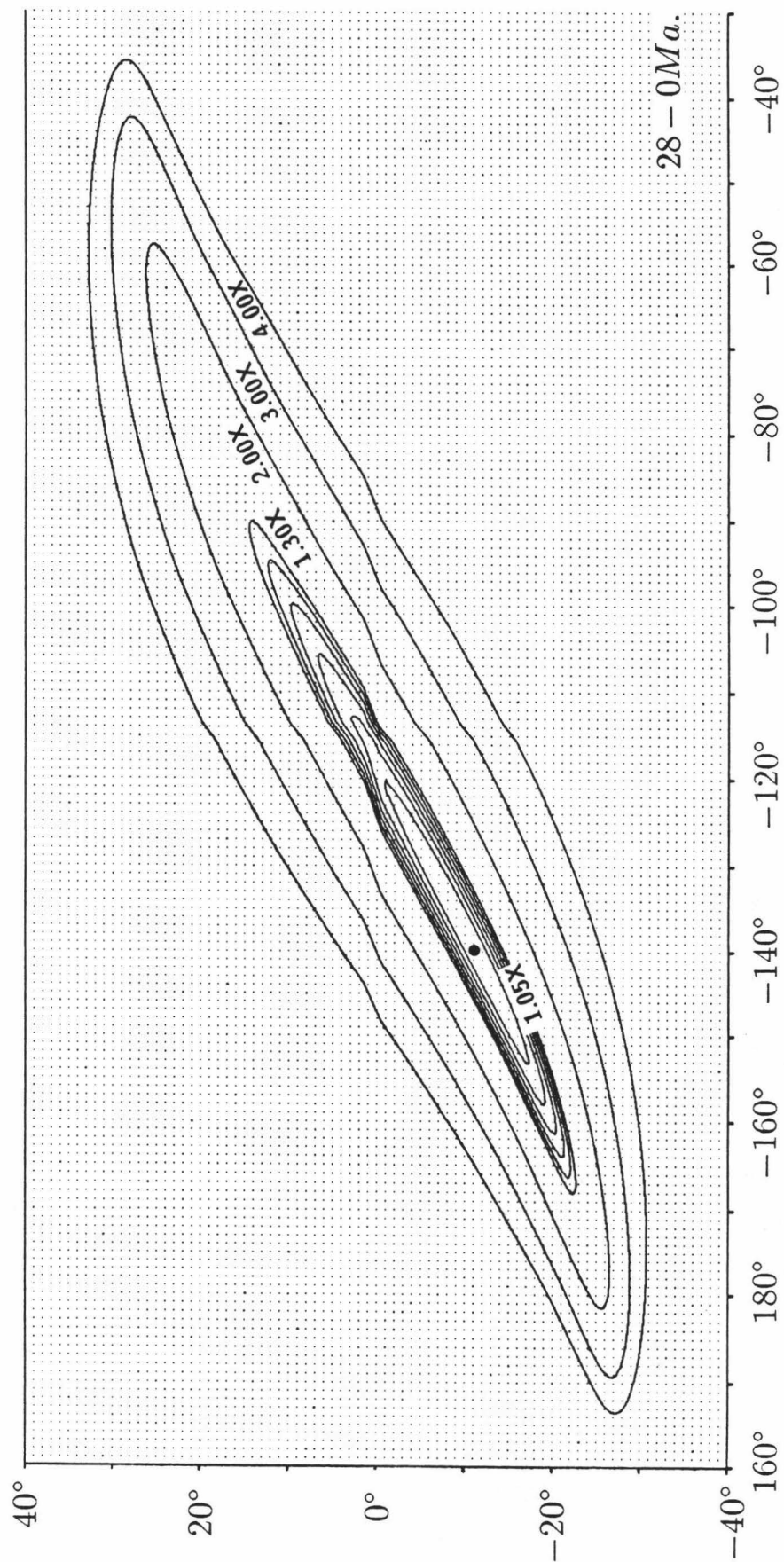


Figure 23 Contour map of standard deviation (σ) of the poles of rotation in angular distance for the 28-0 Ma time span. Contour levels are chosen at either 0.05 or 1.00 increments of the minimum standard deviation of angular distance (0.350°) as indicated. The dotted pattern is the distribution of data points contoured. Solid dot marks the location of the minimum σ value.



Appendix D:
Plots of Angular Distance vs. Age

Plots of angular distances of the volcanic centers or basaltic lava fields vs. radiometric ages (Ma) along parallels about the poles of rotation from a reference volcanic center or basaltic lava field. The slopes of the graphs are the rates of rotation about the poles for these time spans.

Figure 24 A plot of the angular distances of the volcanic centers from the 27.7 Ma volcanic center along parallels about the preferred pole of rotation at $25.2^{\circ}S$, $173.2^{\circ}W$ versus radiometric ages (Ma) for the 43-28 Ma time span. The slope of the line is the rate of rotation for the 43-28 Ma time span. The slope of the graph ($0.70^{\circ}/Ma$) is the rate of rotation about the pole for the 43-28 Ma time span.

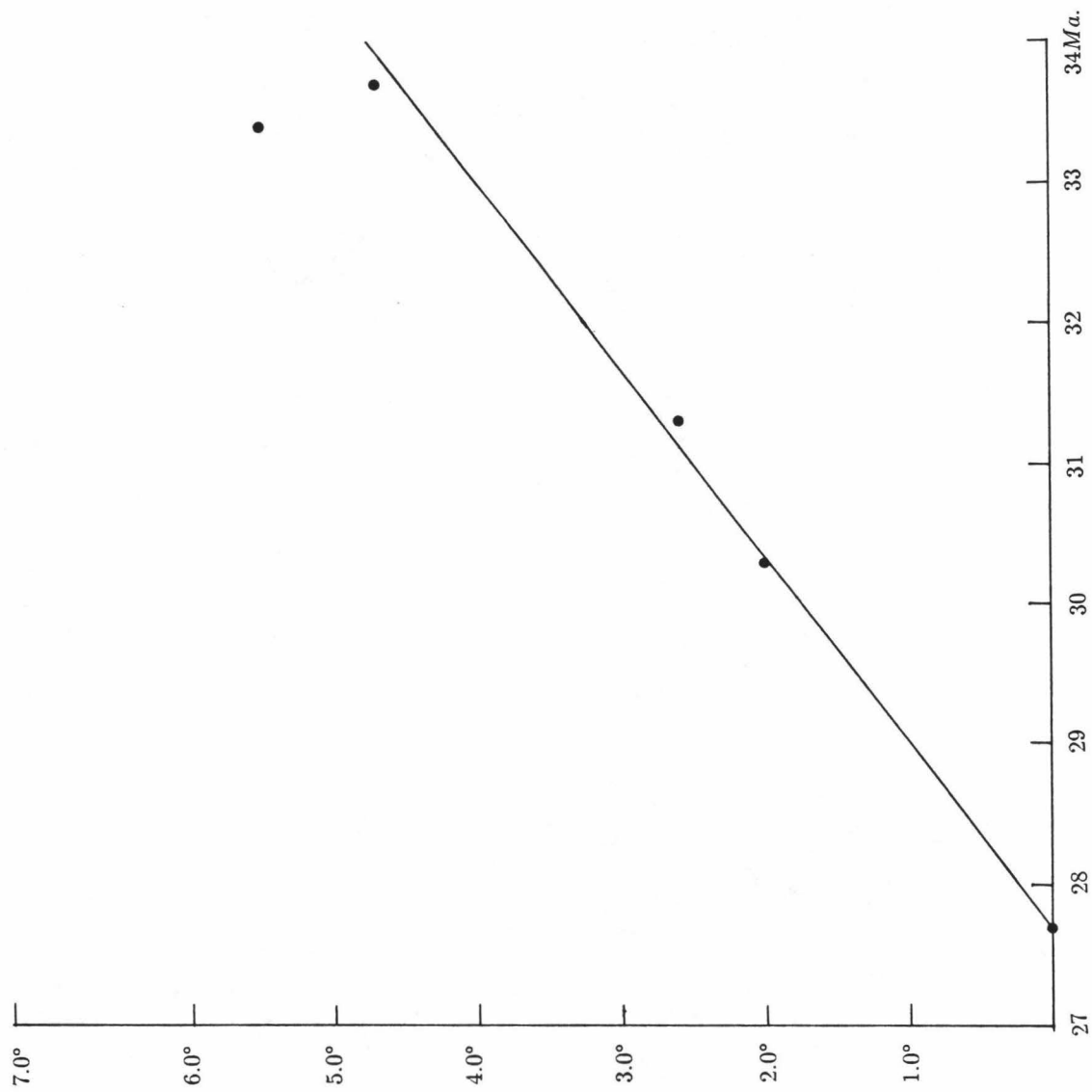


Figure 25 A plot of the angular distances of the basaltic lava fields from the Nr and Wa basaltic lava fields in the southeast Australia (without the inclusion of the chain of geoid anomalies in the southwestern Tasman Sea) along the parallels about the pole at $2.85^{\circ}S$, $81.75^{\circ}W$ versus radiometric ages (Ma) within the 55-43 Ma time span. The data is a combination of the Ipswich Trail and the Barrington Trail. See Figure 4 for symbols of the southeastern Australian basaltic lava fields. The slope of the graph ($0.56^{\circ}/Ma$) is the rate of rotation about the pole for the 55-43 Ma time span.

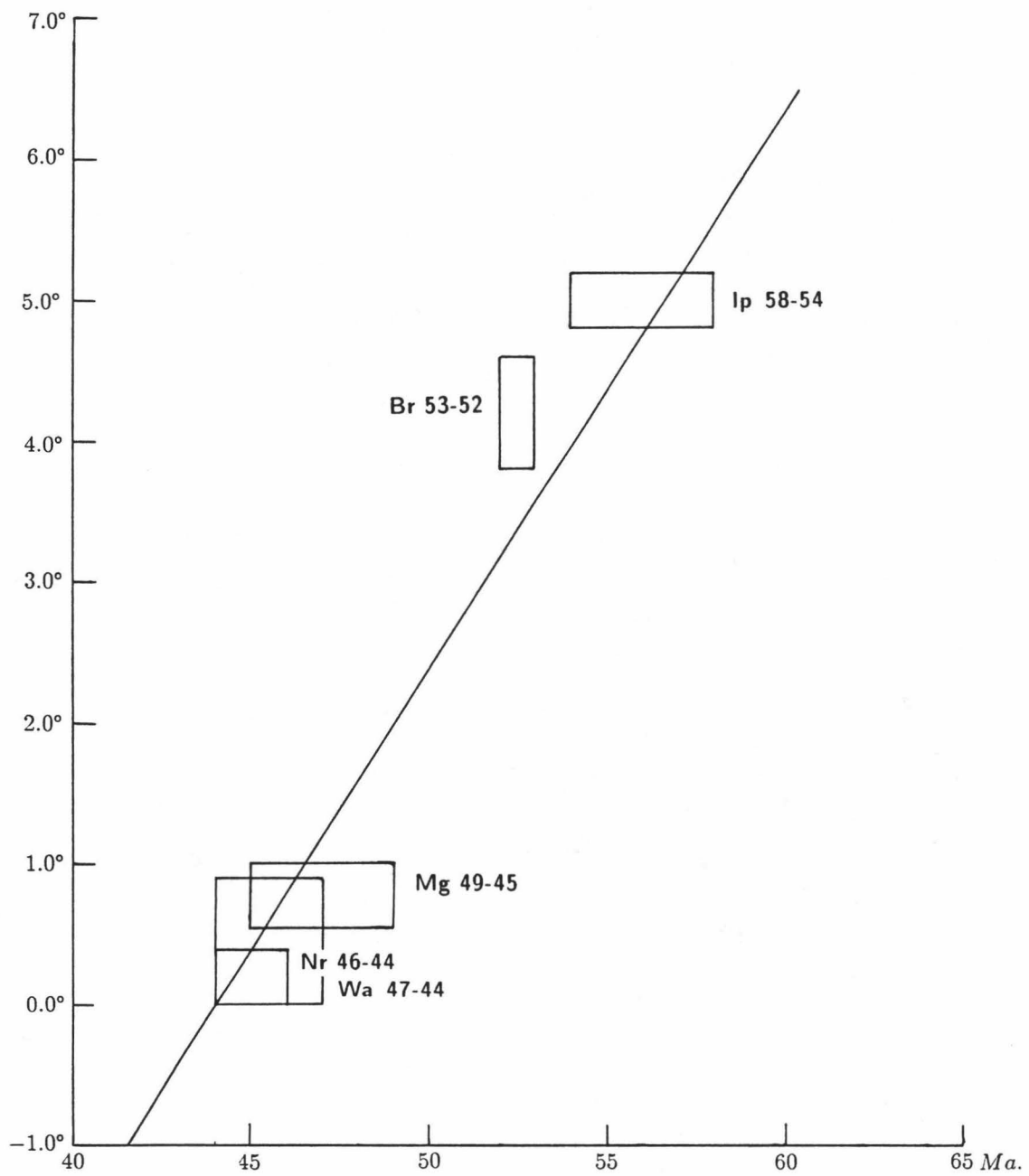
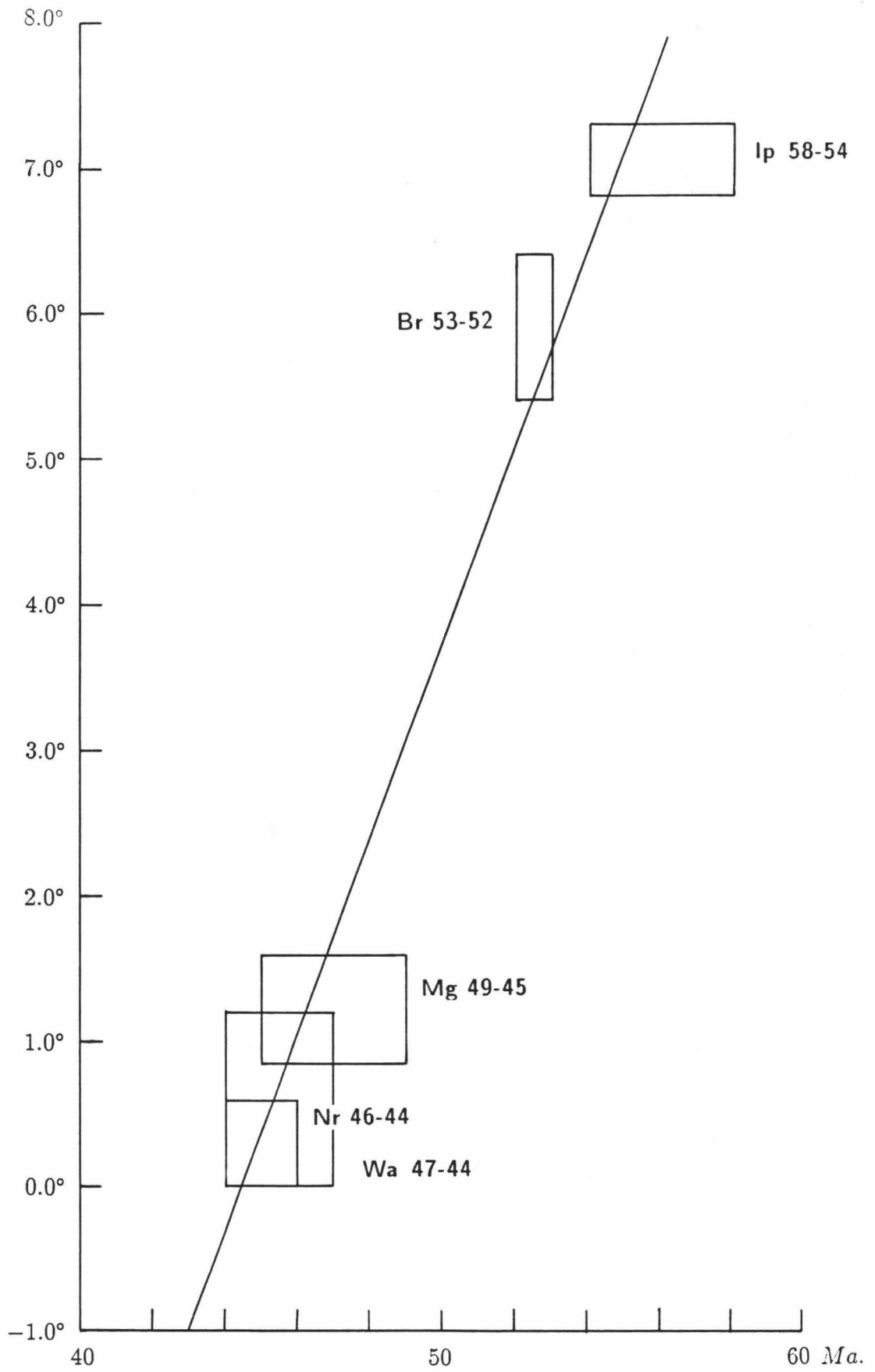


Figure 26 A plot of the angular distances of the basaltic lava fields from the Nr and Wa basaltic lava fields in the southeast Australia (with the inclusion of the chain of geoid anomalies in the southwestern Tasman Sea) along the parallels about the preferred pole at $14.4^{\circ}S$, $65.8^{\circ}W$ versus radiometric ages (Ma) within the 55-43 Ma time span. The data is a combination of the Ipswich Trail and the Barrington Trail. See Figure 4 for symbols of the southeatern Australian basaltic lava fields. The slope of the graph ($0.67^{\circ}/Ma$) is the rate of rotation about the pole for the 55-43 Ma time span.



References

- Barron, E.J., 1987, Cretaceous plate tectonic reconstructions, *Paleogeogr., Paleoclimatol., Paleoecol.*, 59, 3-29.
- Baudry, N., Diament, M., and Albouy, Y., 1987, Precise location of unsurveyed seamounts in the Austral archipelago area using SEASAT data, *Geophys. J.R. astr. Soc.*, 89, 869-888.
- Blackburn, G., Allison, G.B., and Leaney, F.W.J., 1982, Further evidence on the age of tuff at Mt. Gambier, South Australia, *Trans. R. Soc. S. Aust.*, 106(4), 163-167.
- Bonatti, E., Harrison, C.G.A., Fisher, D.E., Honnorez, J., Schilling, J.-G., Stipp, J.J., and Zentilli, M., 1977, Easter volcanic chain (Southeast Pacific): A mantle hot line, *J. Geophys. Res.*, 82, 2457-2478.
- Briden, J.C., Hurley, A.M., and Smith, A.G., 1981, Paleomagnetism and Mesozoic-Cenozoic paleocontinental maps, *J. Geophys. Res.*, 86, 11631-11656.
- Burke, K., Kidd, W.S.K., Wilson, J.T., 1973, Relative and latitudinal motion of Atlantic hot spots, *Nature*, 245, 133-137.
- Cande, S.C. and Mutter, J.C., 1982, A revised identification of the oldest sea-floor spreading anomalies between Australia and Antarctica, *Earth Planet. Sci. Lett.*, 58, 151-160.
- Clague, D.A. and Dalrymple, G.B., 1987, The Hawaiian-Emperor volcanic chain, Part I, Geologic evolution, *U.S. Geol. Surv. Prof. Pap.*, 1350, 5-54.
- Cleary, J., 1973, Australian crustal structure, *Tectonophysics*, 20, 241-248.
- Cox, A. and Hart, R.B., 1986, Plate tectonic how it works, *Blackwell Scientific Publications*, 392 pp.
- Denham, D., 1985, The Tasman Sea earthquake of 25 November 1983 and stress in the Australia Plate, *Tectonophysics*, 111, 329-338.
- Denham, D., Weekes, J., and Krayshek, C., 1981, Earthquake evidence for compressive stress in the southeast Australian crust, *J. Geol. Soc. Aust.*, 28,

- Duncan, R.A., 1981, Hotspots in the Southern Oceans - an absolute frame of reference for motion of the Gondwana continents. In: S.C.Solomon, R. Van der Voo and M.A. Chinnery (editors), Quantitative methods of assessing plate motions, *Tectonophysics*, 74, 29-42.
- Duncan, R.A., 1984, Age progressive volcanism in the New England Seamounts and the opening of the Central Atlantic Ocean, *J. Geophys. Res.*, 89, 9980-9990.
- Duncan, R.A. and McDougall, I., in press, Time-space relationships for Cainozoic intraplate volcanism in eastern Australia, the Tasman Sea, and New Zealand, in *Intraplate volcanic activity in Australia and New Zealand*.
- Embleton, B.J.J. and McElhinny, M.W., 1982, Marine magnetic anomalies, paleomagnetism and the drift history of Gondwanaland, *Earth Planet. Sci. Lett.*, 58, 141-150.
- Epp, D., 1978, Age and tectonic relationships among volcanic chains on the Pacific plate, Ph. D. dissertation, Univ. of Hawaii, Honolulu.
- Epp, D., 1984, Possible perturbations to hotspot traces and implications for the origin and structure of the Line Islands, *J. Geophys. Res.*, 89, 11273-11286.
- Ewart, A., 1987, The East Australian Cainozoic volcanic provinces - an overview of their petrology and chemistry, *Pacific Proceedings, Pacific Rim Congress 87*, The Geology, structure, mineralization and economic of the Pacific Rim, The Australian Institute of Mining and Metallurgy, 567-571.
- Falconer, R.H.K. and Tharp, M., 1983, General bathymetric chart of the oceans (GEBCO), *The Canadian Hydrographic Service*, Ottawa, Canada.
- Falvey, D.A. and Mutter, J.C., 1981, Regional plate tectonics and the evolution of Australia's passive continental margins, *BMR J. Aust. Geol. Geophys.*, 6, 1-29.
- Gill, E.D., 1964, Rocks contiguous with the basaltic cuirass of western Victoria, *Royal Soc. Victoria Proc.*, 77, 331-355.

- Green, D.H., Barsdell, M., Crawford, A.J., Eggins, S.M., Falloon, T.J., and Wallace, M.E., 1987, Petrology of upper mantle processes in the S.W., *Pacific Proceedings, Pacific Rim Congress 1987*, The Geology, structure, mineralization and economic of the Pacific Rim, The Australian Institute of Mining and Metallurgy, 621-632.
- Grim, P.J., 1969, Heat flow measurements in the Tasman Sea, *J. Geophys. Res.*, 74, 3933-3934.
- Harrison, C.G.A., 1972, Poles of rotation, *Earth Planet. Sci. Lett.*, 14, 31-38.
- Haxby, W.F., 1987, Gravity field of the World's oceans, *Geophysical Data Center, NOAA/National Ocean Office*.
- Hayes, D.E. and Ringis, J., 1973, Seafloor spreading in the Tasman Sea, *Nature*, 243, 454-458.
- Hess, H.H. and Maxwell, J.C., 1949, Major structural features of the southwest Pacific: *7th Pacific Sci. Cong. Proc.*, 2, 14-17.
- Idnurm, M., 1985, Late Mesozoic and Cenozoic palaeomagnetism of Australia - I. A redetermined apparent polar wander path, *Geophys. J.R. astr. Soc.*, 83, 399-418.
- Idnurm, M., 1986, Late Mesozoic and Cenozoic palaeomagnetism of Australia - III. Bias-corrected pole paths for Australia, Antarctica and India, *Geophys. J.R. astr. Soc.*, 86, 277-287.
- Jurdy, D.M. and Van der Voo, R., 1974, A method for the separation of true polar wander and continental drift, including results for the last 55 m.y., *J. Geophys. Res.*, 79, 2945-2952.
- Kent, D.V. and Gradstein, F.M., 1986, A Jurassic to recent chronology; in Vogt, P.R., and Tucholke, B.E. (ed.), *The geology of North America, Volume M, The Western North Atlantic Region*: 45-50, Geological Society of America.
- Klitgord, K.D. and Schouten, H., 1986, Plate kinematics of the central Atlantic, in Vogt, P.R., and Tucholke, B.E. (ed.), *The geology of North America*,

Volume M, *The Western North Atlantic Region*: Geological Society of America, 351-378.

- Konig, M., 1987, Geophysical data from the continental margin off Wilkes Land, Antarctica - Implications for breakup and dispersal of Australia - Antarctica, in Eittreim, S.L., and Hampton, M.A. (ed.), *The Antarctic Continental Margin: Geology and Geophysics of Offshore Wilkes Land*, CPCEMR Earth Sci. Ser., 5A, 117-145: Houston, Texas, Circumpacific Council for Energy and Mineral Resources.
- Kroenke, L.W., Jouannic, C., and Woodward, P., 1983, Bathymetry of the Southwest Pacific, Chart 1 of the Geological Atlas of the Southwest Pacific (2 sheets), Suva, Fiji, *CCOP/SOPAC*.
- Kroenke, L.W., 1986, Tectonic evolution of the Southwest Pacific, 3-20, in Johnson, C.J. and Clark, A.L. (ed.), *Pacific mineral resources physical, economic, and legal issues, Proceedings of the Pacific marine mineral resources training course*, held at East-West Center, Honolulu, Hawaii, June 1985.
- Larue, B.M., Daniel, J., Jouannic, C., and Recy, J., 1977, The south Rennell Trough: Evidence for a fossil spreading zone, *Intel. Sym. on Geodym. in Southwest Pacific*, 51-62.
- Lawver, L.A. and Dick, H.J.B., 1983, The American-Antarctic Ridge, *J. Geophys. Res.*, 88, 8193-8202.
- Lawver, L.A., Sclater, J.G., and Meinke, L., 1985, Mesozoic and Cenozoic reconstructions of the South Atlantic, *Tectonophysics*, 114, 233-254.
- Le Pichon, X., Francheteau, J., and Bonnin, J., 1973, Plate tectonics, 200pp., Development in Geotectonics, 6, *Elsevier Scientific Publishing Company*.
- Lilley, F.E.M., 1975, Electrical conductivity anomalies and continental seismicity in Australia, *Nature*, 257, 381-382.
- Lilley, F.E.M., 1976, A magnetometer array study across southern Victoria and the Bass Strait area, Australia, *Geophys. J.R. astr. Soc.*, 46, 165-184.

- Livermore, R.A., Vine, F.J., and Smith, A.G., 1984, Plate motions and the geomagnetic field - II. Jurassic to Tertiary, *Geophys. J.R. astr. Soc.*, 79, 939-961.
- Lonsdale, P., 1988, Geography and history of the Louisville hot-spot chain in the Southwest Pacific, *J. Geophys. Res.*, 93, 3078-3104.
- McDonough, W.F., McCulloch, M.T., and Sun, S.S., 1985, Isotopic and geochemical systematics in Tertiary-Recent basalts from southeastern Australia and implications for the evolution of the sub-continental lithosphere, *Geochimica et Cosmochimica Acta*, 49, 2051-2067.
- McDougall, I., Embleton, B.J.J., and Stone, D.B., 1981, Origin and evolution of Lord Howe Island, Southwest Pacific Ocean, *J. Geol. Soc. Aust.*, 28, 155-176.
- McElhinny, M.W., 1979, Paleomagnetism and plate tectonics, *Cambridge Earth Science Series, Cambridge Univ. Press.*
- McElhinny, M.W., Embleton, B.J.J., and Wellman, P., 1974, A synthesis of Australian Cenozoic palaeomagnetic results, *Geophys. J.R. astr. Soc.*, 36, 141-151.
- Minster, J.B., Jordan, T.H., Molnar, P., and Haines, E., 1974, Numerical modelling of instantaneous plate tectonics, *Geophys. J. R. astr. Soc.*, 36, 541-576.
- Minster, J.B. and Jordan, T.H., 1978, Present-day plate motions, *J. Geophys. Res.*, 83, 5331-5354.
- Molnar, P., and Atwater, T., 1973, Relative motion of hot spots in the mantle, *Nature*, 246, 288-291.
- Molnar, P. and Francheteau, J., 1975, The relative motion of 'hot spots' in the Atlantic and Indian Oceans during the Cenozoic, *Geophys. J.R. astr. Soc.*, 43, 763-774.
- Molnar, P. and Stock, J., 1987, Relative motions of hotspots in the Pacific, Atlantic and Indian Oceans since late Cretaceous time *Nature*, 327, 587-591.
- Monahan, D., Falconer, R.H.K., and Tharp, M., 1984, General bathymetric chart

of the oceans (GEBCO), *The Canadian Hydrographic Service*, Ottawa, Canada.

- Morgan, W.J., 1971, Convection plumes in the lower mantle, *Nature*, 230, 42-43.
- Morgan, W.J., 1972a, Deep mantle convection plumes and plate motions, *Am. Assoc. Petro. Geol. Bull.*, 56, 203-213.
- Morgan, W.J., 1972b, Plate motion and deep mantle convection, *Geol. Soc. Amer.*, Memoir, 132, 7-22.
- Morgan, W.J., 1981, Hotspot tracks and the opening of the Atlantic and Indian Oceans, 443-487, in *The Sea*, Vol. 7, C. Emiliani Ed., Wiley, New York.
- Morgan, W.J., 1983, Hotspot tracks and the early rifting of the Atlantic, *Tectonophysics*, 94, 123-139.
- Muirhead, K.J., Cleary, J.R., and Finlayson, D.M., 1977, A long-range seismic profile in South-eastern Australia, *Geophys. J.R. astr. Soc.*, 48, 509-519.
- Owen, H.G., 1984, Atlas of continental displacement, 200 million years to the present, *Cambridge Press*, New York, 159 pp.
- Pilger, R.H., Jr., 1982, The origin of hotspot traces: Evidence from eastern Australia, *J. Geophys. Res.*, 87, 1825-1834.
- Sandwell, D.T., 1984, A detailed view of the South Pacific geoid from satellite altimetry, *J. Geophys. Res.*, 89, 1089-1104.
- Sass, J.H. and Lachenbruch, A.H., 1979, Thermal regime of the Australian continental crust, in *The Earth - Its origin, structure and evolution*, McElinny, M.W. (ed.), Academic Press, London, 301-351.
- Schmidt, P.W. and Embleton, B.J.J., 1981, Magnetic overprinting in southeastern Australia and the thermal history of its rifted margin, *J. Geophys. Res.*, 86, 3998-4008.
- Schult, F.R. and Gordon, R.G., 1984, Root mean square velocities of the continents with respect to the hot spots since the Early Jurassic, *J. Geophys. Res.*,

89, 1789-1800.

- Shaw, R.D., 1979, On the evolution of the Tasman Sea and adjacent continental margins, Ph. D. dissertation, Univ. of Sydney, Australia.
- Sheard, M.J., 1978, Geological history of the Mount Gambier volcanic complex, Southeast South Australia, *Trans. R. Soc. S. Aust.*, 102, 125-139.
- Slater, R.A. and Goodwin, R.H., 1973, Tasman Sea guyots, *Marine Geology*, 14, 81-99.
- Smith, A.G., 1982, Late Cenozoic uplift of stable continents in a reference frame fixed to South America, *Nature*, 296, 400-404.
- Smith, B.W. and Prescott, J.R., 1987, Thermoluminescence dating of the eruption at Mt. Schank, South Australia, *Aust. J. Earth Sci.*, 34, 335-342.
- Sprigg, R.C., 1959, Presumed submarine volcanic activity near Beachport, South-east South Australia, *Trans. Roy. Soc. S. Aust.*, 82, 195-203.
- Standard, J.C., 1961, Submarine geology of the Tasman Sea, *Geol. Soc. Amer. Bull.*, 72, 1777-1788.
- Stephenson, P.J., Griffin, T.J., and Sutherland, F.L., 1980, Cainozoic volcanism in Northeastern Australia Cainozoic volcanism, in *Northeastern Australia*, 349-374, Henderson, R.A. and Stephenson, P.J. (ed.), Geol. Soc. Aust. Qld. Division.
- Sutherland, F.L., 1981, Migration in relation to possible tectonic and regional controls in eastern Australian volcanism, *J. Volcanol. Geotherm. Res.*, 9, 181-213.
- Sutherland, F.L., 1983, Timing, trace and origin of basaltic migration in eastern Australia, *Nature*, 305, 123-126.
- Sutherland, F.L., 1985, Regional controls in eastern Australian volcanism. In: Sutherland, F.L., Franklin, B.J., and Waltho, A.E., (eds.), *Volcanism in Eastern Australia*, 13-32, Geol. Soc. Aust., New South Wales Division, Publication No. 1, Sydney.

- Vogt, P.R. and Conolly, J.R., 1971, Tasmantid Guyots, the age of the Tasman Basin, and motion between the Australia Plate and the mantle, *Geol. Soc. Amer. Bull.*, 82, 2577-2584.
- Watanabe, T., Langseth, M.G., and Anderson, R.N., 1977, Heat flow in back-arc basins of the Western Pacific, 137-161, in *Island arcs, deep sea trenches and back-arc basins*, Maurice Ewing Ser. 1, AGU, Washington, D.C..
- Watts, D.R., Watts, G.C., and Bramall, A.M., 1984, Cretaceous and early Tertiary paleomagnetic results from the Antarctic Peninsula, *Tectonics*, 3, 333-346.
- Weissel, J.K. and Hayes, D.E., 1972, Magnetic anomalies in the Southeast Indian Ocean, in *Antarctic Oceanology II: The Australia-New Zealand Sector*, Antarctic Res. Ser., 19, edited by D.E. Hayes, 165-196, AGU, Washington, D.C..
- Weissel, J.K. and Hayes, D.E., 1977, Evolution of the Tasman Sea reappraised, *Earth Planet. Sci. Lett.*, 36, 77-84.
- Weissel, J.K., Hayes, D.E., and Herron, E.M., 1977, Plate tectonics synthesis: The displacements between Australia, New Zealand, and Antarctica since the Late Cretaceous, *Marine Geology*, 25, 231-277.
- Weissel, J.K. and Watts, A.B., 1979, Tectonic evolution to the Coral Sea basin, *J. Geophys. Res.*, 84, 4572-4582.
- Wellman, P., 1983, Hotspot volcanism in Australia and New Zealand: Cainozoic and Mid-Mesozoic, *Tectonophysics*, 96, 225-243.
- Wellman, P., McElhinny, M.W., and McDougall, I., 1969, On the polar-wander path for Australia during the Cenozoic, *Geophys. J.R. astr. Soc.*, 18, 371-395.
- Wellman, P. and McDougall, I., 1974, Cainozoic igneous activity in eastern Australia, *Tectonophysics*, 23, 49-65.
- Whitman J.M., Harrison, C.G.A., and Brass, G.W., 1983, Tectonic evolution of the Pacific Ocean since 74 Ma, *Tectonophysics*, 99, 241-249.

- Wilson, J.T., 1963, A possible origin of the Hawaiian Islands, *Canad. J. Phys.*, 41, 863-870.
- Wilson, J.T., 1965, Convection currents and continental drift, *Royal Soc. London, Philos. Trans.*, 258 A, 145-167, Symposium on continental drift.
- Wong, P.P.K., Greggory, C., and Handschumacher, D.W., 1975, Computer program projecting fictitious longitude and latitude systems onto standard Mercator grids, *Hawaii Institute of Geophysics, Data Report No. 30, HIG-75-19*, Honolulu.